Passive scalar mixing in turbulent flow

Wouter J.T. Bos

N° d'ordre : 2005–14 Année 2005

THÈSE

présentée devant

L'ÉCOLE CENTRALE DE LYON

École doctorale MEGA

pour obtenir

le titre de DOCTEUR

Spécialité: Mécanique

par

Wouter Bos

Passive scalar mixing in turbulent flow

Soutenue le 24 juin 2005 devant la Commission d'Examen

Jury:	MM.	J.-P.	Bertoglio	- *Directeur de Thèse*
		C.	Cambon	
		J.-N.	Gence	
	Mme	M.	Larchevêque	- *Rapporteur*
	MM.	E.	Lévêque	- *Président*
		M.	Reeks	
		Z.	Warhaft	- *Rapporteur*

Preface

What you are reading is the beginning of my PhD-manuscript. It tells in more or less chronological order what I discovered and learned during the last four years about turbulence and mixing. A big part of it I learned directly from my supervisor Jean-Pierre Bertoglio. I deeply respect him for his scientific skills, but also for the way he guided my thesis in a wise and human way. Thank you Jean-Pierre, it is a pleasure and a privilege working with you.

I want to thank the two referees of my manuscript, professor Zellman Warhaft and professor Michèle Larchevêque for the time and energy they have put in reading my manuscript and their interesting and valuable comments on my work.

I am also grateful to Professor Michael Reeks and Dr. Emmanuel Lévêque for accepting to be members of the jury. I especially want to thank Dr. Claude Cambon for interesting discussions on spectral closures and Professor Jean-Noël Gence for discussions on dimensional analysis and for his patience in explaining fluid mechanics to me.

This work would not have been the same without the help of Hatem Touil (il faut toujours avoir un Hatem dans son bureau) and the help, critical remarks and pedagogical skills of Yohann Duguet; you were always there to help me with whatever numerical, physical, mathematical, political or linguistic problem. I thank you as colleagues but even more as friends.

Without the numerical simulations of Liang Shao, this work would not have been complete, thank you Liang. I thank Fabien Godeferd for the answers on the uncountable number of questions, Guillevic Lamaison and Lukas Liechtenstein for the many interesting discussions. Thank you, Rob Poole, for proof-reading my introduction.

I thank the (ex-)thesards Sam, Manu, Denis, Dominique, Charles, Antoine, Laure, Steph, Thomas, Aurélien, Walid, Valeria, Pietro and all the other people of the LMFA for the famous french coffee breaks and the nice atmosphere in the lab.

Thanks also to the friends from Lyon, Confluants, and others, with a special mentioning of Greg, Yohann and Lukas. You made my stay in Lyon more than pleasant. Thanks also to the friends of Borrelnood.

My parents were always there to encourage and help me, thank you Spechten (that includes Bram and Annemieke). Elena, thank you for being there, for always encouraging me, thank you.

A special word for Professor Frans Nieuwstadt, who died a few weeks before the end of my thesis. Without his enthousiasm I would probably not have chosen to do a PhD in turbulence. I dedicate this thesis to him.

Contents

Nomenclature

$A^T, A^{\Pi}..$	Model constants
B	Relative intensity ratio
$C_K, C_{CO}, C_{w\theta}$	Constant of Kolmogorov, Corrsin-Obukhov, Scalar flux spectrum
D_{ij}	Turbulent diffusivity tensor
D_{ll}, D_{lll}	Second, third order velocity correlation
$D_{\theta\theta}, D_{\theta\theta l}$	Second, third order scalar and mixed correlation
$D_{ij}(K)$	Inhomogeneous transport
$E(K)$	Kinetic energy spectrum, $\int E(K)dK = \frac{3}{2}\mathcal{U}^2 = k$
$E_\theta(K)$	Scalar spectrum, $\int E_\theta(K)dK = \frac{1}{2}\overline{\theta^2}$
E^+	Thermalized energy
$\mathcal{F}_{u_i\theta}(\boldsymbol{K})$	Three-dimensional scalar flux spectrum
$F_{u_i\theta}(K), F(K)$	Scalar flux spectrum, $\int F_{u_i\theta}(K)dK = \overline{u_i\theta}$
FT	Fourier transform
$g^{sg}_{u_i\theta}$	Subgrid scalar flux
k	Kinetic Energy
$\boldsymbol{K}, \boldsymbol{P}, \boldsymbol{Q}, K_i$	Wave vector
K, P, Q	Wave number
K_η	Kolmogorov spatial frequency
K_c	Cut-off wavenumber (LES), Infrared spectral cut-off
K_f	Forced wavenumber
K^-	Wavenumber containing minimum energy in a partially thermalized spectrum
$\mathcal{L}$	Integral length scale
n	Inertial range spectral slope
P	Total pressure ($= \overline{P} + p$)
$P(K)$	Production
$P_{ij}(\boldsymbol{K})$	Projection operator
$P_{ijk}(\boldsymbol{K})$	$= K_j P_{ik}(\boldsymbol{K}) + K_k P_{ij}(\boldsymbol{K})$
Pe	Peclet number
Pr, Pr_T	Prandtl number, turbulent Prandtl number
R_{ij}	Two-point velocity correlation
R_λ	Taylor-scale Reynolds number
R	Velocity-scalar time scale ratio
$\boldsymbol{r}, r_i$	Separation vector
S_{ij}	Rate of strain tensor
S	Mean velocity gradient

T	Total temperature $= \Theta + \theta$
T^{NL}	Non-linear transfer
$T^{<}, T^{>}$	Resolved, unresolved non-linear transfer
T^{L}	Linear transfer
T_{ijk}	Triple correlation
$\mathcal{T}', \mathcal{T}$	Single particle, two-particle correlation time
u, u_i	Velocity fluctuation
$\overline{U}, \overline{U}_i$	Mean velocity
U, U_i	Total velocity $(= \overline{U}_i + u_i)$
$\mathcal{U}$	Integral velocity scale
$\mathcal{U}_i(x, t \mid \tau)$	Lagrangian velocity
V^{SG}	Subgrid diffusion, destruction
$\boldsymbol{x}, x_i$	Spatial variable
α	Molecular diffusivity of scalar
α_e	Eddy diffusivity of scalar
γ	Coefficient governing the scalar flux in the inertial range
Γ	Mean scalar gradient
δ_{ij}	Kronecker delta
$\delta(\boldsymbol{K})$	Dirac delta
ϵ	Viscous dissipation
ϵ^{F}	Spectral flux
$\epsilon_\theta, \epsilon_{u\theta}$	Molecular diffusion of scalar variance, scalar flux
$\eta(K)$	Spectral eddy viscosity
Θ	Mean temperature
$\Theta(K, t)$	Triple correlation relaxation time
θ	Temperature fluctuation
λ	EDQNM model constant
μ	Cosine of the angle between $\boldsymbol{K}$ and the mean scalar gradient
$\mu(K)$	Eddy damping
ν	Kinematic viscosity
ν_e	Eddy viscosity
Π	Slow or non-linear pressure term
Π^{L}	Rapid or linear pressure term
${}^{R}\Pi$	Wall reflection pressure term
ρ	Density
$\rho_{u\theta}$	Scalar-velocity cross correlation coefficient
$\tau(K)$	Local spectral timescale
τ_{ij}^{sg}	Subgrid stress tensor
$\Phi_{ij}(\boldsymbol{K})$	Spectral tensor
$\Phi_\theta(\boldsymbol{K})$	Three-dimensional scalar spectrum
$\varphi_{ij}(K)$	Spherically averaged spectral tensor, $\int \varphi_{ij}(K) dK = \overline{u_i u_j}$

Introduction

It is hard to give a precise definition of what turbulence is. As a consequence turbulence is generally described by its properties. One of its most striking properties is its ability to mix. Turbulence enhances the mixing of pollution in the atmosphere, salt in the sea, sugar in our coffee, fuel in a combustion engine, but most importantly, turbulence mixes turbulence, and this may be seen as the main problem in predicting a turbulent flow: the convection of momentum by the velocity field itself is a nonlinear mechanism that prevents a simple description.

The apparent randomness and complexity of a turbulent flow stem from this nonlinearity and make a statistical description appealing. The most relevant information of a turbulent flow can often be retained by considering the averaged properties. A very common way of describing a turbulent flow is therefore by statistical means. The velocity U_i, for example, can be divided into a mean part $\overline{U}_i$ and a fluctuation u_i.

If one wants to predict the mean velocity field $\overline{U}_i$ one should take into account the effect of the turbulent fluctuations on the mean field which act as a stress $\overline{u_i u_j}$, called the Reynolds stress. We can interpret this stress as the mixing of momentum by turbulent movement. The essential problem of predicting the mean velocity of a turbulent flow could then be solved by an accurate knowledge of the Reynolds stress as an explicit function of the mean quantities. However, such a relation is to date not satisfactorily established.

The subject of this thesis is the mixing of a passive scalar by a turbulent flow. A passive scalar is a scalar quantity that does not influence the flow field by which it is advected. Examples are the concentration of non-reacting chemical species and temperature, as long as the temperature fluctuations remain small. Also the separation distance of a fluid particle from its initial position is a non-diffusive passive scalar (see section 7.2). The benefits of studying passive scalars are therefore twofold. On one hand it is of practical importance when predicting for example the mixing of pollutants in the air or the performance of heat exchangers, on the other hand the study is of theoretical importance: understanding the mixing of the fluid particles should help to describe a turbulent flow.

The equation governing the transport of a passive scalar is linear. The advection of the scalar by a turbulent velocity field is however not simple. Once again, description by statistical means is the most widely used approach. The scalar T is then divided into a mean value Θ and a fluctuating part θ. The effect of the turbulent fluctuations on the mean scalar field is now represented by a turbulent scalar flux, $\overline{u_i\theta}$. The scalar flux is thus the key quantity in the prediction of the mean scalar field and its understanding and modelling is the main issue of this thesis. In order to investigate the contributions of the different turbulent lengthscales to the scalar flux we examine the spectral distribution of scalar flux with wavenumber, i.e. the scalar flux spectrum.

Theoretically the simplest configuration with which to study the turbulent scalar flux is isotropic turbulence with a uniform mean scalar gradient. The scalar field is in this case anisotropic. At the same time it is the simplest way to study anisotropy in a turbulent flow because the scalar field is homogeneous and also axisymmetric: in a plane perpendicular to the mean scalar gradient axis there is no preferential direction. The scalar flux spectrum reduces in this case to one single scalar function.

Isotropic turbulence with a mean scalar gradient is the subject of the first four chapters of the manuscript. In the first chapter the basic quantities and equations are introduced. In particular the wavenumber spectra of the kinetic energy, the scalar flux and the scalar variance are discussed because those quantities will receive our main attention in this thesis.

In the second chapter, experimental results from the literature concerning the scalar flux spectrum are reviewed. Apparent discrepancies between experimental results and classical scaling laws are examined. Detailed dimensional analysis as well as Direct Numerical Simulation and Large Eddy Simulations (approaches explained in section 1.3) are used to examine the behaviour of the scalar flux spectrum. As will be seen, these approaches do not yield conclusive answers about the asymptotic (high Reynolds number) spectral behaviour of this spectrum.

In the third chapter we use an analytical theory of turbulence, the Eddy-Damped Quasi-Normal Markovian theory (EDQNM), to study the scalar flux spectrum. The basic idea of this theory stems from the observation that turbulent velocity and scalar fluctuations are close to Gaussianity. Using the assumption of Gaussianity leads to a closed evolution equation for the scalar flux spectrum. Subsequently, the equation is numerically integrated. EDQNM is very suitable to studying wave-number spectra of turbulent quantities at high Reynolds numbers. This allows us to investigate the anomalous behaviour of the scalar flux spectrum observed in chapter 2.

We use the EDQNM theory to analyze some parameters that might influence the Large Eddy Simulations of isotropic turbulence with a mean scalar gradient in chapter 4. The influence of resolution, forcing and sub-

gridmodel on the velocity and scalar field are examined. EDQNM allows a better interpretation of the LES results, initially discussed in chapter 2, to be made.

After the extensive validation of the EDQNM theory in isotropic turbulence, we apply it to homogeneous shear flow. More assumptions and modelling have to be introduced, but it is shown that the analytical theory can here again provide insights in to the behaviour of the turbulent scalar fluxes. In this chapter the velocity field is modelled by an extension of the EDQNM theory to homogeneous anisotropic turbulence by Touil [1].

These positive results encouraged us to extend the closure to inhomogeneous turbulent flows. Therefore in chapter 6 we propose, and subsequently derive, an extension of the closure for the scalar flux and scalar variance to inhomogeneous turbulence to show that the extension to complex flows is feasible. This extension is compatible with the Simplified spectral Closure for Inhomogeneous Turbulence (SCIT), developed at the *Laboratoire de Mécanique des Fluides de l'Ecole Centrale de Lyon.* The SCIT model constitutes a closure of the Reynolds stresses in inhomogeneous turbulent flows.

One of the advantages of an analytical approach is that it is straight forward to study the limiting behaviour of zero viscosity or zero diffusivity. The first of those cases, inviscid turbulence, is treated in section 7.1 and insights are obtained in to the theoretical issue of relaxation towards a thermal equilibrium. The second case, the non-diffusive scalar is treated in section 7.2, where we illustrate the link between passive scalar mixing and single particle dispersion.

This link allows to formulate a single-time two-point closure for the energy spectrum, without any model constants. In this new closure, the characteristic time scale (or damping term) is built on the spectrum of the velocity-scalar correlation. The model is presented in section 7.3 where it is shown to yield good estimates of the Kolmogorov and Corrsin-Obukhov constants.

An extensive french abstract of this thesis can be found in chapter 8.

Chapter 1

Scalar mixing in Isotropic Turbulence

1.1 Isotropic turbulence

1.1.1 Generalities

The dynamics of an incompressible Newtonian fluid are entirely determined by the Navier-Stokes equations and the incompressibility condition:

$$\frac{\partial U_i}{\partial t} + U_j \frac{\partial U_i}{\partial x_j} = -\frac{1}{\rho}\frac{\partial P}{\partial x_i} + \nu \frac{\partial^2 U_i}{\partial x_j^2} \tag{1.1}$$

$$\frac{\partial U_i}{\partial x_i} = 0 \tag{1.2}$$

In this equation U_i is the velocity vector, ρ is the density, P is the pressure and ν is the kinematic viscosity. The second term in equation (1.1) is non-linear. If this term becomes large compared to the last term, the viscous stress, the regime of the flow changes from laminar to turbulent. The movements of the fluid particles becomes dependent on small variations of the initial conditions. If the exact initial conditions are unknown the movement of the fluid particles becomes unpredictable.

Most of the flows encountered in practice are turbulent. The unpredictable nature of the fluid particles makes an exact description of most of the real-life turbulent flows practically unfeasible. A statistical study of the flow can provide valuable information. We decompose a turbulent quantity in its mean and its fluctuation. For the velocity vector we write:

$$U_i = \overline{U_i} + u_i \tag{1.3}$$

The average that we use in theoretical approaches is the 'ensemble' average, the average value after an infinity of realizations of the same flow. The

chaotic nature of the flow ensures that every realization yields a different result. One could assume that this average is equivalent to the long-time average in a stationary flow, or the space average in an infinitely large homogeneous flow. This assumption is called *ergodicity* .

1.1.2 Statistical description of isotropic turbulence

Homogeneous turbulence is a turbulence that is statistically identical at every point in space. Observers at different spatial positions in the velocity field will experience the same statistical behaviour. In other words: the turbulence is statistically invariant under translations.

If in addition the statistics are invariant under rotation the field is called isotropic. This means that the different observers experience the same when looking in different directions. The mean flow $\overline{U_i}$ must be zero or uniform in such a flow, because a non-uniform mean flow would immediately introduce a preferential direction in the flow. An isotropic turbulence is from a statistical point of view the most simple configuration of turbulence. Experimentally, however, creating a proper isotropic turbulent flow is not that simple because the influence of boundaries and mean flow easily breaks the isotropy. By carrying out experiments far enough away from boundaries we can try to eliminate most of the boundary effects. In atmospheric experiments we could hope that this is the case. The meteorological conditions (stratification, rotation and shear) prevent however the atmosphere from being isotropic. In laboratories we can eliminate most of those factors and we might be able to create locally isotropic turbulence at a smaller scale than in the atmosphere. Now the question is: how can we create turbulence in an isotropic way? The conventional way of generating nearly isotropic turbulence in a laboratory is by use of a grid in a wind tunnel. One could object that the velocity fluctuations generated in this way are convected by a mean velocity, and that this velocity breaks the isotropy by imposing directionality on the flow field. For an observer moving with the same velocity as the mean velocity of the flow, the turbulence can however be considered isotropic.

Let us assume now that we have generated isotropic turbulence. Perhaps statistically this is the simplest kind of turbulence but while studying it, we notice that the flow is not that simple: we see a large variety of eddies convecting each other, interacting by local shearing and straining. Big scales breaking up in smaller ones, whirls exchanging momentum with other whirls. The complexity of isotropic turbulence appears to be related to its variety of lengthscales. We could state that 'turbulence consists of chaotic whirly structures with a large range of lengthscales' [2]. This wide variety in lengthscales is found in all turbulent flows even in the most simple kind, isotropic turbulence. It might be clever to study first this kind of flow.

The tools and concepts derived in this framework could be very valuable in studying more complex flows such as sheared or inhomogeneous turbulence.

To get more insights in those complex dynamics, a fruitful approach is statistically studying the different turbulent lengthscales. The simplest statistical feature would be the statistical mean of the velocity of each lengthscale. In isotropic turbulence, the average velocity is however zero at each lengthscale. As one rather studies a non-zero statistic, one could consider the kinetic energy k of the velocity field.

$$k(\boldsymbol{x},t) = \frac{1}{2}\left(\overline{u^2(\boldsymbol{x},t)} + \overline{v^2(\boldsymbol{x},t)} + \overline{w^2(\boldsymbol{x},t)}\right) \tag{1.4}$$

Because of isotropy u, v and w are statistically equivalent so that: $k(\boldsymbol{x},t) = 3/2\ \overline{u^2(\boldsymbol{x},t)}$. In freely decaying isotropic turbulence one can write:

$$\frac{\partial k(t)}{\partial t} = -\epsilon(t), \tag{1.5}$$

That is: the decrease of the kinetic energy is equal in value to the viscous dissipation ϵ. The value of k does not tell us much about the different lengthscales, its value is the sum of the contributions of all different scales. For instance, a flow field with only one lengthscale could have the same kinetic energy. To study the multi-scale behaviour it is more convenient to evaluate the kinetic energy contained by each different lengthscale. By measuring the mean kinetic energy at one point we will not have access to information on the different lengthscales. In order to obtain the energy distribution over the different scales of motion in a homogeneous turbulence we consider therefore the two point velocity-correlations:

$$R_{ij}(\boldsymbol{r},t) = \overline{u_i(\boldsymbol{x},t)u_j(\boldsymbol{x}+\boldsymbol{r},t)} \tag{1.6}$$

and we vary the separation distance $\boldsymbol{r}$ between the two observation points. $R_{ij}(\boldsymbol{r},t)$ is independent of the position $\boldsymbol{x}$ because of homogeneity. It is common use and rather suitable to consider multi-scale phenomena in Fourier space:

$$\Phi_{ij}(\boldsymbol{K},t) = FT_{/\boldsymbol{r}}\left[R_{ij}(\boldsymbol{r},t)\right] \tag{1.7}$$

in which $FT_{/\boldsymbol{r}}$ indicates a Fourier transform:

$$FT_{/\boldsymbol{r}}\left[f(\boldsymbol{r},t)\right] = \frac{1}{(2\pi)^3}\int f(\boldsymbol{r},t)e^{-i\boldsymbol{K}\cdot\boldsymbol{r}}d\boldsymbol{r} \tag{1.8}$$

The quantity $\Phi_{ij}(\boldsymbol{K},t)$ is called the spectral tensor. In isotropic turbulence, this tensor should show the same behaviour in all directions of $\boldsymbol{K}$. It should therefore be possible to describe its behaviour by a function that is independent of the direction of the wavevector $\boldsymbol{K}$. We obtain such a function

by integrating over all directions, that is, over spherical shells with a radius $K = \|\boldsymbol{K}\|$. In other words: isotropy allows to use the wavenumber (the norm of the wavevector) as the main variable instead of the three dimensional wavevector. This yields one scalar function, the energy spectrum $E(K,t)$. The relation between the two quantities is (using the fact that the velocity field is incompressible):

$$\Phi_{ij}(\boldsymbol{K},t) = \left(\delta_{ij} - \frac{K_i K_j}{K^2}\right) \frac{E(K,t)}{4\pi K^2} \tag{1.9}$$

This one scalar function $E(K,t)$ describes the entire statistical distribution of turbulent kinetic energy k over all different lengthscales in an isotropic turbulent velocity field. The integral of $E(K,t)$ over all wavenumbers yields the kinetic energy:

$$\int_0^\infty E(K,t)dK = k(t) \tag{1.10}$$

In the following we will omit the time dependence of the different quantities.

Let us consider a turbulence with a broad range of lengthscales. Most of the kinetic energy is contained in the large scales. We define the quantity

$$\mathcal{U} = \sqrt{\overline{u^2}}, \tag{1.11}$$

as the typical velocity scale of those energy-containing eddies and we can define a typical lengthscale $\mathcal{L}$, also called the integral lengthscale, corresponding to the size of those large eddies[1]. The dissipation of the kinetic energy takes mainly place in the small scales (or large wavenumbers). In those smallest scales the velocity gradients are the strongest and it is therefore at those scales that the viscous stresses (the last term in equation 1.1) become non-negligible and that the kinetic energy is converted to heat. We assume that a tiny little eddy is only convected by a large scale and that in the reference frame following this little eddy the large scale parameters $\mathcal{L}$ and $\mathcal{U}$ will not directly influence its behaviour. The dissipation ϵ takes however place in such small whirls and is governed by viscous effects so that the dynamics at the dissipation lengthscale η should be determined by the quantities ν and ϵ. Dimensional analysis allows to define this dissipation lengthscale:

$$\eta = \frac{\nu^{3/4}}{\epsilon^{1/4}} \tag{1.13}$$

[1] This is rather an order of magnitude than a rigorous definition. A frequently used definition of the integral lengthscale in isotropic turbulence is

$$\mathcal{L} = \frac{3\pi}{4} \frac{\int_0^\infty \frac{E(K)}{K} dK}{\int_0^\infty E(K) dK}. \tag{1.12}$$

The ratio of convective to viscous effects at a scale $\mathcal{L}$ is given by the Reynolds number.

$$R_{\mathcal{L}} = \frac{\mathcal{U}\mathcal{L}}{\nu} \tag{1.14}$$

The subscript $\mathcal{L}$ indicates that the typical lengthscale used in this definition of the Reynolds number is the integral lengthscale. Another definition, generally used in isotropic turbulence, is based on the Taylor microscale λ. This definition reads (see for example Pope [3]):

$$R_\lambda = \sqrt{\frac{20}{3}\frac{k^2}{\nu\epsilon}} \tag{1.15}$$

A large Reynolds number corresponds to a large range of lengthscales. In between the largest 'integral' scales and the dissipative scales we find in this case a range of intermediate sized eddies. If their size is much smaller then $\mathcal{L}$ but much larger then η we say that they are in the inertial subrange. *Much larger* and *much smaller* are still to be defined.

Similarly, in spectral space the region of the energy containing scales is separated from the wavenumber range of dissipative eddies by a zone of intermediate length-scales that we can call the inertial range. Inertial because neither the largest scales nor the dissipation scales are directly influencing their behaviour. The role of those inertial scales consists of transferring energy from the former to the latter[2]. In equilibrium this spectral energy flux must be equal to the dissipation ϵ. For a given turbulent scale l, the only relevant parameters are therefore the wavenumber K proportional to the inverse of the local lengthscale l and ϵ. The energy spectrum should thus, by dimensional analysis, obey in this region a scaling first proposed by Kolmogorov [4]:

$$E(K) = C_K \epsilon^{2/3} K^{-5/3}, \tag{1.16}$$

with C_K a constant of about 1.5. Even in flows that are not perfectly isotropic this inertial range is expected to appear if the Reynolds number is high enough. See for example the turbulent boundary layer data of Saddoughi and Veeravalli [5], showing a neat $K^{-5/3}$ slope of the energy spectrum. The reason is that during the cascade process the anisotropy is reduced each time that an eddy breaks up into smaller pieces so that the dissipation scales in such flows are much more isotropic then the largest scales. This is a rather simplistic view and for a more profound discussion of the assumption of local isotropy we refer to the papers of Sreenivasan [6] and Sreenivasan and Antonia [7].

[2]Indeed, interactions transferring energy from small to large scales, i.e. backscatter, are not negligible. For turbulence in equilibrium the net flux of energy in the inertial range will however be from large to small scales.

Let us now write the evolution equation of $E(K)$:

$$\frac{\partial E(K)}{\partial t} = T^{NL}(K) - 2\nu K^2 E(K) \tag{1.17}$$

This equation can be derived starting from the Navier-Stokes equations in Fourier space. For details we refer to standard textbooks like Pope [3]. The molecular dissipation of kinetic energy for each wavenumber is represented by the last term. This term is an explicit function of the molecular viscosity ν and the energy spectrum. and can therefore be calculated without difficulty in spectral models. This in contrast to one-point modelling, where the dissipation equation is generally the weakness of the model. The total dissipation can be calculated by its integration:

$$\int_0^\infty 2\nu K^2 E(K) dK = \epsilon \tag{1.18}$$

The first term on the RHS of (1.17) is the non-linear transfer. This transfer involves the interaction of scales at different wavenumbers:

$$T^{NL}(K) = -2\pi i K_m \left(\delta_{il} - \frac{K_i K_l}{K^2}\right) K^2 \int_{\boldsymbol{K}=\boldsymbol{P}+\boldsymbol{Q}} \overline{u_l(\boldsymbol{P}) u_m(\boldsymbol{Q}) u_i(-\boldsymbol{K})} d\boldsymbol{P} d\boldsymbol{Q} \tag{1.19}$$

If we consider the fact that by definition the dissipation is the time derivative of the kinetic energy:

$$\frac{\partial k}{\partial t} = -\epsilon, \tag{1.20}$$

and considering equation (1.10) we find that the integral of the nonlinear transfer must be zero:

$$\int_0^\infty T^{NL}(K) dK = 0 \tag{1.21}$$

The nonlinear transfer represents in this scenario the role of the energy cascade from the kinetic energy reservoir at the small wavenumbers to the kinetic energy destruction at the large wavenumbers. It is therefore this terms that contains the dynamics of the interaction of the different length-scales in the inertial range. In fig. 1.1 we illustrate the foregoing. We show for a small[3] Reynolds on the left and a large on the right a sketch of the spectral behaviour. The two top figures show the energy spectra in *log-log* representation. The bottom figures show the nonlinear transfer terms and dissipation. Their values are multiplied by K to account for the deformation of the contributions by the log-linear representation. We observe that

[3] We call $R_\lambda = 30$ a small R_λ. This choice is rather arbitrary. To give an idea: a well resolved direct numerical simulation at a 128^3 wavenumber resolution would attain such a R_λ. $R_\lambda = 10^4$ is here called large because this is the typical value in atmospheric measurements.

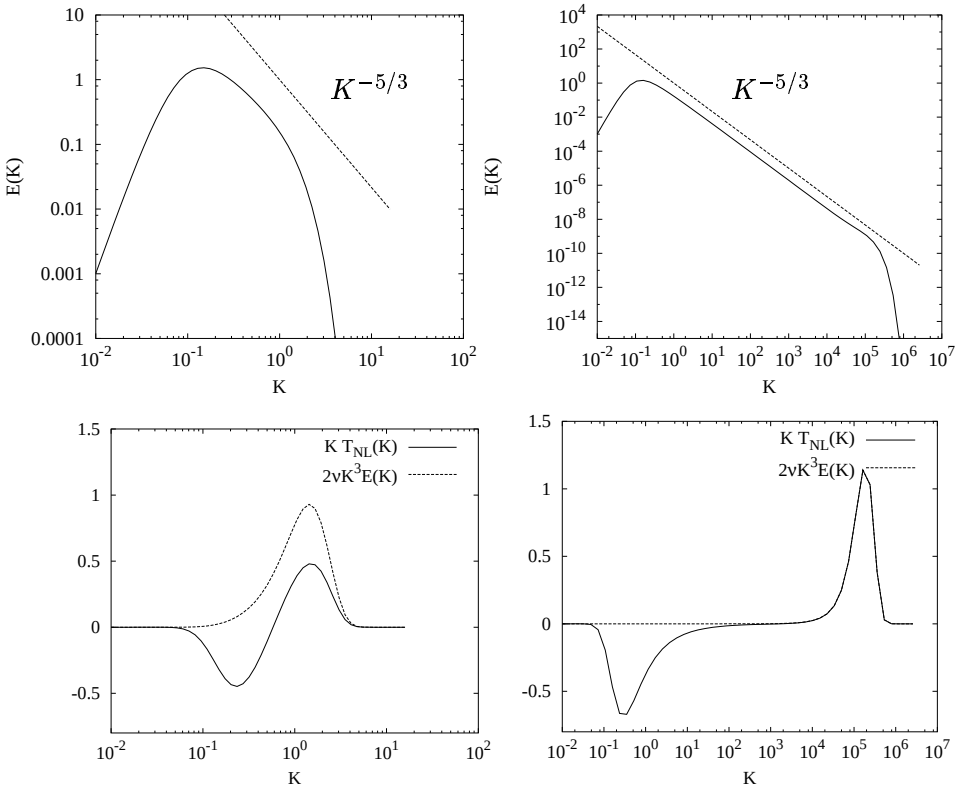

Figure 1.1: Typical spectra (top), nonlinear transfer and viscous dissipation (bottom) in isotropic turbulence at $R_\lambda = 30$ (left) and $R_\lambda = 10000$ (right). x and y scales are chosen arbitrarily.

the integral value of the transfer terms is zero in agreement with (1.21). The transfer is negative at the low wavenumbers and positive at the high wavenumbers: energy is taken from the large scales and transferred to the small scales where it is dissipated. For the large Reynolds number we see that the dissipation range is entirely located at the large wave numbers. In between the large and the small scales we observe a region that appears to be unaffected by the dissipation and the transfer. The energy entering this range is in equilibrium with the energy leaving it so that the net balance is zero. This is the inertial range, only passing energy from scale to scale. In this range (1.16) should apply. At low R_λ the dissipation is acting at all scales and the $K^{-5/3}$ zone is not observed.

1.1.3 Mixing of an isotropic passive scalar

The mixing of temperature or chemical species in a turbulent flow can also be described from a spectral point of view. We uniquely consider the case of small temperature fluctuations and species that not influence the flow field: we study in this work the passive scalar. Temperature fluctuations can be considered as passive scalar fluctuations as long as they are small enough. We will throughout this work only consider this case and the terms temperature and passive scalar will both be used to denote the same quantity. The evolution of a passive scalar T in a fluid is described by:

$$\frac{\partial T}{\partial t} + U_j \frac{\partial T}{\partial x_j} = \alpha \frac{\partial^2 T}{\partial x_j^2}, \tag{1.22}$$

with α the diffusivity of the scalar. We will decompose the passive scalar in a mean value Θ and a fluctuation θ:

$$T = \Theta + \theta \tag{1.23}$$

The mixing of a scalar is a process involving all the lengthscales described in the previous section. The large velocity scales mix the scalar by advection. The eventual molecular mixing or diffusion takes place in smaller scales. For a highly diffusive scalar the molecular mixing takes place in scales larger than the smallest velocity scales. For a scalar with a small diffusivity α, scalar structures even smaller than the Kolmogorov scale can be observed. The ratio of advective to diffusive effects at the large scales is proportional to the Péclet number:

$$Pe_{\mathcal{L}} = \frac{\mathcal{U}\mathcal{L}}{\alpha} \tag{1.24}$$

The relation between the size of the smallest eddies and the smallest scalar structures is a function of the the ratio of the Péclet and the Reynolds number. This ratio is called the Prandtl number:

$$Pr = \frac{\nu}{\alpha} \tag{1.25}$$

This number for heat in water at $20\,^{\circ}C$ is 7.01 and varies strongly with the temperature, for heat in air it is 0.71, almost independent of the ambient temperature. Like in the foregoing for the velocity field we can define a temperature variance spectrum. We start from the two point scalar fluctuations:

$$R_\theta(\boldsymbol{r},t) = \frac{1}{2}\overline{\theta(\boldsymbol{x})\theta(\boldsymbol{x}+\boldsymbol{r})} \tag{1.26}$$

and we can similarly take the Fourier transform:

$$\Phi_\theta(\boldsymbol{K}) = \frac{1}{2}FT_{/\boldsymbol{r}}\left[\overline{\theta(\boldsymbol{x})\theta(\boldsymbol{x}+\boldsymbol{r})}\right] \tag{1.27}$$

Again, we take advantage of isotropy to reduce this function of the wavevector $\boldsymbol{K}$ to a function of the wavenumber $K = \|\boldsymbol{K}\|$ by integrating over spherical shells. Hence we define the scalar spectrum:

$$E_\theta(K) = \int_{\Sigma(K)} \Phi_\theta(\boldsymbol{K}) d\Sigma(K) \tag{1.28}$$

In which $\Sigma(K)$ is a spherical shell with radius K. By definition the integral of the scalar spectrum is:

$$\int_0^\infty E_\theta(K)dK = \frac{1}{2}\overline{\theta}^2 \tag{1.29}$$

One can derive the equation for the scalar spectrum in isotropic turbulence. This equation resembles the equation for the energy spectrum:

$$\frac{\partial E_\theta(K)}{\partial t} = T_\theta^{NL}(K) - 2\alpha K^2 E_\theta(K) \tag{1.30}$$

and the molecular diffusion of scalar variance can be calculated:

$$\int_0^\infty 2\alpha K^2 E_\theta(K)dK = \epsilon_\theta \tag{1.31}$$

The analogies between the turbulent scalar and velocity are striking in some aspects. We can for example define an inertial range just like we did for the velocity field. Most of the scalar variance is contained in the largest scales and destroyed in the smallest scales. This incited Obukhov [8] and Corrsin [9] to extend Kolmogorov's idea to the scalar spectrum:

$$E_\theta(K) = C_{CO}\ \epsilon^{-1/3}\epsilon_\theta K^{-5/3} \tag{1.32}$$

The experimental value of the Corrsin-Obukhov constant C_{CO} shows considerable scatter but according to the work of Sreenivasan [10] the value of 0.4 is a good estimate.

The nonlinear transfer and diffusion behave similarly as in fig. 1.1. Using the analogy between the passive scalar and the velocity to describe the scalar is tempting but risky. The scalar equation does not contain the pressure and the scalar fluctuations are therefore governed by a pure advection-diffusion process.

The $K^{-5/3}$ scaling (1.32) is indeed observed in experiments, but seems to be dependent on the scale of injection (Warhaft and Lumley [11]). The way of generating the fluctuations is another parameter (Jayesh *et al.* [12]). Using the same grid to generate the turbulent velocity fluctuations and the scalar fluctuations by heating the rods, yields a $-5/3$ scaling at a relatively low Reynolds number, a value at which we would not expect it because proper scale separation is not fulfilled. Also the fluctuations generated by imposing a mean scalar gradient as discussed in the next section show this low Reynolds $-5/3$ scaling. In this case scale separation and local isotropy are both lacking. When the fluctuations are on the other hand introduced by use of heated wires, independent of the grid and therefore also independent of the generation of the velocity fluctuations, a much higher Reynolds is needed to observe the $-5/3$ scaling. This situation grows even worse if one considers scalar spectra in shear flows [6], but this issue will not be addressed until chapter 5.

We should mention here that the inertial range scaling is also dependent on the Prandtl number. Recent papers reporting the influence of the Prandtl number on the scalar spectrum are Yeung, Xu and Sreenivasan [13] and Brethouwer, Hunt and Nieuwstadt [14]. All through this dissertation the Prandtl number is assumed around unity.

1.2 Isotropic turbulence with a mean scalar gradient

A way to generate temperature fluctuations in an isotropic turbulence is by imposing a mean temperature gradient. This case was first considered by Corrsin [15] and experimentally by Wiskind [16]. The turbulent movements in the direction of the gradient will transport hot fluid towards a colder part and vice versa. This mechanism creates a turbulent heat flux in the direction opposite to the gradient[4] . This mechanism is illustrated in fig. 1.2. The scalar field ceases to be isotropic as the gradient imposes a preferential direction.

[4]If this gradient is positive, the scalar flux and the scalar flux spectrum are negative. In the first 4 chapters of this thesis, the gradient will be chosen negative in which case the production of scalar flux is positive so that scalar flux and scalar flux spectrum are positive.

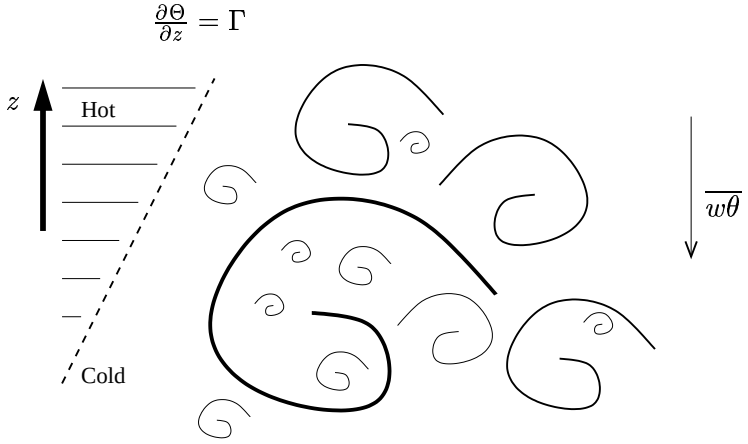

Figure 1.2: Sketch of the physical mechanism of turbulent scalar flux. The turbulent eddies transport cold fluid towards the hot part of the fluid and vice versa. This creates a mean turbulent flux $\overline{w\theta}$ of heat in the opposite direction of the gradient Γ.

1.2.1 The anisotropic scalar spectrum

The equation of the scalar variance contains now an extra term: the production by the scalar flux:

$$\frac{\partial \frac{1}{2}\overline{\theta}^2}{\partial t} = -\frac{\partial \Theta}{\partial x_i}\overline{u_i\theta} - \epsilon_\theta \tag{1.33}$$

or for the spectrum:

$$\frac{\partial E_\theta(K)}{\partial t} = -F_{u_i\theta}(K)\frac{\partial \Theta}{\partial x_i} + T_\theta^{NL}(K) - 2\alpha K^2 E_\theta(K) \tag{1.34}$$

Eddies of all different sizes contribute to this scalar flux: it is also a multi-scale phenomenon and introduces a new spectral quantity: the scalar flux spectrum.

1.2.2 The spectrum of the scalar flux

We choose the scalar gradient without loss of generality in the z-direction.The one-point scalar flux equation reads then:

$$\frac{\partial}{\partial t}\overline{w\theta} = -\frac{\partial \Theta}{\partial z}\overline{ww} - \frac{1}{\rho}\theta\overline{\frac{\partial p}{\partial z}} - (\nu+\alpha)\overline{\frac{\partial w}{\partial x_j}\frac{\partial \theta}{\partial x_j}} \tag{1.35}$$

To study the scalar flux spectrum we derive its equation starting from the two-point correlation:

$$R_{u_i\theta}(\boldsymbol{r}) = \overline{(u_i(\boldsymbol{x})\theta(\boldsymbol{x}+\boldsymbol{r})} \tag{1.36}$$

and we can take the Fourier transform:

$$\mathcal{F}_{u_i\theta}(\boldsymbol{K}) = FT_{/\boldsymbol{r}}\left[\overline{u_i(\boldsymbol{x})\theta(\boldsymbol{x}+\boldsymbol{r})}\right] \tag{1.37}$$

The scalar field is not isotropic. The spectrum is however axisymmetric around the gradient axis. Homogeneity, linearity of the scalar equation and incompressibility allow to describe $\mathcal{F}_{u_i\theta}(\boldsymbol{K})$ by one scalar function $F_{w\theta}(K)$ that we will call the scalar flux spectrum. The argument that we show here is due to Lumley [17].

Consider an isotropic turbulent velocity field on which we impose a uniform mean temperature gradient in an arbitrary direction $\partial\Theta/\partial x_j$. If we ignore the molecular diffusion, the equation for the scalar fluctuations is:

$$\frac{d\theta}{dt} + u_j\frac{\partial\Theta}{\partial x_j} = 0 \tag{1.38}$$

This equation can be solved to yield:

$$\theta(\boldsymbol{x},t) = -\frac{\partial\Theta}{\partial x_j}(x_j - s_j(\boldsymbol{x},t)) \tag{1.39}$$

with $s_j(\boldsymbol{x},t)$ the position of the fluid particle at $t=0$ that arrives at $\boldsymbol{x}$ at time t. We can subsequently write

$$\overline{\theta(\boldsymbol{x},t)u_i(\boldsymbol{x}',t)} = -\frac{\partial\Theta}{\partial x_j}\overline{(-s_j(\boldsymbol{x},t)u_i(\boldsymbol{x}',t))} \tag{1.40}$$

The two-point velocity scalar correlation can thus be written as a linear function of the scalar gradient and a second order tensor $a_{ij}(\boldsymbol{x},\boldsymbol{x}')$:

$$\overline{u_i(\boldsymbol{x})\theta(\boldsymbol{x}')} = -\frac{\partial\Theta}{\partial x_j}a_{ij}(\boldsymbol{x},\boldsymbol{x}') \tag{1.41}$$

We consider a homogeneous scalar and velocity fluctuation field so that the two point quantity depends only on its separation vector $\boldsymbol{r} = \boldsymbol{x}'-\boldsymbol{x}$:

$$\overline{u_i(x)\theta(x+\boldsymbol{r})} = -\frac{\partial\Theta}{\partial x_j}a_{ij}(\boldsymbol{r}) \tag{1.42}$$

and its equivalent in Fourier space:

$$\mathcal{F}_{u_i\theta}(\boldsymbol{K}) = -\frac{\partial\Theta}{\partial x_j}A_{ij}(\boldsymbol{K}) \tag{1.43}$$

with the tensor $A_{ij}(\mathbf{K})$ dependent uniquely on the velocity field. In isotropic turbulence, $A_{ij}(\mathbf{K},t)$ independent on the scalar gradient, is an isotropic quantity. Lumley states that this tensor must be an even

function of $\boldsymbol{r}$ and its general form is therefore (in an incompressible fluid):

$$\mathcal{F}_{u_i\theta}(\boldsymbol{K}) = -\frac{\partial\Theta}{\partial x_j} f(K,t)\left(\delta_{ij} - \frac{K_i K_j}{K^2}\right) \tag{1.44}$$

$\mathcal{F}_{u_i\theta}(\boldsymbol{K})$ can subsequently be written as an isotropic function multiplied by the scalar gradient. Choosing without loss of generality the scalar gradient in the z-direction and defining μ as the cosine of the angle between $\mathbf{K}$ and the scalar gradient:

$$\mathbf{K} \cdot e_3 \equiv K_3 = \mu K, \tag{1.45}$$

we can write:

$$\begin{aligned} \mathcal{F}_{w\theta}(\boldsymbol{K}) &= \mathcal{F}_{w\theta}(K,\mu) \\ &= -\frac{\partial\Theta}{\partial z}(1-\mu^2) f(K,t) \end{aligned} \tag{1.46}$$

This expression can be integrated over wavenumber shells to yield after proper normalization the function $F_{w\theta}(K)$ so that:

$$\int F_{w\theta}(K) dK = \overline{w\theta} \tag{1.47}$$

The effect of diffusivity was ignored in the previous derivation. The introduction of diffusivity is not expected to reintroduce angular dependence in the expression for $F_{w\theta}(K)$, the diffusion term being small, isotropic and non-negligible only at the largest wavenumbers. A formal proof of (1.46) using tensor-invariant theory for homogeneous axisymmetric tensors can be found in the papers of Batchelor [18] and Chandrasekhar [19]. This yields a more general expression in which the spherically averaged spectrum is still a function of μ. It is however shown in Herr *et al.* [20], that this angular dependence vanishes if it is absent in the initial conditions and they even claim that if it is present in the initial conditions it will decay if the production term in the equation of $F_{w\theta}(K,\mu)$ has no angular dependence, which is the case in isotropic turbulence.

The evolution equation of the scalar flux spectrum will be derived in detail in chapter 3. The equation reads schematically:

$$\frac{\partial}{\partial t} F_{w\theta}(K) + (\nu+\alpha)K^2 F_{w\theta}(K) = P(K) + T_{w\theta}^{NL}(K) + \Pi(K) \tag{1.48}$$

The second term on the left hand side is the molecular destruction term of scalar flux, with ν and α respectively the kinematic viscosity and molecular diffusion coefficient. $P(K)$ is the production by the mean gradient:

$$P(K) = -\frac{2}{3}\frac{\partial\Theta}{\partial x_j} E(K) \tag{1.49}$$

$\Pi(K)$ is the pressure term, corresponding to the spherically integrated value of $\Pi(\boldsymbol{K})$:

$$\Pi(\boldsymbol{K}) = FT_{/\boldsymbol{r}}\left(\frac{1}{\rho}\overline{\theta(\boldsymbol{x})\frac{\partial}{\partial z}p(\boldsymbol{x}+\boldsymbol{r})}\right), \tag{1.50}$$

$FT_{/\boldsymbol{r}}$ denoting a Fourier transform with respect to $\boldsymbol{r}$, ρ the density, p the fluctuating pressure, z the direction of the mean scalar gradient. The non-linear triple correlation term (or non-linear transfer), $T^{NL}_{w\theta}(K)$ is the spherically integrated value of $T^{NL}_{w\theta}(\boldsymbol{K})$:

$$\begin{aligned} T^{NL}_{w\theta}(\boldsymbol{K}) = iK_j\Big(FT_{/\boldsymbol{r}}\Big(&\overline{\theta(\boldsymbol{x})u_j(\boldsymbol{x})w(\boldsymbol{x}+\boldsymbol{r})} \\ &-\overline{\theta(\boldsymbol{x})u_j(\boldsymbol{x}+\boldsymbol{r})w(\boldsymbol{x}+\boldsymbol{r})}\Big)\Big) \end{aligned} \tag{1.51}$$

it can easily be seen by taking the value of $\boldsymbol{r} = 0$ that the integral value of $T^{NL}_{w\theta}(\boldsymbol{K})$ is zero. We note that we can divide this transfer into two contributions:

$$\begin{aligned} [T^{NL}_{w\theta}(\boldsymbol{K})]_\theta &= \quad iK_j\left(FT_{/\boldsymbol{r}}\left(\overline{\theta(\boldsymbol{x})u_j(\boldsymbol{x})w(\boldsymbol{x}+\boldsymbol{r})}\right)\right) \\ \left[T^{NL}_{w\theta}(\boldsymbol{K})\right]_U &= -iK_j\left(FT_{/\boldsymbol{r}}\left(\overline{\theta(\boldsymbol{x})u_j(\boldsymbol{x}+\boldsymbol{r})w(\boldsymbol{x}+\boldsymbol{r})}\right)\right) \end{aligned} \tag{1.52}$$

The first of these contributions stems from the advection term in the scalar equation, the second term from the nonlinear or convection term in the Navier-Stokes equations. We will need this distinction in chapter 3.

The molecular destruction of scalar flux can be calculated as:

$$\int_0^{K_\eta} (\nu+\alpha)K^2 F_{w\theta}(K)dK \tag{1.53}$$

with K_η the (Kolmogorov) cut-off frequency.

It is worth noting that, contrary to what happens in the equations for the energy and scalar spectrum, the pressure intervenes explicitly in the equation through the term $\Pi(K)$. This pressure term is a destructive term that acts at all wavenumbers. The spectral flux in the inertial range is therefore not constant, but decreases. We have a cascade that is leaking its spectral flux. We sketch the situation situation in figure 1.3.

It is generally believed that the small scale structure of a turbulent quantity is more isotropic than the large scales. The scalar flux is a purely anisotropic quantity and its spectrum is therefore expected to decrease faster than the scalar spectrum in the inertial range. A measure of the anisotropy at each lengthscale is given by the correlation spectrum:

$$\rho_{w\theta}(K) = \frac{F_{w\theta}(K)}{\sqrt{E(K)E_\theta(K)}} \tag{1.54}$$

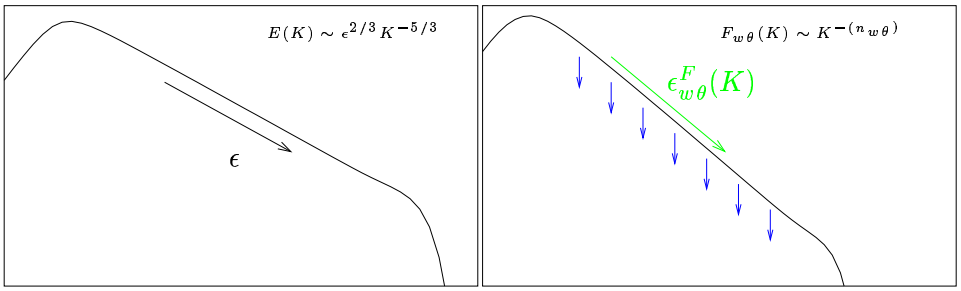

Figure 1.3: The kolmogorov spectral cascade of kinetic energy placed next to the 'leaking' cascade of scalar flux.

The slope of the $F_{w\theta}(K)$ spectrum is expected to be steeper than $K^{-5/3}$. If not the small scales would not be more isotropic than the large scales. An argument based on local isotropy to determine the slope of the scalar flux spectrum similar to a Kolmogorov or Obukhov argument does not work as the spectrum would be zero in an isotropic scalar field. The inertial range behaviour of the scalar flux spectrum will be investigated in the next chapter. We will first discuss three different methods of studying the scalar flux spectrum.

1.3 Simulations and analytical theory of scalar mixing

Three different approaches are used in this thesis to study scalar mixing: Direct Numerical Simulation, Large Eddy Simulation and two-point closures or analytical theory. Those methods are now briefly discussed.

1.3.1 Direct Numerical Simulation

In section 1.1 we discussed experimental difficulties in generating isotropic turbulence. Computers allow us nowadays to simulate perfectly isotropic turbulence. Direct Numerical Simulations (DNS) resolve the full range of turbulent lengthscales. The Navier-Stokes equations 1.1 are discretized and this discretized set of equations is solved. The simulations provide an abundance of information about all the different variables in a turbulent flow. DNS is often considered as the numerical equivalent of ideal real-life turbulence. However, one should be careful because the creation of the turbulent flow by forcing or by generating initial conditions may have a non negligible influence on the turbulent statistics. DNS is severely restricted in Reynolds number due to limits in computational resources. Results of DNS of isotropic

turbulence with a mean scalar gradient can be found in the next chapter.

1.3.2 Large Eddy Simulation

A second approach to study scalar mixing is Large Eddy Simulation (LES). In LES the large scales are numerically resolved but the small scales and the interaction between small and large scales are replaced by a so-called subgrid model. The concept of LES is based on the universal behaviour of the small scales in a turbulent flow. There is no Reynolds number limitation to LES but the computer power limits the range of scales that can be resolved. In general, we can not afford resolutions that resolve a large part of the inertial range before introducing the cut-off so that studying the inertial range by LES becomes a delicate job. LES will be discussed in detail in chapter 4, but results can already be found in section 2.5.

1.3.3 Analytical theory

Scalar mixing in isotropic turbulence

Next to DNS (limited in Reynolds number) and LES (limited in resolution), the third approach that is employed in this dissertation to study scalar mixing is a closure approach. We use the Eddy-Damped Quasi-Normal Markovian theory (EDQNM). The approach is based on an assumption of Gaussianity of the fourth order moments of turbulent quantities. The EDQNM theory is suitable to study wavenumber spectra of turbulent second order moments such as $E(K,t)$ (as prosed by Orszag [21]), $E_\theta(K,t)$ (Herring *et al.* [22], Vignon and Cambon [23]) and $F_{w\theta}(K,t)$ (Herr *et al.* [20]). Information is obtained about statistical averages: no information on instantaneous velocity and scalar fluctuations $u_i(\boldsymbol{x},t)$ and $\theta(\boldsymbol{x},t)$ can be obtained. The advantage of the method is that at the same time the approach has virtually no restriction in Reynolds number (calculations up to $R_\lambda = 10^7$ are performed in this work) and the whole wavenumber spectrum is resolved. The only limitations are the assumptions within the theory. This closure-theory will be presented and applied to the case of isotropic turbulence with a mean scalar gradient in chapter 3.

Fig. 1.4 shows an example of typical spectra of the scalar flux obtained with the three different methods. The picture shows in particular the attractivity of EDQNM, which gives information on the whole wavenumber spectrum at large Reynolds numbers.

Scalar mixing in homogeneous shear flow

The EDQNM closure was applied to homogeneously sheared turbulence in the works of Cambon *et al.* [24] and Bertoglio [25]. In chapter 5 the EDQNM closure will be applied to scalar mixing in homogeneous shear flow. In

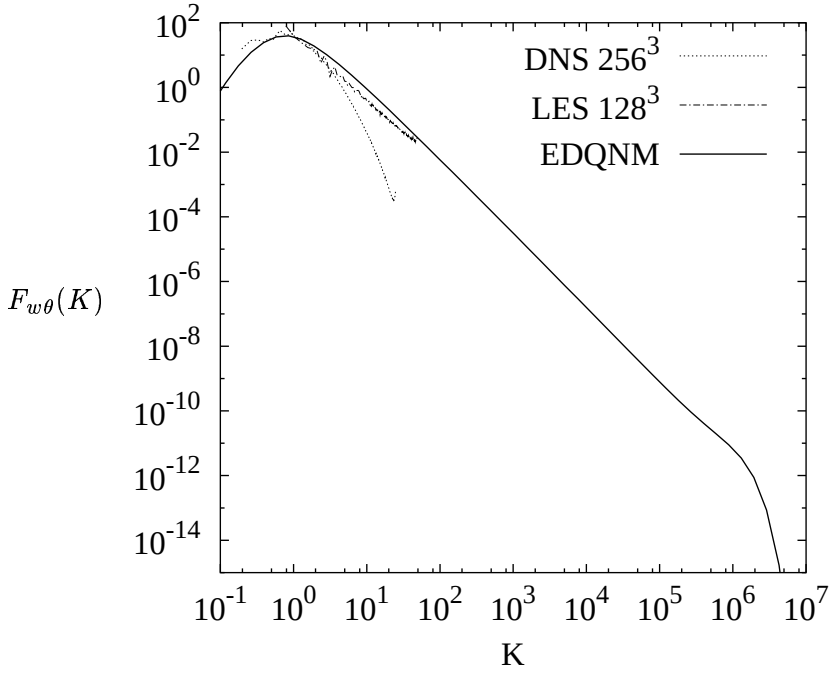

Figure 1.4: Typical LES (128^3) and DNS (256^3, $R_\lambda = 50$) spectra, compared to the result of an EDQNM calculation ($R_\lambda = 10^5$). The large wavenumber extent of EDQNM calculations explains its attractivity to study high Reynolds number flows

the presence of shear $\mathcal{F}_{u_i\theta}(\boldsymbol{K})$ and $\Phi_{ij}(\boldsymbol{K})$ can not be expressed exactly as a function of the wavenumber only. A full EDQNM approach of the problem would then require to build and numerically integrate a wavevector dependent closed set of equations. In order to simplify the numerical task that would result of this complete approach, we integrate the equation over spherical shells with radius K to obtain the variable:

$$F_{u_i\theta}(K,t) = \iint_{\Sigma k} \mathcal{F}_{u_i\theta}(\mathbf{K},t)dA(\mathbf{K}) \tag{1.55}$$

and for the spectral tensor as proposed by Cambon *et al.* [24]:

$$\varphi_{ij}(K,t) = \iint_{\Sigma k} \Phi_{ij}(\mathbf{K},t)dA(K) \tag{1.56}$$

The model for $\varphi_{ij}(K,t)$ can be found in Touil [1]. The triple correlations appearing in the evolution equation for $F_{u_i\theta}(K,t)$ are treated with the EDQNM model as discussed in chapter 3. Even though the closure was derived for isotropic turbulence we will use it here in the case of an anisotropic velocity field. The approach is not rigorous and has to be seen as an approximation.

Scalar mixing in inhomogeneous turbulence

The EDQNM equations for inhomogeneous turbulence can be found in the works of Menoret [26] and Burden [27]. Numerically exploitable equations were derived by Laporta [28] who derived the extension of the EDQNM theory to weakly inhomogeneous turbulence. Bertoglio and Jeandel [29] proposed to use the EDQNM closure in wall-bounded flows, introducing a infrared cut-off frequency to take into account the scale limitation of turbulent structures by the presence of walls. Parpais [30] implemented the equations derived by Laporta [28] and the approach of Bertoglio and Jeandel [29] in a finite element code. This model, the SCIT model for Simplified spectral Closure for Inhomogeneous Turbulence, is able to calculate complex flows and take into account the interactions between the different turbulent length scales by use of the EDQNM closure. The main variable of this SCIT-0 version is the variable $E(\boldsymbol{x},K,t)$. The anisotropic extension of this model, the SCIT-1 version, can be found in the PhD dissertation of Touil [1]. The variable in this work is $\varphi_{ij}(\boldsymbol{x},K,t)$. We propose in chapter 6 an extension of the model to inhomogeneous scalar mixing. This model is compatible with the full inhomogeneous SCIT-1 approach.

Chapter 2

On the behaviour of the velocity-scalar cross correlation spectrum in the inertial range

This chapter appeared as a publication in *Physics of fluids*. The sections 2.1 and 2.2 are rewritten for a better transition with the rest of the thesis. The reference of the original paper is: W. BOS, H. TOUIL, L. SHAO, J.-P. BERTOGLIO " On the behaviour of the velocity-scalar cross correlation spectrum in the inertial range", Phys. Fluids 16 (10), 2004.

2.1 Introduction

In section 1.2.2 the scalar flux spectrum was introduced. We also mentioned that the inertial range slope for high Reynolds numbers can not be determined by using an argument of local isotropy, because the scalar flux is a purely anisotropic quantity. Lumley [17, 31] suggested the scaling law:

$$F_{w\theta}(K) \sim \Gamma \epsilon^{1/3} K^{-7/3} \tag{2.1}$$

for the behaviour in the inertial range of the scalar flux spectrum at high Reynolds number. This analysis is based on an assumption that in the inertial range all spectral behaviour is governed by the quantities ϵ and K.

We will review experiments that measured the slope of $F_{w\theta}(K)$ in the next section. A $K^{-7/3}$ behaviour is found in two works reporting atmospheric measurements. In most of the high and moderate Reynolds number experiments the spectra are however more compatible with a -2 inertial range slope. This chapter is an attempt to clarify those observations and we will examine the possibility of an asymptotic K^{-2} inertial range.

We start in the following section with a short review of experimental data on the scalar flux spectrum. The terms in the equation for the scalar flux spectrum are studied in section 2.3 using direct numerical simulation (DNS). In section 2.4 we present a model based on the physics observed in our DNS and dimensional arguments. This model allows for both a -2 and $-7/3$ inertial range slope for the scalar flux. The Large Eddy Simulations in 2.5 support the K^{-2} scaling. We conclude this chapter consequently with a big question mark: is the scaling (2.1) wrong or should we rather suspect the Large Eddy Simulations?

2.2 Review of experimental data

In the early seventies the paper of Wyngaard and Coté [32] based on experiments in the atmospheric surface layer of Kaimal *et al.* [33], reports a $-7/3$ inertial slope and similar results are found in Kader and Yaglom [34]. Atmospheric measurements are however affected by external effects like shear and measurement filtering methods are subject of discussion (see for example Massman and Lee [35]). In the works of Feigenwinter *et al.* [36] and Korrman *et al.* [37] no distinction between a $K^{-7/3}$ or a K^{-2} spectral slope can be made. In the recent atmospheric experiment of Su *et al.* [38] a K^{-2} range clearly appears. Finally, we mention that a K^{-2} scaling was already proposed by Horst [39] to fit atmospheric data.

If we examine laboratory results, this K^{-2} is confirmed: in the grid-generated turbulence experiment of Mydlarski and Warhaft [40] (M&W), the spectrum of the scalar flux is found to be close to a K^{-2} scaling. As stated by the authors this behaviour can be suspected to be a low Reynolds

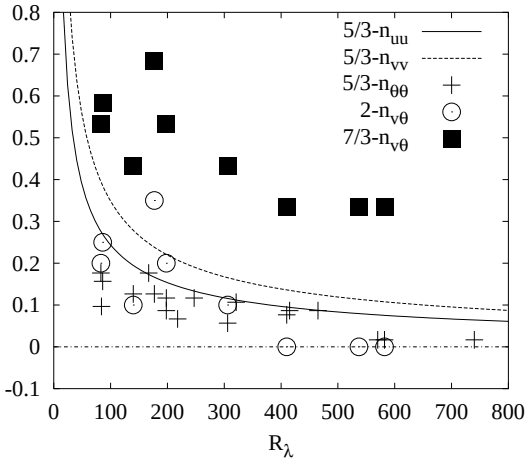

Figure 2.1: Behaviour of the spectral slope in the inertial range as a function of the Reynolds number. n_{uu}: slope of the $E_{11}(K_1)$ spectrum, n_{vv}: $E_{22}(K_1)$, from Mydlarski and Warhaft 1996; [43] $n_{\theta\theta}$: $E_\theta(K_1)$, $n_{v\theta}$: $F_{v\theta}(K_1)$ from Mydlarski and Warhaft 1998 [40].

number effect. It is however observed for values of R_λ up to 582, that is to say for Reynolds numbers high enough for the scalar spectrum $E_\theta(K)$ to show a $K^{-5/3}$ inertial range, and the longitudinal velocity spectrum having a $K_1^{-1.58}$ slope. In a recent paper Mydlarski [41] evaluated the structure function of the turbulent scalar flux $\langle \Delta u \Delta\theta \rangle(r)$. This function should behave as $r^{4/3}$ if the spectrum behaves as $K^{-7/3}$ in the inertial range. Mydlarski found $\langle \Delta u \Delta\theta \rangle(r) \sim r^{1.02}$ which provides support to a K^{-2} scaling for the spectrum, r^1 corresponding to K^{-2}. In a laboratory boundary layer experiment of Antonia and Smalley [42], the scalar flux spectrum shows a $K^{-1.80}$ spectral slope at a R_λ of 390.

To illustrate the evolution of the different spectra towards their asymptotic limits as observed by M&W, the slopes are plotted in Fig. 2.1 as functions of the Taylor-scale Reynolds number. The expected slope (e.g. $-5/3$ for the scalar spectrum) is substracted from the measured slope so that all presented quantities should tend to zero at high Reynolds number. For the scalar flux spectrum two different asymptotic slopes are attempted, $-7/3$ and -2. We observe that when $-7/3$ is used as an asymptote, the behaviour of the scalar flux spectrum is clearly different from that of the other spectra and that, when using -2 as an asymptote, all values are comparable.

2.3 Direct numerical simulation

The code used for the DNS is a classical pseudo-spectral code with a second order Runge-Kutta time integration scheme. The calculations are performed

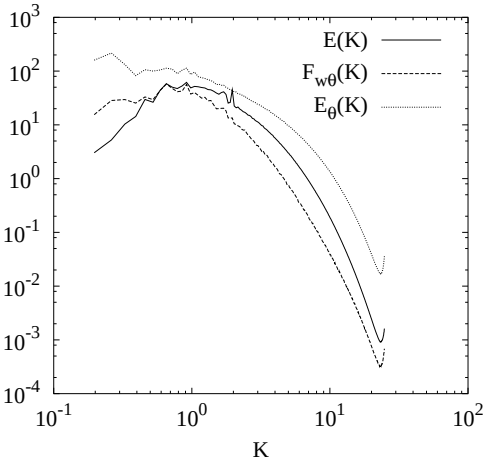

Figure 2.2: Kinetic energy, scalar flux and scalar variance spectra (DNS results), $R_\lambda = 50$, $Pr = 1$.

at a 256^3 resolution. Details about the method can be found in Zhou *et al.* [44]. The velocity field is maintained statistically stationary by forcing the large scales. A deterministic forcing is used (Deutsch. [45]) A constant mean scalar gradient Γ creates the scalar fluctuations. Results are analyzed once the energy and scalar spectra have reached their statistically steady states. The Reynolds number based on the Taylor micro-scale in this DNS is 50 and the Prandtl number is 1.

Figure 2.2 shows the kinetic energy, scalar variance and scalar flux spectra. $F_{w\theta}(K)$ is clearly steeper than $E(K)$, but the Reynolds number is too low to observe an inertial range.

We recall equation (1.48) for the scalar flux spectrum in isotropic turbulence with a mean scalar gradient:

$$\frac{\partial}{\partial t}F_{w\theta}(K) + (\nu+\alpha)K^2 F_{w\theta}(K) = P(K) + T_{w\theta}^{NL}(K) + \Pi(K) \qquad (2.2)$$

The production $P(K)$, dissipation $(\nu+\alpha)K^2F_{w\theta}(K)$, non-linear transfer term $T_{w\theta}^{NL}(K)$ and pressure term $\Pi(K)$ are plotted in Fig. 2.3 as a function of the wave-number. We note that:

- The dissipation is small compared to the production as observed in previous works, [46, 41] so it is essentially the pressure term that balances the production.

- The balance between pressure and production is not local in the spectrum: the production exceeds the pressure term at small wavenumbers, whereas the opposite is true at higher wavenumbers.

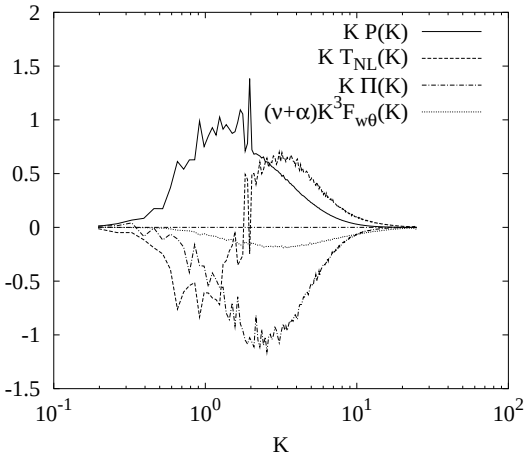

Figure 2.3: Spectra of the different contributions in the equation of the scalar flux (DNS results).

- This imbalance between production and pressure can be explained by the existence of a transfer term, that can also be observed in Fig. 2.3.
- At higher wavenumbers, the production is small compared to the pressure and a local balance between pressure and transfer is observed

Note that the values in the figures are normalized by the maximum value (peaks being ignored) of the production term.

2.4 Dimensional arguments and scaling

In this section we consider the case of high Reynolds number and assume the *Kolmogorov [4]* and *Corrsin-Obukhov [9, 8]* spectra for the kinetic energy and scalar variance:

$$E(K) = C_K \epsilon^{2/3} K^{-5/3} \tag{2.3a}$$

$$E_\theta(K) = C_{CO} \epsilon^{-1/3} \epsilon_\theta K^{-5/3} \tag{2.3b}$$

with ϵ_θ the dissipation of scalar fluctuations, C_K, C_{CO} being constants. The analysis could be improved, adding a K^4 zone at the small wavenumbers and taking into account the rounding of the spectra in the vicinity of the wavenumber where the spectra attain their maxima, but this would not affect the resulting scaling expressions.

2.4.1 Inertial scaling of the scalar flux spectrum

Lumley [31] proposed that the turbulent scalar flux spectrum in isotropic turbulence with a mean scalar gradient in the inertial range should depend

on the variables ϵ, the local flux of kinetic energy (equal to the viscous dissipation in the limit of infinite Reynolds number), Γ, the mean scalar gradient and the wavenumber K:

$$F_{w\theta}(K) = f(\Gamma, \epsilon, K) \tag{2.4}$$

A dimensional analysis then leads to the expression:

$$F_{w\theta}(K) \sim \Gamma \epsilon^{1/3} K^{-7/3} \tag{2.5}$$

If, instead of Γ, a spectral flux of $F_{w\theta}(K)$, $\epsilon^F_{w\theta}(K)$, is introduced in the analysis,

$$F_{w\theta}(K) \sim f(\epsilon^F_{w\theta}(K), \epsilon, K) \tag{2.6}$$

a different scaling is obtained:

$$F_{w\theta}(K) = C_F \epsilon^F_{w\theta}(K) \epsilon^{-1/3} K^{-5/3} \tag{2.7}$$

with C_F a constant. It can be noticed that (2.7) is similar to the Corrsin-Obukhov scaling for $E_\theta(K)$ (2.3b), in which $\epsilon^F_{w\theta}(K)$ replaces ϵ_θ. The flux $\epsilon^F_{w\theta}(K)$ is a quantity that is associated with the non-linear transfer term $T^{NL}_{w\theta}(K)$. It is not conserved in the cascade (unlike ϵ_θ that is conserved in the inertial range), $F_{w\theta}(K)$ being destroyed by the pressure effect. We suppose that the flux follows a power-law dependence with K:

$$\epsilon^F_{w\theta}(K) = f_\epsilon K^{-\gamma} \tag{2.8}$$

with f_ϵ independent of K. This yields:

$$F_{w\theta}(K) = C_F f_\epsilon \epsilon^{-1/3} K^{-(5/3+\gamma)} \tag{2.9}$$

To express f_ϵ, (2.9) is integrated over K assuming an inertial range extending from K_0 to infinity:

$$\begin{aligned} \overline{w\theta} = \int_{K_0}^{\infty} F_{w\theta}(K) dK &= \frac{C_F}{2/3+\gamma} f_\epsilon \epsilon^{-1/3} K_0^{-(2/3+\gamma)} \\ &\sim f_\epsilon \epsilon^{-(1+\gamma)} \overline{u^2}^{(1+3\gamma/2)} \end{aligned} \tag{2.10}$$

Introducing the correlation coefficient $\rho_{w\theta}$ leads to:

$$\overline{w\theta} = \rho_{w\theta} \sqrt{\overline{u^2}} \sqrt{\overline{\theta^2}} \tag{2.11}$$

Evaluating $\overline{u^2}$ and $\overline{\theta^2}$ by integration of (2.3a) and (2.3b) and using an assumption of proportionality between production and dissipation to express ϵ_θ:

$$\epsilon_\theta \sim \Gamma \overline{w\theta} \tag{2.12}$$

lead to:

$$\overline{w\theta} \sim \rho_{w\theta}^2 \Gamma \overline{u^2}^2 \epsilon^{-1} \tag{2.13}$$

Using (2.10) and (2.13) we can express equation (2.9) as:

$$F_{w\theta}(K) \sim \rho_{w\theta}^2 \Gamma \overline{u^2}^{(1-3\gamma/2)} \epsilon^{\gamma-1/3} K^{-(5/3+\gamma)} \tag{2.14}$$

Note that the proportionality between production and destruction of temperature fluctuations (2.12) has been observed experimentally by Sirivat and Warhaft [47] as well as in LES by Chasnov [48], and that $\rho_{w\theta}$ is known to tend to an asymptotic value of approximately 0.7 (Sirivat and Warhaft [47] and Budwig *et al.* [49]).

The value of γ is still to be determined, $\gamma = 2/3$ leading to Lumley's original scaling.

2.4.2 The non-linear interaction in the inertial range

To understand the physics behind γ, one has to investigate the balance of the different terms in equation (1.48). We will neglect the instationary term in the inertial range. The flux $\epsilon_{w\theta}^F(K)$ is supposed to be a function of the parameters governing the non-linear transfer, ϵ, K and $F_{w\theta}(K)$. Classical reasoning allows to give a crude estimation for the non linear transfer:

$$T_{w\theta}^{NL}(K) \sim \frac{\partial}{\partial K} g(\epsilon, K, F_{w\theta}(K)) \tag{2.15}$$

Dimensional analysis gives:

$$T_{w\theta}^{NL}(K) = -A_T \frac{\partial}{\partial K} \left[\epsilon^{1/3} K^{5/3} F_{w\theta}(K) \right] \tag{2.16}$$

or in the inertial range:

$$T_{w\theta}^{NL}(K) = \gamma A_T \epsilon^{1/3} K^{2/3} F_{w\theta}(K) \tag{2.17}$$

Using a Rotta-like hypothesis, we assume the pressure term $\Pi(K)$ to be proportional to the inverse of a local time-scale $\tau(K)$ and to $F_{w\theta}(K)$ [50]:

$$\Pi(K) \sim -\frac{1}{\tau(K)} F_{w\theta}(K) \tag{2.18}$$

Taking a time-scale built on the spectral energy flux ϵ and the wave-vector:

$$\tau(K) \sim \epsilon^{-1/3} K^{-2/3} \tag{2.19}$$

it is found:

$$\Pi(K) = -A_\Pi \, \epsilon^{1/3} K^{2/3} F_{w\theta}(K) \tag{2.20}$$

We can proceed by supposing the molecular dissipation sufficiently small compared to the pressure destruction at high Reynolds numbers. The non-linear transfer has a zero integral value, so that:

$$\int_{K_0}^{K_\eta} \Pi(K)dK = -\int_{K_0}^{K_\eta} P(K)dK \tag{2.21}$$

The production is equal to:

$$\int_{K_0}^{K_\eta} P(K)dK = \Gamma\overline{u^2} \tag{2.22}$$

which determines A_Π.

If we furthermore assume that in the inertial range there is a local balance between pressure and non-linear transfer as observed in the DNS, we obtain:

$$A_T = A_\Pi \gamma^{-1} \tag{2.23}$$

so that there is only one free parameter in the model: γ. Writing the sum of transfer and pressure and using (2.23) give:

$$T_{w\theta}^{NL}(K) + \Pi(K) = A_T \epsilon^{1/3} K^{-\gamma} \frac{\partial}{\partial K}\left[K^{5/3+\gamma} F_{w\theta}(K)\right] \tag{2.24}$$

which is the model of the global effect of the triple correlations. We observe that this term is zero for a $K^{-(5/3+\gamma)}$ inertial range.

The value $\gamma = 0$ corresponds to the limiting case where the flux $\epsilon_{w\theta}^F(K)$ would be constant in the cascade which is excluded by the presence of the pressure term. Negative γ would even correspond to a flux increasing with K and are also excluded. The case $\gamma = 2/3$, corresponding to Lumley's scaling appears as the other limit. $F_{w\theta}(K)$ then reads:

$$\gamma = 2/3 \quad \rightarrow \quad F_{w\theta}(K) \sim \rho_{w\theta}^2 \Gamma \epsilon^{1/3} K^{-7/3} \tag{2.25}$$

In this case production and pressure terms decay in the inertial range with the same exponent: $-5/3$. Larger γ are excluded because production would then be compensated nor by transfer neither by pressure[1]. It is thus plausible that γ belongs to the interval $]0, 2/3]$. $\gamma = 1/3$ is within this interval and in this case we have:

$$\gamma = 1/3 \quad \rightarrow \quad F_{w\theta}(K) \sim \rho_{w\theta}^2 \Gamma \mathcal{U} K^{-2} \tag{2.28}$$

[1]This situation is observed at small Pr: in the large wavenumber region of the inertial range the molecular destruction becomes dominant compared to the nonlinear interaction. A local balance between the production and the molecular destruction,

$$(\nu + \alpha)K^2 F_{w\theta}(K) = \frac{2}{3}\Gamma E(K), \tag{2.26}$$

and expression (2.3a) yields then a $K^{-11/3}$ wavenumber dependence:

$$F_{w\theta}(K) = \frac{2}{3}(\nu + \alpha)^{-1} C_K \Gamma \epsilon^{2/3} K^{-11/3}. \tag{2.27}$$

This behaviour is observed in a recent paper of O'Gorman and Pullin [51].

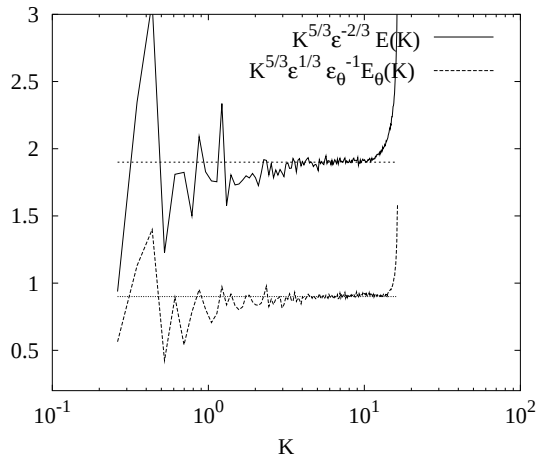

Figure 2.4: Compensated Energy and Scalar Variance spectrum, LES results.

2.5 Large eddy simulation

Laboratory experiments and DNS calculations are restricted to relatively low Reynolds numbers, whereas atmospheric experiments are subjected to large measurement and filtering errors and secondary effects. For this reason Large Eddy Simulations (LES) were performed. LES should provide indications on the value of γ and thus on the asymptotic slope of the scalar flux spectrum.

The code used for the LES is the same as described in section 2.3. The calculations were performed at a 128^3 resolution. The subgrid model is the Chollet and Lesieur eddy viscosity model [52] for the velocity field. To model the subgrid scalar field, a constant subgrid Prandtl number is assumed: $Pr_T = 0.6$.

We show in Fig. 2.4 the compensated kinetic energy and scalar variance spectrum. The spectra are compensated according to the Kolmogorov and Corrsin-Obukhov scaling laws (2.3a) and (2.3b) and good agreement with the theory is observed. The Kolmogorov constant in our calculation is 1.9, the Corrsin-Obukhov constant 0.9. This last value is slightly high but in perfect agreement with previous LES using a constant turbulent Prandtl number (see Lesieur and Rogallo [53]). In Fig. 2.5 we show the scalar flux spectrum. In Fig. 2.6 we show the same spectrum in compensated form. The scalar flux spectrum is compensated according to the scaling relations (2.25) and (2.28). In both figures the K^{-2} slope of the scalar flux spectrum is clear.

Figure 2.7 shows the compensated spectrum of the pressure term $\Pi(K)$. Equation (2.20) predicts that a $\gamma = 1/3$ corresponds to a $K^{-4/3}$ slope of the

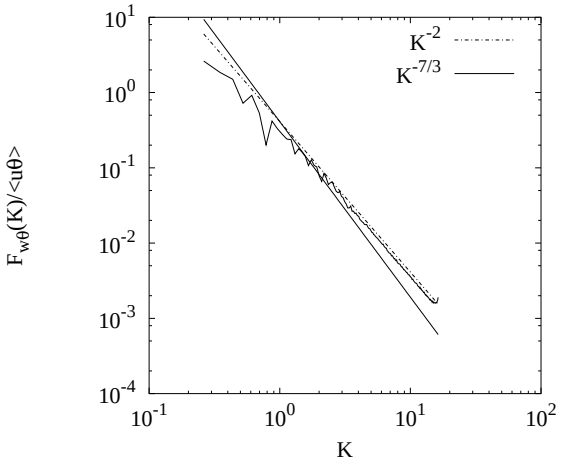

Figure 2.5: Scalar Flux spectrum, LES results.

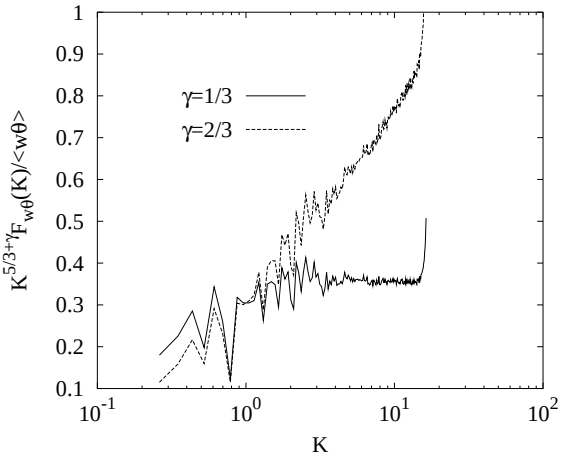

Figure 2.6: Compensated Scalar Flux spectrum, LES results.

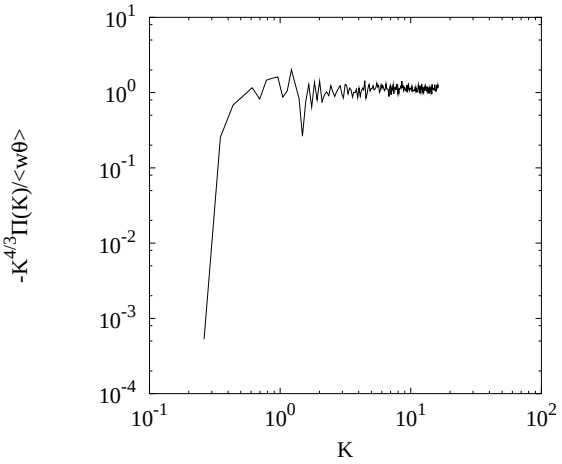

Figure 2.7: Spectrum of the pressure term in the equation of the scalar flux compensated with $K^{4/3}$ (LES results).

pressure term. This $K^{-4/3}$ slope for the pressure term is clearly observed.

2.6 Conclusion

DNS shows the existence of a spectral range in which $F_{w\theta}(K)$ is not produced by the production by the mean gradient, but by the non linear interaction. This observation provides support to a cascade type of analysis. When a spectral flux of scalar flux, $\epsilon^F_{w\theta}(K)$, is introduced, dimensional analysis yields an inertial range slope for $F_{w\theta}(K)$ dependent on a parameter γ that reflects the evolution of the spectral flux in the cascade of $F_{w\theta}(K)$. The asymptotic spectrum obtained allows for a slope between $K^{-5/3}$ and $K^{-7/3}$.

Our Large eddy simulations show a clear K^{-2} scaling for the scalar flux spectrum, and also confirm the related $K^{-4/3}$ scaling of the pressure term. We stress however that although in our LES the value of γ is clearly much more likely to be 1/3 than 2/3, the present analysis does not exclude the possibility of a $K^{-7/3}$ spectrum.

It has to be noticed that the EDQNM equations in the presence of a mean scalar gradient have been derived by Herr et al. [20, 54] Comparisons with the present analysis would constitute an interesting direction for future work[2].

We would like to thank Professor G.X. Cui and Professor Z.S. Zhang of the Department of Engineering Mechanics, Tsinghua University, Beijing, for providing the DNS results used in this work.

[2]This will be the subject of the next chapter

Chapter 3

The Eddy-Damped Quasi-Normal Markovian Theory

In the previous chapter we showed that LES, DNS and dimensional analysis give no definite answer to the question: what is the slope of the inertial range of the scalar flux spectrum? Spectral closures such as the Eddy-Damped Quasi-Normal Markovianized (EDQNM) theory are adequate tools to examine triadic interactions between wavevectors and therefore contribute to the understanding of the behaviour of spectra of turbulent quantities.

The EDQNM theory was formalized by Orszag [21] for the kinetic energy spectrum and applied to an isotropic scalar by Herring *et al.* [22] (see also Vignon and Cambon [23, 55]). We refer to Lesieur [56] for an extensive discussion of the EDQNM theory for the isotropic energy spectrum $E(K)$ and the isotropic scalar spectrum $E_\theta(K)$. More recently this closure was extended to the scalar flux spectrum by Herr [20] (see also the papers of Nakauchi and Sega [57], Ulitsky *et al.* [54, 58]). We will discuss this derivation and rewrite it in detail in section 3.1. For these readers who are not interested in the details of the derivation, we refer to section 3.1.1 for an overview of the derivation and section 3.1.7 in which we show the final equation.

In section 3.3 it will be shown that the two model constants involving the Eddy Damping can be determined in another way than proposed in previous works. This choice is not the same as the choice in the papers mentioned before [20, 54, 58]. In this same section we discuss the influence of the mean scalar gradient on the non-linear interactions.

In section 3.4 we will analyze the results of EDQNM calculations in a broad range of Reynolds numbers. We will focus on inertial and dissipation range statistics because spectral closures are particularly well suited to study

this part of the spectrum: the dissipation is calculated exactly and the triadic interaction is present to give meaningful inertial range behaviour. Those results are unattainable by LES, because they are not or only partly resolved, and restricted to low Reynolds numbers in DNS.

3.1 Derivation of the EDQNM equations

3.1.1 Overview

In this section the evolution-equation for the scalar-velocity cross-correlation spectrum is derived and closed by the EDQNM theory. We consider an isotropic, incompressible, turbulent velocity field. The passive scalar fluctuations are generated by a mean scalar gradient, resulting in an axisymmetric distribution of scalar fluctuations. Starting from the Fourier representation of the equations of the scalar and velocity fluctuations, we will derive the equation of the velocity-scalar cross-correlation. Schematically this equation reads:

$$\left[\frac{\partial}{\partial t} + (\nu+\alpha)K^2\right]\overline{u\theta} = f(\overline{uu\theta}) - \Gamma\overline{uu} \tag{3.1}$$

This is the same equation as (1.48). On the left-hand side we see the time derivative and the viscous dissipation and diffusion. The pressure term and non-linear transfer term in equation (1.48) are here gathered in the triple correlation term $\overline{uu\theta}$ and the last term is the production term. The triple correlations are the unclosed term. To close them, we write in section 3.1.3 the equation for those triple correlations:

$$\left[\frac{\partial}{\partial t} + (\nu+\alpha)K^2\right]\overline{uu\theta} = f_2(\overline{uuu\theta}) - \Gamma\overline{uuu} \tag{3.2}$$

This equation introduces quadruple correlations $\overline{uuu\theta}$ and triple correlations $\overline{uuu}$. The quadruple correlations will be closed by assuming that the turbulent and scalar field are close to a Gaussian state. Gaussian fourth-order moments can be expressed as a sum of products of second order moments:

$$\overline{uuu\theta} \rightarrow \sum \overline{uu}\ \overline{u\theta} \tag{3.3}$$

As a result of the absence of the fourth order cumulants, the triple correlations are only damped by viscous forces. The non linear damping caused by the interaction amongst turbulent scales that has thus been removed can be modeled by adding an eddy damping $\mu(K)$ to the equation.

$$\left[\frac{\partial}{\partial t} + (\nu+\alpha)K^2 + \mu(K)\right]\overline{uu\theta} = \sum \overline{uu}\ \overline{u\theta} - \Gamma\overline{uuu} \tag{3.4}$$

This differential equation can simply be solved yielding a solution, depending on the entire history of the triple correlations:

$$\overline{uu\theta} = \int_0^t G(\tau) \left[\sum \overline{uu}\ \overline{u\theta}(\tau) - \Gamma \overline{uuu}(\tau) \right] d\tau \tag{3.5}$$

with

$$G(\tau) = exp\left[- \int (\nu + \alpha) K^2 + \mu(K, \tau) d\tau \right] \tag{3.6}$$

The process of Markovianization, assuming the characteristic time scale of G small compared to the time scale of the correlations $\overline{uu}$ and $\overline{u\theta}$, allows a substantial simplification. If, in addition, the time variation of the eddy damping is neglected, the solution reads:

$$\overline{uu\theta} = \Theta(t) \left[\sum \overline{uu}\ \overline{u\theta}(t) - \Gamma \overline{uuu}(t) \right] \tag{3.7}$$

with

$$\Theta(t) = \int G(\tau) d\tau. \tag{3.8}$$

Equation (3.7) still contains triple correlations $\overline{uuu}$, that will be treated in section 3.1.4 in exactly the same manner as the triple correlations $\overline{uu\theta}$. Those terms, containing the mean gradient, cause difficulties in the Markovianization step and a common practice is to neglect those terms (this is the EDQNM1 approach). Taking into account the effect of those terms is called EDQNM2. This subject will be treated in detail in section 3.3.4.

Applying the quasi normal assumption, eddy damping and Markovianization to the velocity correlations gives:

$$\overline{uuu} = \Theta^u(t) \sum \overline{uu}\ \overline{uu}(t) \tag{3.9}$$

We use this expression in equation (3.7) to obtain a closed expression for the triple correlations $\overline{uu\theta}$:

$$\overline{uu\theta} = \Theta(t) \left[\sum \overline{uu}\ \overline{u\theta}(t) - \Gamma \Theta^u(t) \sum \overline{uu}\ \overline{uu}(t) \right] \tag{3.10}$$

this expression is used to close (3.1) in section 3.1.5. As mentioned before, the triple correlations $\overline{uu\theta}$ contain the contributions of non-linear transfer and pressure. If one wants to investigate those terms separately, one needs to identify their individual contributions. This is done in section 3.1.6.

3.1.2 Two point correlation between the velocity and the scalar fluctuation

We write the spectral formulation of the Navier-Stokes and scalar fluctuation equation for incompressible isotropic turbulence with a passive scalar gradient Γ in the z-direction:

$$\left[\frac{\partial}{\partial t}+\nu K^2\right]\hat{u}_k(\mathbf{K},t) = -iK_a P_{kj}(\mathbf{K})\int_{\mathbf{K}=\mathbf{P}+\mathbf{Q}}\hat{u}_j(\mathbf{P},t)\hat{u}_a(\mathbf{Q},t)d\mathbf{P} \quad (3.11)$$

and

$$\left[\frac{\partial}{\partial t}+\alpha M^2\right]\hat{\theta}(\mathbf{M},t) = -iM_a\int_{\mathbf{M}=\mathbf{P}+\mathbf{Q}}\hat{u}_a(\mathbf{P},t)\hat{\theta}(\mathbf{Q},t)d\mathbf{P} - \hat{u}_3(\mathbf{M},t)\Gamma \quad (3.12)$$

in which we use the projection operator $P_{ij}(\mathbf{K}) = \delta_{ij} - K_iK_j/(K^2)$. In the following we will omit the time dependence but one should keep in mind that every quantity involving a scalar or velocity fluctuation is a function of time. We multiply the first equation by $\hat{\theta}(\mathbf{M})$, the second by $\hat{u}_k(\mathbf{K})$, sum and average, to obtain:

$$\begin{aligned}\left[\frac{\partial}{\partial t}+\nu K^2+\alpha M^2\right]\overline{\hat{u}_k(\mathbf{K})\hat{\theta}(\mathbf{M})} = &-\frac{i}{2}P_{kaj}(\mathbf{K})\int_{\mathbf{K}=\mathbf{P}+\mathbf{Q}}\overline{\hat{u}_j(\mathbf{P})\hat{u}_a(\mathbf{Q})\hat{\theta}(\mathbf{M})}d\mathbf{P}\\ &-iM_a\int_{\mathbf{M}=\mathbf{P}+\mathbf{Q}}\overline{\hat{u}_a(\mathbf{P})\hat{\theta}(\mathbf{Q})\hat{u}_k(\mathbf{K})}d\mathbf{P}\\ &-\overline{\hat{u}_3(\mathbf{M})\hat{u}_k(\mathbf{K})}\Gamma\end{aligned} \quad (3.13)$$

in which we used the symmetry property that

$$-iK_aP_{kj}(\mathbf{K})\int_{\mathbf{K}=\mathbf{P}+\mathbf{Q}}\hat{u}_j(\mathbf{P})\hat{u}_a(\mathbf{Q})d\mathbf{P} = -\frac{i}{2}P_{kaj}(\mathbf{K})\int_{\mathbf{K}=\mathbf{P}+\mathbf{Q}}\hat{u}_j(\mathbf{P})\hat{u}_a(\mathbf{Q})d\mathbf{P} \quad (3.14)$$

with $P_{ijk}(\mathbf{K}) = K_jP_{ik}(\mathbf{K}) + K_kP_{ij}(\mathbf{K})$. In homogeneous turbulence the velocity correlation $\overline{\hat{u}_i(\mathbf{M})\hat{u}_k(\mathbf{K})}$ can be rewritten as:

$$\overline{\hat{u}_i(\mathbf{M})\hat{u}_j(\mathbf{K})} = \Phi_{ij}(\mathbf{K})\delta(\mathbf{K}+\mathbf{M}) \quad (3.15)$$

with $\Phi_{ij}(\mathbf{K})$ the spectral tensor. If, in addition, the turbulent velocity field is incompressible and isotropic one can express the spectral tensor as a function of the kinetic energy spectrum:

$$\Phi_{ij}(\mathbf{K}) = P_{kj}(\mathbf{K})\frac{E(K)}{4\pi K^2} \quad (3.16)$$

Homogeneity, incompressibility and axisymmetry allow similarly to express $\overline{\hat{u}_k(\mathbf{K})\hat{\theta}(\mathbf{M})}$ as a function of the scalar flux spectrum. We showed the argument in section 1.2.2. Similar arguments can be found in [54] or O'Gorman & Pullin [59].

As in equation (1.43) we can write:

$$\overline{\hat{u}_k(\mathbf{K},t)\hat{\theta}(\mathbf{M},t)} = -\frac{\partial\Theta}{\partial x_j}A_{ij}(\mathbf{K},t)\delta(\mathbf{K}+\mathbf{M}) \tag{3.17}$$

with the tensor $A_{ij}(\mathbf{K},t)$ dependent uniquely on the velocity field. In isotropic turbulence, $A_{ij}(\mathbf{K},t)$ independent on the scalar gradient, is an isotropic quantity and its general form is therefore (in an incompressible fluid):

$$\overline{\hat{u}_k(\mathbf{K},t)\hat{\theta}(\mathbf{M},t)} = -\frac{\partial\Theta}{\partial x_j}f(K,t)P_{ij}(\mathbf{K})\delta(\mathbf{K}+\mathbf{M}) \tag{3.18}$$

Normalizing the function $f(K,t)$ and choosing the scalar gradient in the z-direction:

$$\overline{\hat{u}_k(\mathbf{K})\hat{\theta}(\mathbf{M})} = \frac{3}{2}P_{k3}(\mathbf{K})\frac{F(K)}{4\pi K^2}\delta(\mathbf{K}+\mathbf{M}) \tag{3.19}$$

Substituting identities (3.19) and (3.16) into equation (3.13):

$$\begin{aligned}\left[\frac{\partial}{\partial t}+\nu K^2+\alpha M^2\right]P_{k3}(\mathbf{K})\frac{F(K)}{4\pi K^2}\delta(\mathbf{K}+\mathbf{M}) = \\ -\frac{i}{2}P_{kaj}(\mathbf{K})\frac{2}{3}\int_{\mathbf{K}=\mathbf{P}+\mathbf{Q}}\overline{\hat{u}_j(\mathbf{P})\hat{u}_a(\mathbf{Q})\hat{\theta}(\mathbf{M})}d\mathbf{P} \\ -iM_a\frac{2}{3}\int_{\mathbf{M}=\mathbf{P}+\mathbf{Q}}\overline{\hat{u}_a(\mathbf{P})\hat{\theta}(\mathbf{Q})\hat{u}_k(\mathbf{K})}d\mathbf{P} \\ -\frac{2}{3}P_{k3}(\mathbf{K})\frac{E(K)}{4\pi K^2}\delta(\mathbf{K}+\mathbf{M})\Gamma\end{aligned} \tag{3.20}$$

Multiplying both sides by $P_{k3}(\mathbf{K})$ and taking $\mathbf{M}=-\mathbf{K}$

$$\begin{aligned}\left[\frac{\partial}{\partial t}+\nu K^2+\alpha K^2\right]P_{k3}(\mathbf{K})P_{k3}(\mathbf{K})\frac{F(K)}{4\pi K^2} = \\ -\frac{i}{2}P_{kaj}(\mathbf{K})P_{k3}(\mathbf{K})\frac{2}{3}\int_{\mathbf{K}=\mathbf{P}+\mathbf{Q}}\overline{\hat{u}_j(\mathbf{P})\hat{u}_a(\mathbf{Q})\hat{\theta}(-\mathbf{K})}d\mathbf{P} \\ +iK_aP_{k3}(\mathbf{K})\frac{2}{3}\int_{-\mathbf{K}=\mathbf{P}+\mathbf{Q}}\overline{\hat{u}_a(\mathbf{P})\hat{\theta}(\mathbf{Q})\hat{u}_k(\mathbf{K})}d\mathbf{P} \\ -\frac{2}{3}P_{k3}(\mathbf{K})P_{k3}(\mathbf{K})\frac{E(K)}{4\pi K^2}\Gamma\end{aligned} \tag{3.21}$$

We define μ as the cosine of the angle between $\mathbf{K}$ and the scalar gradient:

$$\mathbf{K}\cdot e_3 = \mu K \tag{3.22}$$

We note that $P_{k3}(\mathbf{K})P_{k3}(\mathbf{K}) = 1-\mu^2$ and $P_{i3}(\mathbf{K})P_{ijk}(\mathbf{K}) = P_{3jk}(\mathbf{K})$ and write:

$$\begin{aligned}\left[\frac{\partial}{\partial t}+(\nu+\alpha)K^2\right]F(K)+\frac{2}{3}E(K)\Gamma = \\ \frac{8i\pi K^2}{3(1-\mu^2)}\left[\frac{1}{2}P_{3aj}(-\mathbf{K})\int_{\mathbf{K}=\mathbf{P}+\mathbf{Q}}\overline{\hat{u}_a(\mathbf{Q})\hat{u}_j(\mathbf{P})\hat{\theta}(-\mathbf{K})}d\mathbf{P}\right. \\ \left.+K_aP_{k3}(\mathbf{K})\int_{-\mathbf{K}=\mathbf{P}+\mathbf{Q}}\overline{\hat{u}_k(\mathbf{K})\hat{u}_a(\mathbf{P})\hat{\theta}(\mathbf{Q})}d\mathbf{P}\right]\end{aligned} \tag{3.23}$$

Rewriting the integral:

$$\int_{-\mathbf{K}=\mathbf{P}+\mathbf{Q}}d\mathbf{P} = \iint\delta(\mathbf{K}+\mathbf{P}+\mathbf{Q})d\mathbf{P}d\mathbf{Q} \tag{3.24}$$

and replacing the variables $\boldsymbol{P}$ by $-\boldsymbol{P}$ and $\boldsymbol{Q}$ by $-\boldsymbol{Q}$ in the first integral we obtain:

$$\begin{aligned}\left[\frac{\partial}{\partial t}+(\nu+\alpha)K^2\right]F(K)+\frac{2}{3}E(K)\Gamma = \\ \frac{8i\pi K^2}{3(1-\mu^2)}\left[\frac{1}{2}P_{3aj}(-\mathbf{K})\iint\delta(-\mathbf{K}-\mathbf{P}-\mathbf{Q})\overline{\hat{u}_a(-\mathbf{Q})\hat{u}_j(-\mathbf{P})\hat{\theta}(-\mathbf{K})}d(-\mathbf{P})d(-\mathbf{Q})\right. \\ \left.+K_aP_{k3}(\mathbf{K})\iint\delta(\mathbf{K}+\mathbf{P}+\mathbf{Q})\overline{\hat{u}_k(\mathbf{K})\hat{u}_a(\mathbf{P})\hat{\theta}(\mathbf{Q})}d\mathbf{P}d\mathbf{Q}\right]\end{aligned} \tag{3.25}$$

noting that $\hat{u}_p(-\mathbf{M}) = \hat{u}_p(\mathbf{M})^*$, $*$ denoting complex conjugated, and using the fact that $a^*b^* = (ab)^*$ we write:

$$\begin{aligned}\left[\frac{\partial}{\partial t}+(\nu+\alpha)K^2\right]F(K)+\frac{2}{3}E(K)\Gamma = \\ \frac{8i\pi K^2}{3(1-\mu^2)}\left[\frac{1}{2}P_{3aj}(-\mathbf{K})\iint\delta(\mathbf{K}+\mathbf{P}+\mathbf{Q})\overline{\left(\hat{u}_a(\mathbf{Q})\hat{u}_j(\mathbf{P})\hat{\theta}(\mathbf{K})\right)^*}d\mathbf{P}d\mathbf{Q}\right. \\ \left.+K_aP_{k3}(\mathbf{K})\iint\delta(\mathbf{K}+\mathbf{P}+\mathbf{Q})\overline{\hat{u}_k(\mathbf{K})\hat{u}_a(\mathbf{P})\hat{\theta}(\mathbf{Q})}d\mathbf{P}d\mathbf{Q}\right]\end{aligned} \tag{3.26}$$

noting that $P_{ijk}(-\mathbf{K}) = -P_{ijk}(\mathbf{K})$ we obtain after some shuffling of the indexes

$$\begin{aligned}\left[\frac{\partial}{\partial t}+(\nu+\alpha)K^2\right]F(K) = \\ \frac{8i\pi K^2}{3(1-\mu^2)}\iint\left[K_jP_{a3}(\mathbf{K})\delta(\mathbf{K}+\mathbf{P}+\mathbf{Q})\overline{\hat{u}_a(\mathbf{K})\hat{u}_j(\mathbf{P})\hat{\theta}(\mathbf{Q})}\right. \\ \left.-\frac{1}{2}P_{3aj}(\mathbf{K})\delta(\mathbf{K}+\mathbf{P}+\mathbf{Q})\overline{\left(\hat{u}_a(\mathbf{Q})\hat{u}_j(\mathbf{P})\hat{\theta}(\mathbf{K})\right)^*}\right]d\mathbf{P}d\mathbf{Q} \\ -\frac{2}{3}E(K)\Gamma\end{aligned} \tag{3.27}$$

Defining:

$$T_{aj}(\mathbf{K},\mathbf{P},\mathbf{Q}) = \delta(\mathbf{K}+\mathbf{P}+\mathbf{Q})\overline{\hat{u}_a(\mathbf{K})\hat{u}_j(\mathbf{P})\hat{\theta}(\mathbf{Q})} \tag{3.28}$$

$$T^*_{aj}(\mathbf{Q},\mathbf{P},\mathbf{K}) = \delta(\mathbf{K}+\mathbf{P}+\mathbf{Q})\overline{\Big(\hat{u}_a(\mathbf{Q})\hat{u}_j(\mathbf{P})\hat{\theta}(\mathbf{K})\Big)^*} \tag{3.29}$$

we obtain the expression:

$$\left[\frac{\partial}{\partial t}+(\nu+\alpha)K^2\right]F(K) = \frac{8i\pi K^2}{3(1-\mu^2)}\iint\Big[K_nP_{j3}(\mathbf{K})T_{jn}(\mathbf{K},\mathbf{P},\mathbf{Q}) - \frac{1}{2}P_{3jn}(\mathbf{K})T^*_{jn}(\mathbf{Q},\mathbf{P},\mathbf{K})\Big]d\mathbf{P}d\mathbf{Q} - \frac{2}{3}E(K)\Gamma \tag{3.30}$$

This expression is exact, but the triple-correlations are unknown. To proceed we will write the equation for the triple correlations in the following.

3.1.3 Velocity-scalar triple correlations $\overline{uu\theta}$

Following the same procedure as for the double correlations we write the equations for $\hat{u}_k(\mathbf{K})$, $\hat{u}_l(\mathbf{L})$ and $\hat{\theta}(\mathbf{M})$. We find after multiplication, summing and averaging:

$$\begin{aligned}\left[\frac{\partial}{\partial t}+\nu(K^2+L^2)+\alpha M^2\right]&\overline{\hat{u}_k(\mathbf{K})\hat{u}_l(\mathbf{L})\hat{\theta}(\mathbf{M})} = \\ -\frac{i}{2}P_{kaj}(\mathbf{K})&\int_{\mathbf{K}=\mathbf{P}+\mathbf{Q}}\overline{\hat{u}_j(\mathbf{P})\hat{u}_a(\mathbf{Q})\hat{u}_l(\mathbf{L})\hat{\theta}(\mathbf{M})}d\mathbf{P} \\ -\frac{i}{2}P_{laj}(\mathbf{L})&\int_{\mathbf{L}=\mathbf{P}+\mathbf{Q}}\overline{\hat{u}_j(\mathbf{P})\hat{u}_a(\mathbf{Q})\hat{u}_k(\mathbf{K})\hat{\theta}(\mathbf{M})}d\mathbf{P} \\ -iM_a&\int_{\mathbf{M}=\mathbf{P}+\mathbf{Q}}\overline{\hat{u}_a(\mathbf{P})\hat{\theta}(\mathbf{Q})\hat{u}_k(\mathbf{K})\hat{u}_l(\mathbf{L})}d\mathbf{P} \\ &-\overline{\hat{u}_k(\mathbf{K})\hat{u}_l(\mathbf{L})\hat{u}_3(\mathbf{M})}\Gamma\end{aligned} \tag{3.31}$$

The quasi normal assumption consists of assuming Gaussianity of the quadruple correlations and thus neglecting the fourth-order cumulants. Gaussian fourth-order moments can be written as a sum of products of second order moments:

$$\begin{aligned}\overline{\hat{u}_j(\mathbf{P})\hat{u}_a(\mathbf{Q})\hat{u}_l(\mathbf{L})\hat{\theta}(\mathbf{M})} &= \overline{\hat{u}_j(\mathbf{P})\hat{u}_a(\mathbf{Q})}\ \overline{\hat{u}_l(\mathbf{L})\hat{\theta}(\mathbf{M})} + \\ \overline{\hat{u}_j(\mathbf{P})\hat{u}_l(\mathbf{L})}\ &\overline{\hat{u}_a(\mathbf{Q})\hat{\theta}(\mathbf{M})} + \overline{\hat{u}_j(\mathbf{P})\hat{\theta}(\mathbf{M})}\ \overline{\hat{u}_a(\mathbf{Q})\hat{u}_l(\mathbf{L})}\end{aligned} \tag{3.32}$$

The first term on the right hand side can not form triads except for $K=0$ so it disappears in equation (3.31). Using equations (3.16) and (3.19) and noting that

$$\int P_{jl}(\mathbf{P})\frac{E(P)}{4\pi P^2}\delta(\mathbf{P}+\mathbf{L})d\mathbf{P} = P_{jl}(-\mathbf{L})\frac{E(L)}{4\pi L^2} = P_{jl}(\mathbf{L})\frac{E(L)}{4\pi L^2}$$
$$\int P_{a3}(\mathbf{Q})\frac{F(Q)}{4\pi Q^2}\delta(\mathbf{Q}+\mathbf{M})d\mathbf{Q} = P_{a3}(-\mathbf{M})\frac{F(M)}{4\pi M^2} = P_{a3}(\mathbf{M})\frac{F(M)}{4\pi M^2} \tag{3.33}$$

defining:

$$f(K,P) = \frac{1}{(4\pi KP)^2} \tag{3.34}$$

we find:

$$\begin{aligned}\left[\frac{\partial}{\partial t}+\nu(K^2+L^2)+\alpha M^2\right]\overline{\hat{u}_k(\mathbf{K})\hat{u}_l(\mathbf{L})\hat{\theta}(\mathbf{M})} = \\ -\frac{i}{2}P_{kaj}(\mathbf{K})\left[P_{jl}(\mathbf{L})E(L)P_{a3}(\mathbf{M})F(M)+P_{al}(\mathbf{L})E(L)P_{j3}(\mathbf{M})F(M)\right]\frac{3}{2}f(L,M) \\ -\frac{i}{2}P_{laj}(\mathbf{L})\left[P_{jk}(\mathbf{K})E(K)P_{a3}(\mathbf{M})F(M)+P_{ak}(\mathbf{K})E(K)P_{j3}(\mathbf{M})F(M)\right]\frac{3}{2}f(K,M) \\ -iM_a\left[P_{ak}(\mathbf{K})E(K)P_{l3}(\mathbf{L})F(L)+P_{al}(\mathbf{L})E(L)P_{k3}(\mathbf{K})F(K)\right]\frac{3}{2}f(K,L) \\ -\overline{\hat{u}_k(\mathbf{K})\hat{u}_l(\mathbf{L})\hat{u}_3(\mathbf{M})}\Gamma\end{aligned} \tag{3.35}$$

One can use the symmetry of a and j in the first two terms on the RHS to simplify the equation:

$$\begin{aligned}\left[\frac{\partial}{\partial t}+\nu(K^2+L^2)+\alpha M^2\right]\overline{\hat{u}_k(\mathbf{K})\hat{u}_l(\mathbf{L})\hat{\theta}(\mathbf{M})} = \\ -iP_{kaj}(\mathbf{K})\left[P_{jl}(\mathbf{L})E(L)P_{a3}(\mathbf{M})F(M)\right]\frac{3}{2}f(L,M) \\ -iP_{laj}(\mathbf{L})\left[P_{jk}(\mathbf{K})E(K)P_{a3}(\mathbf{M})F(M)\right]\frac{3}{2}f(K,M) \\ -iM_a\left[P_{ak}(\mathbf{K})E(K)P_{l3}(\mathbf{L})F(L)+P_{al}(\mathbf{L})E(L)P_{k3}(\mathbf{K})F(K)\right]\frac{3}{2}f(K,L) \\ -\overline{\hat{u}_k(\mathbf{K})\hat{u}_l(\mathbf{L})\hat{u}_3(\mathbf{M})}\Gamma\end{aligned} \tag{3.36}$$

We add a damping term to the left hand side of the last equation:

$$\begin{aligned}\left[\frac{\partial}{\partial t}+\nu(K^2+L^2)+\alpha M^2\right] \rightarrow \\ \left[\frac{\partial}{\partial t}+\nu(K^2+L^2)+\alpha M^2+\eta'(K)+\eta'(L)+\eta''(M)\right]\end{aligned} \tag{3.37}$$

We will discuss the need for this eddy damping and its form in section 3.3.1.

One can solve equation (3.36) to obtain a solution for the triple correlations. We assume zero triple correlations at $t = 0$ and find:

$$\begin{aligned}\overline{\hat{u}_k(\mathbf{K})\hat{u}_l(\mathbf{L})\hat{\theta}(\mathbf{M})} = \\ -\frac{3i}{2}\int_0^t G^{KLM}_{EDQN}\Big(P_{kaj}(\mathbf{K})P_{jl}(\mathbf{L})P_{a3}(\mathbf{M})E(L,\tau)F(M,\tau)f(L,M) \\ +P_{laj}(\mathbf{L})P_{jk}(\mathbf{K})P_{a3}(\mathbf{M})E(K,\tau)F(M,\tau)f(K,M) \\ +M_a\left[P_{ak}(\mathbf{K})P_{l3}(\mathbf{L})E(K,\tau)F(L,\tau)+P_{al}(\mathbf{L})P_{k3}(\mathbf{K})E(L,\tau)F(K,\tau)\right]f(K,L) \\ +\frac{2}{3i}\overline{\hat{u}_k(\mathbf{K},\tau)\hat{u}_l(\mathbf{L},\tau)\hat{u}_3(\mathbf{M},\tau)}\Gamma\Big)d\tau\end{aligned} \tag{3.38}$$

with

$$G^{KLM}_{EDQN} = exp\left[-\int(\nu(K^2+L^2)+\alpha M^2+\eta'(K,\tau)+\eta'(L,\tau)+\eta''(M,\tau))d\tau\right] \tag{3.39}$$

Apart from the triple velocity correlations in (3.38) that we will treat in the next section, this EDQN approximation represents a closed solution for the evolution equation of the scalar spectrum (3.30). *Markovianization* allows then a substantial simplification of equation (3.38). Assuming the time scale of Θ^{KLM}_{EDQN} small compared to the timescale of the energy and flux spectra, equation (3.38) can be rewritten:

$$\begin{aligned}\overline{\hat{u}_k(\mathbf{K})\hat{u}_l(\mathbf{L})\hat{\theta}(\mathbf{M})} = \\ -\frac{3i}{2}\int_0^t \Theta^{KLM}_{EDQN}d\tau\Big(P_{kaj}(\mathbf{K})P_{jl}(\mathbf{L})P_{a3}(\mathbf{M})E(L,t)F(M,t)f(L,M) \\ +P_{laj}(\mathbf{L})P_{jk}(\mathbf{K})P_{a3}(\mathbf{M})E(K,t)F(M,t)f(K,M) \\ +M_a\left[P_{ak}(\mathbf{K})P_{l3}(\mathbf{L})E(K,t)F(L,t)+P_{al}(\mathbf{L})P_{k3}(\mathbf{K})E(L,t)F(K,t)\right]f(K,L) \\ +\frac{2}{3i}\overline{\hat{u}_k(\mathbf{K},t)\hat{u}_l(\mathbf{L},t)\hat{u}_3(\mathbf{M},t)}\Gamma\Big)\end{aligned} \tag{3.40}$$

Leith [60] proposed to neglect the time variation of the eddy damping, yielding

$$\begin{aligned}\Theta^{KLM} = \int_0^t \Theta^{KLM}_{EDQN}d\tau = \\ \frac{1-exp-\left[\nu(K^2+L^2)+\alpha M^2+\eta'(K)+\eta'(L)+\eta''(M)\right]t}{\nu(K^2+L^2)+\alpha M^2+\eta'(K)+\eta'(L)+\eta''(M)}\end{aligned} \tag{3.41}$$

We still need to close the triple velocity correlations in (3.40).

3.1.4 Velocity triple correlations $\overline{uuu}$

Following exactly the same approach as in the last section, one can write the equation for the triple velocity correlations.

$$\begin{aligned}\left[\frac{\partial}{\partial t}+\nu(K^2+L^2+M^2)\right]\overline{\hat{u}_k(\mathbf{K})\hat{u}_l(\mathbf{L})\hat{u_m}(\mathbf{M})} = \\ -\frac{i}{2}P_{kaj}(\mathbf{K})\int_{\mathbf{K}=\mathbf{P}+\mathbf{Q}}\overline{\hat{u}_j(\mathbf{P})\hat{u}_a(\mathbf{Q})\hat{u}_l(\mathbf{L})\hat{u_m}(\mathbf{M})}d\mathbf{P} \\ -\frac{i}{2}P_{laj}(\mathbf{L})\int_{\mathbf{L}=\mathbf{P}+\mathbf{Q}}\overline{\hat{u}_j(\mathbf{P})\hat{u}_a(\mathbf{Q})\hat{u}_k(\mathbf{K})\hat{u_m}(\mathbf{M})}d\mathbf{P} \\ -\frac{i}{2}P_{maj}(\mathbf{M})\int_{\mathbf{M}=\mathbf{P}+\mathbf{Q}}\overline{\hat{u}_j(\mathbf{P})\hat{u}_a(\mathbf{Q})\hat{u}_k(\mathbf{K})\hat{u_l}(\mathbf{L})}d\mathbf{P}\end{aligned} \tag{3.42}$$

applying the assumption of Gaussianity to the fourth order moments:

$$\begin{aligned}\left[\frac{\partial}{\partial t}+\nu(K^2+L^2+M^2)\right]\overline{\hat{u}_k(\mathbf{K})\hat{u}_l(\mathbf{L})\hat{u_m}(\mathbf{M})} = \\ -\frac{i}{2}P_{kaj}(\mathbf{K})\left[P_{jl}(\mathbf{L})P_{am}(\mathbf{M})+P_{al}(\mathbf{L})P_{jm}(\mathbf{M})\right]f(L,M)E(L)E(M) \\ -\frac{i}{2}P_{laj}(\mathbf{L})\left[P_{jk}(\mathbf{K})P_{am}(\mathbf{M})+P_{ak}(\mathbf{K})P_{jm}(\mathbf{M})\right]f(K,M)E(K)E(M) \\ -\frac{i}{2}P_{maj}(\mathbf{M})\left[P_{jk}(\mathbf{K})P_{al}(\mathbf{L})+P_{ak}(\mathbf{K})P_{jl}(\mathbf{L})\right]f(K,L)E(K)E(L)\end{aligned} \tag{3.43}$$

and using the symmetry of $P_{ijk}=P_{ikj}$ we have:

$$\begin{aligned}\left[\frac{\partial}{\partial t}+\nu(K^2+L^2+M^2)\right]\overline{\hat{u}_k(\mathbf{K})\hat{u}_l(\mathbf{L})\hat{u_m}(\mathbf{M})} = \\ -iP_{kaj}(\mathbf{K})P_{jl}(\mathbf{L})P_{am}(\mathbf{M})f(L,M)E(L)E(M) \\ -iP_{laj}(\mathbf{L})P_{jk}(\mathbf{K})P_{am}(\mathbf{M})f(K,M)E(K)E(M) \\ -iP_{maj}(\mathbf{M})P_{jk}(\mathbf{K})P_{al}(\mathbf{L})f(K,L)E(K)E(L)\end{aligned} \tag{3.44}$$

After Eddy damping and Markovianization this gives:

$$\begin{aligned}\overline{\hat{u}_j(\mathbf{K})\hat{u}_n(\mathbf{P})\hat{u_3}(\mathbf{Q})} = -i\Theta^U\big[\\ P_{jab}(\mathbf{K})P_{bn}(\mathbf{P})P_{a3}(\mathbf{Q})f(P,Q)E(P)E(Q) \\ +P_{nab}(\mathbf{P})P_{bj}(\mathbf{K})P_{a3}(\mathbf{Q})f(K,Q)E(K)E(Q) \\ +P_{3ab}(\mathbf{Q})P_{bj}(\mathbf{K})P_{an}(\mathbf{P})f(K,P)E(K)E(P)\ \big]\end{aligned} \tag{3.45}$$

In which we changed the indices and wavenumbers: $k\to j$, $l\to n$, $m\to 3$, $j\to b$, $\mathbf{L}\to\mathbf{P}$, $\mathbf{M}\to\mathbf{Q}$ and with a damping term:

$$\Theta^U=\frac{1-exp-\left[\nu(K^2+P^2+Q^2)+\eta(K)+\eta(P)+\eta(Q)\right]t}{\nu(K^2+P^2+Q^2)+\eta(K)+\eta(P)+\eta(Q)} \tag{3.46}$$

3.1.5 The EDQNM equation for the scalar flux spectrum

Replacing the expression for the triple velocity correlation $\overline{uuu}$ (3.45) in the expression for the mixed correlation $\overline{uu\theta}$ (3.40) and using equation (3.28), $T_{jn}(\mathbf{K},\mathbf{P},\mathbf{Q})$ can be expressed as:

$$\begin{aligned}T_{jn}(\mathbf{K},\mathbf{P},\mathbf{Q}) = -\frac{3i}{2}\Theta^{KPQ}\delta(\mathbf{K}+\mathbf{P}+\mathbf{Q})\Big\{&P_{jab}(\mathbf{K})P_{bn}(\mathbf{P})E(P)P_{a3}(\mathbf{Q})F(Q)f(P,Q)\\ &+P_{nab}(\mathbf{P})P_{bj}(\mathbf{K})E(K)P_{a3}(\mathbf{Q})F(Q)f(K,Q)\\ &+Q_a\left[P_{aj}(\mathbf{K})E(K)P_{n3}(\mathbf{P})F(P)+P_{an}(\mathbf{P})E(P)P_{j3}(\mathbf{K})F(K)\right]f(K,P)\\ &-\frac{2}{3}\Gamma\Theta^{U}\Big[P_{jab}(\mathbf{K})P_{bn}(\mathbf{P})P_{a3}(\mathbf{Q})f(P,Q)E(P)E(Q)\\ &+P_{nab}(\mathbf{P})P_{bj}(\mathbf{K})P_{a3}(\mathbf{Q})f(K,Q)E(K)E(Q)\\ &+P_{3ab}(\mathbf{Q})P_{bj}(\mathbf{K})P_{an}(\mathbf{P})f(K,P)E(K)E(P)\Big]\Big\}\end{aligned} \tag{3.47}$$

It can be seen from equations (3.36) and (3.43) that, at least in the Quasi Normal approximation, $\overline{\left(\hat{u}_a(\mathbf{Q})\hat{u}_j(\mathbf{P})\hat{\theta}(\mathbf{K})\right)^*}$ is a purely imaginary quantitity so that we can replace $T^*_{jn}(\mathbf{Q},\mathbf{P},\mathbf{K})$ by $-T_{jn}(\mathbf{Q},\mathbf{P},\mathbf{K})$. We substitute (3.47) in equation (3.30) to obtain the closed equation for the scalar flux spectrum:

$$\begin{aligned}\left[\frac{\partial}{\partial t}+(\nu+\alpha)K^2\right]F(K)+\frac{2}{3}E(K)\Gamma = \frac{K^2}{4\pi(1-\mu^2)}\iint\Bigg[&\\ K_nP_{j3}(\mathbf{K})\Big(\Theta^{KPQ}\delta(\mathbf{K}+\mathbf{P}+\mathbf{Q})\Big\{&P_{jab}(\mathbf{K})P_{bn}(\mathbf{P})P_{a3}(\mathbf{Q})E'(P)F'(Q)\\ &+P_{nab}(\mathbf{P})P_{bj}(\mathbf{K})P_{a3}(\mathbf{Q})E'(K)F'(Q)\\ &+Q_a\left[P_{aj}(\mathbf{K})P_{n3}(\mathbf{P})E'(K)F'(P)+P_{an}(\mathbf{P})P_{j3}(\mathbf{K})E'(P)F'(K)\right]\\ &-\frac{2}{3}\Gamma\Theta^{U(K,P,Q)}\Big[P_{jab}(\mathbf{K})P_{bn}(\mathbf{P})P_{a3}(\mathbf{Q})E'(P)E'(Q)\\ &+P_{nab}(\mathbf{P})P_{bj}(\mathbf{K})P_{a3}(\mathbf{Q})E'(K)E'(Q)\\ &+P_{3ab}(\mathbf{Q})P_{bj}(\mathbf{K})P_{an}(\mathbf{P})E'(K)E'(P)\Big]\Big\}\Big)\\ +\frac{1}{2}P_{3jn}(\mathbf{K})\Big(\Theta^{QPK}\delta(\mathbf{K}+\mathbf{P}+\mathbf{Q})\Big\{&P_{jab}(\mathbf{Q})P_{bn}(\mathbf{P})P_{a3}(\mathbf{K})E'(P)F'(K)\\ &+P_{nab}(\mathbf{P})P_{bj}(\mathbf{Q})P_{a3}(\mathbf{K})E'(Q)F'(K)\\ &+K_a\left[P_{aj}(\mathbf{Q})P_{n3}(\mathbf{P})E'(Q)F'(P)+P_{an}(\mathbf{P})P_{j3}(\mathbf{Q})E'(P)F'(Q)\right]\\ &-\frac{2}{3}\Gamma\Theta^{U(Q,P,K)}\Big[P_{jab}(\mathbf{Q})P_{bn}(\mathbf{P})P_{a3}(\mathbf{K})E'(P)E'(K)\\ &+P_{nab}(\mathbf{P})P_{bj}(\mathbf{Q})P_{a3}(\mathbf{K})E'(Q)E'(K)\\ &+P_{3ab}(\mathbf{K})P_{bj}(\mathbf{Q})P_{an}(\mathbf{P})E'(Q)E'(P)\Big]\Big\}\Big)\Bigg]d\mathbf{P}d\mathbf{Q}\end{aligned} \tag{3.48}$$

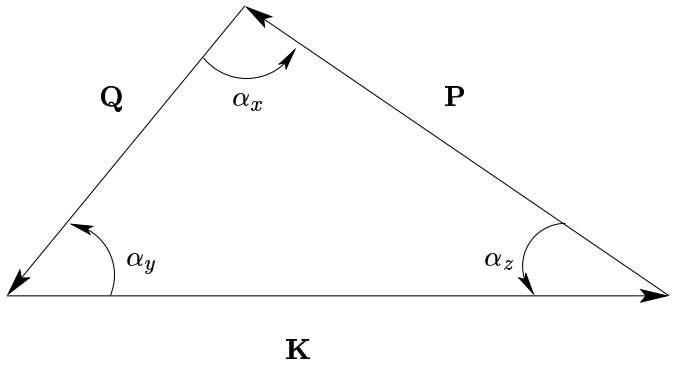

Figure 3.1: Wavenumber triad, contributing to the non-linear interaction.

with $E'(K) = E(K)/K^2$ and $F'(K) = F(K)/K^2$. In the appendix is shown how one can express the above integral as a function of the norm K, P and Q of the wavevectors, the cosines x, y and z (see figure 3.1) of their interior angles and μ, the cosine of the angle between $\mathbf{K}$ and the direction of the mean scalar gradient. All calculations done we find:

$$\begin{aligned}
\left[\frac{\partial}{\partial t} + (\nu+\alpha)K^2\right] F(K) + \frac{2}{3}E(K)\Gamma = \frac{1}{4}\iint_{\Delta} \Bigg[\\
\Theta^{KPQ}\Big\{ -\frac{2}{3}\Gamma\Theta^{U(K,P,Q)}\Big[H_1E(K)E(P) + H_2E(K)E(Q) + H_3E(P)E(Q)\Big] \\
+H_4E(P)F(K) + H_5E(K)F(Q) + H_6E(P)F(Q) + H_7E(K)F(P)\Big\} \\
+\frac{1}{2}\Theta^{QPK}\Big\{ -\frac{2}{3}\Gamma\Theta^{U(Q,P,K)}\Big[J_1E(P)E(K) + J_2E(Q)E(K) + J_3E(Q)E(P)\Big] \\
+J_4E(Q)F(K) + J_5E(P)F(Q) + J_6E(Q)F(P) + J_7E(P)F(K)\Big\}\Bigg] \frac{dP}{P}\frac{dQ}{Q}
\end{aligned} \tag{3.49}$$

with

$$
\begin{aligned}
H_1 &= Q^3(-2y^3 - yz^2 - zx - 2zxy^2) \\
H_2 &= P^3(y^2z - yx + 2z^2xy) \\
H_3 &= K^3(-z^2 - 2z^2y^2 - xyz + 1 + y^2) \\
H_4 &= Q^3(-2y - 2zx) \\
H_5 &= P^3(-z^3 - yx - zx^2 + z) \\
H_6 &= K^3(-z^2 + y^2 - 2z^2y^2 - yzx + 1) \\
H_7 &= Q^3(-z(yz + x)) \\
J_1 &= Q^3(-2(zx + y^3)) \\
J_2 &= P^3(-2(yx + z^3)) \\
J_3 &= K^3(2 - 4y^2z^2 - 2xyz) \\
J_4 &= P^3(-2(yx + z^3)) \\
J_5 &= K^3(-z^2 - 2z^2y^2 - yzx + 1 + y^2) \\
J_6 &= K^3(-y^2 + 1 + z^2 - 2z^2y^2 - yzx) \\
J_7 &= Q^3(-2(zx + y^3)
\end{aligned} \tag{3.50}
$$

We note that the a factor $(1-\mu^2)$ appears in all terms which, together with the factor $(1-\mu^2)^{-1}$ in equation (3.48) cancels out the μ-dependence of the equation of the scalar flux spectrum. The equation is now closed and suitable for numerical exploitation. At this point it has to be noted that the terms containing the scalar gradient Γ have been obtained by a double Markovianization process and that they contain a double eddy damping. We could say that they are modeled by an EDM-EDQNM procedure and that the derivation of those terms is thus more questionable.

3.1.6 Decoupling the contributions of pressure and non-linear transfer

To investigate independently the different contributions in the scalar flux equation, one needs to decouple the pressure and non-linear transfer. In the above derivation, the influence of the pressure is not observable independently, because in equation (3.11) the pressure is absorbed in the non-linear transfer (the non-linear term is multiplied by the projector $P_{ij}(K)$). We could rewrite the equation in the form:

$$
\left[\frac{\partial}{\partial t} + \nu K^2\right] \hat{u}_k(\mathbf{K},t) = -iK_a \int_{\mathbf{K}=\mathbf{P}+\mathbf{Q}} \hat{u}_k(\mathbf{P},t)\hat{u}_a(\mathbf{Q},t)d\mathbf{P} - iK_k\hat{p}(\mathbf{K}) \tag{3.51}
$$

with $\hat{p}(\mathbf{K})$ the kinematic pressure i.e. the pressure divided by the density. The contribution of the pressure can be written as:

$$
-iK_k\hat{p}(\mathbf{K}) = \frac{K_jK_aK_k}{K^2} \int_{\mathbf{K}=\mathbf{P}+\mathbf{Q}} \hat{u}_j(\mathbf{P})\hat{u}_a(\mathbf{Q})d\mathbf{P} \tag{3.52}
$$

and the convection term can be written as:

$$-K_a\delta_{kj}\int_{\mathbf{K}=\mathbf{P}+\mathbf{Q}}\hat{u}_j(\mathbf{P})\hat{u}_a(\mathbf{Q})d\mathbf{P} \tag{3.53}$$

We could derive the closure starting from the beginning with the two above contributions decoupled. An alternative way is to identify the contribution stemming from the convection term only. The pressure term can then be obtained by substraction.

We derive the equation for the $z-$component of the spectrum: $F_{w\theta}(K)$ without applying the projector $P_{i3}(K)$. The starting equations are now:

$$\left[\frac{\partial}{\partial t}+\nu K^2\right]\hat{u}_3(\mathbf{K}) = -iK_a\int_{\mathbf{K}=\mathbf{P}+\mathbf{Q}}\hat{u}_3(\mathbf{P})\hat{u}_a(\mathbf{Q})d\mathbf{P} - iK_3\hat{p}(\mathbf{K}) \tag{3.54}$$

$$\left[\frac{\partial}{\partial t}+\alpha M^2\right]\hat{\theta}(\mathbf{M}) = -iM_a\int_{\mathbf{M}=\mathbf{P}+\mathbf{Q}}\hat{u}_a(\mathbf{P})\hat{\theta}(\mathbf{Q})d\mathbf{P} - \hat{u}_3(\mathbf{M})\Gamma \tag{3.55}$$

yielding

$$\left[\frac{\partial}{\partial t}+\nu K^2+\alpha M^2\right]\overline{\hat{u}_3(\mathbf{K})\hat{\theta}(\mathbf{M})} = -iK_a\int_{\mathbf{K}=\mathbf{P}+\mathbf{Q}}\overline{\hat{u}_3(\mathbf{P})\hat{u}_a(\mathbf{Q})\hat{\theta}(\mathbf{M})}d\mathbf{P} + \left[T^{NL}_{w\theta}(\boldsymbol{K})\right]_\theta + \Pi(\boldsymbol{K}) + P(\boldsymbol{K}) \tag{3.56}$$

The non linear triple correlation originating from the θ-equation, $\left[T^{NL}_{w\theta}(\boldsymbol{K})\right]_\theta$, corresponding to the H-terms in the previous section are unchanged, the pressure term $\Pi(\boldsymbol{K})$ is unknown but can be obtained by substracting the term $\left[T^{NL}_{w\theta}(\boldsymbol{K})\right]_u$ (the first term on the right hand side of (3.56)) from the J-terms in the previous section. So in the equation:

$$\left[\frac{\partial}{\partial t}+(\nu+\alpha)K^2\right]F(K)(1-\mu^2) = \frac{8i\pi K^2}{3}\iint -K_j(\mathbf{K})T_{j3}(\mathbf{Q},\mathbf{P},\mathbf{K})d\mathbf{P}d\mathbf{Q} + \left[T^{NL}_{w\theta}(\boldsymbol{K})\right]_\theta + \Pi(\boldsymbol{K}) + P(\boldsymbol{K}) \tag{3.57}$$

one only needs to derive an expression for the first term on the right hand side, $\left[T^{NL}_{w\theta}(\boldsymbol{K})\right]_u$. To derive the expression for this term we use the same technique as in the previous sections. The only additional difficulty is that there is no common term $(1-\mu^2)$ appearing on the right hand side. To obtain an expression independent of μ, we integrate both sides of the equation with respect to μ:

$$\left[\frac{\partial}{\partial t}+(\nu+\alpha)K^2\right]\int_0^1 F(K)(1-\mu^2)d\mu = \int_0^1\frac{8i\pi K^2}{3}\iint -K_j(\mathbf{K})T_{j3}(\mathbf{Q},\mathbf{P},\mathbf{K})d\mathbf{P}d\mathbf{Q} + \left[T^{NL}_{w\theta}(\boldsymbol{K})\right]_\theta + \Pi(\boldsymbol{K}) + P(\boldsymbol{K})d\mu \tag{3.58}$$

Eventually we find

$$\left[\frac{\partial}{\partial t}+(\nu+\alpha)K^2\right]F(K)+\frac{2}{3}E(K)\Gamma=\left[T_{w\theta}^{NL}(K)\right]_u+\left[T_{w\theta}^{NL}(K)\right]_\theta+\Pi(K) \quad (3.59)$$

with the non-linear transfer contributions

$$\begin{aligned}&\left[T_{w\theta}^{NL}(K)\right]_u=\\ &\frac{1}{4}\iint_\Delta\Big[\frac{1}{2}\Theta^{QPK}\Big\{-\frac{2}{3}\Gamma\Theta^U\Big[L_1E(P)E(K)+L_2E(Q)E(K)+L_3E(Q)E(P)\Big]\\ &+L_4E(Q)F(K)+L_5E(P)F(Q)+L_6E(Q)F(P)+L_7E(P)F(K)\Big\}\Big]\frac{dP}{P}\frac{dQ}{Q}\end{aligned} \quad (3.60)$$

and

$$\begin{aligned}&\left[T_{w\theta}^{NL}(K)\right]_\theta=\\ &\frac{1}{4}\iint_\Delta\Big[\Theta^{KPQ}\Big\{-\frac{2}{3}\Gamma\Theta^U\Big[H_1E(K)E(P)+H_2E(K)E(Q)+H_3E(P)E(Q)\Big]\\ &+H_4E(P)F(K)+H_5E(K)F(Q)+H_6E(P)F(Q)+H_7E(K)F(P)\Big\}\Big]\frac{dP}{P}\frac{dQ}{Q}\end{aligned} \quad (3.61)$$

and the pressure term

$$\begin{aligned}\Pi(K)=\frac{1}{4}\iint_\Delta\Big[\frac{1}{2}\Theta^{QPK}\Big\{-\frac{2}{3}\Gamma\Theta^U\Big[&(J_1-L_1)E(P)E(K)+(J_2-L_2)E(Q)E(K)+\\ &(J_3-L_3)E(Q)E(P)\Big]+(J_4-L_4)E(Q)F(K)+(J_5-L_5)E(P)F(Q)\\ &+(J_6-L_6)E(Q)F(P)+(J_7-L_7)E(P)F(K)\Big\}\Big]\frac{dP}{P}\frac{dQ}{Q}\end{aligned} \quad (3.62)$$

in which

$$\begin{aligned}L_1&=2Q^3(-zx-y^3+yx^2-y)\\ L_2&=2P^3(y^2z-yx+2z^2xy)\\ L_3&=2K^3(-2z^2y^2+xyz+2y^2+x^2)\\ L_4&=2P^3(y^2z-yx+2z^2xy)\\ L_5&=2K^3(-2z^2+2)\\ L_6&=2K^3(yzx+x^2)\\ L_7&=2Q^3(-zx-y^3+yx^2-y)\end{aligned} \quad (3.63)$$

3.1.7 Final formulation of the model

In the previous 5 sections we showed the derivation of the EDQNM closure for the scalar flux spectrum. The final result is equivalent to the equation in Herr *et al.* [20]. The two expressions differ only by definition of the angles between the wavevectors. Also in our form we have separate information about the non-linear transfer term and the pressure scrambling term, where those contributions where not separated in the formulation of Herr *et al.*

We resume here the derived equation:

$$\left[\frac{\partial}{\partial t} + (\nu + \alpha)K^2\right] F(K) + \frac{2}{3}E(K)\Gamma = \left[T_{w\theta}^{NL}(K)\right]_\theta + \left[T_{w\theta}^{NL}(K)\right]_u + \Pi(K) \quad (3.64)$$

with

$$\left[T_{w\theta}^{NL}(K)\right]_u = \iint_\Delta \left[\sum_{i=1}^{7} \mathcal{L}_i\right] \frac{dP}{P}\frac{dQ}{Q} \quad (3.65)$$

$$\left[T_{w\theta}^{NL}(K)\right]_\theta = \iint_\Delta \left[\sum_{i=1}^{7} \mathcal{H}_i\right] \frac{dP}{P}\frac{dQ}{Q} \quad (3.66)$$

$$\Pi(K) = \iint_\Delta \left[\sum_{i=1}^{7} (\mathcal{J}_i - \mathcal{L}_i)\right] \frac{dP}{P}\frac{dQ}{Q} \quad (3.67)$$

The contributions $\mathcal{H}_i$, $\mathcal{L}_i$ and $\mathcal{J}_i$ can be found in table 3.1. In those expression we find the relaxation time $\Theta(\mu)$:

$$\Theta(\gamma) = \frac{1 - e^{-\alpha t}}{\alpha} \quad (3.68)$$

with

$$\mu_U(K,P,Q) = \lambda(\mu(K) + \mu(P) + \mu(Q)) + \nu(K^2 + P^2 + Q^2) \quad (3.69)$$

and

$$\mu_F(K,P,Q) = \lambda'(\mu(K) + \mu(P)) + \lambda''\mu(Q) + \nu(K^2 + P^2) + \alpha Q^2 \quad (3.70)$$

$\mathcal{H}_1 =$	$-\frac{1}{6}\Gamma\Theta(\mu_F(K,P,Q))\Theta(\mu_U(K,P,Q))$	$(-2y^3 - yz^2 - zx - 2zxy^2)$	$Q^3E(P)E(K)$
$\mathcal{H}_2 =$	$-\frac{1}{6}\Gamma\Theta(\mu_F(K,P,Q))\Theta(\mu_U(K,P,Q))$	$(y^2z - yx + 2z^2xy)$	$P^3E(Q)E(K)$
$\mathcal{H}_3 =$	$-\frac{1}{6}\Gamma\Theta(\mu_F(K,P,Q))\Theta(\mu_U(K,P,Q))$	$(-z^2 - 2z^2y^2 - xyz + 1 + y^2)$	$K^3E(Q)E(P)$
$\mathcal{H}_4 =$	$\frac{1}{4}\Theta(\mu_F(K,P,Q))$	$(-2y - 2zx)$	$Q^3E(P)F(K)$
$\mathcal{H}_5 =$	$\frac{1}{4}\Theta(\mu_F(K,P,Q))$	$(-z^3 - yx - zx^2 + z)$	$P^3E(K)F(Q)$
$\mathcal{H}_6 =$	$\frac{1}{4}\Theta(\mu_F(K,P,Q))$	$(-z^2 + y^2 - 2z^2y^2 - yzx + 1)$	$K^3E(P)F(Q)$
$\mathcal{H}_7 =$	$\frac{1}{4}\Theta(\mu_F(K,P,Q))$	$(-z(yz + x))$	$Q^3E(K)F(P)$
$\mathcal{J}_1 =$	$-\frac{1}{12}\Gamma\Theta(\mu_F(Q,P,K))\Theta(\mu_U(K,P,Q))$	$(-2(zx + y^3))$	$Q^3E(P)E(K)$
$\mathcal{J}_2 =$	$-\frac{1}{12}\Gamma\Theta(\mu_F(Q,P,K))\Theta(\mu_U(K,P,Q))$	$(-2(yx + z^3))$	$P^3E(Q)E(K)$
$\mathcal{J}_3 =$	$-\frac{1}{12}\Gamma\Theta(\mu_F(Q,P,K))\Theta(\mu_U(K,P,Q))$	$(2 - 4y^2z^2 - 2xyz)$	$K^3E(Q)E(P)$
$\mathcal{J}_4 =$	$\frac{1}{8}\Theta(\mu_F(Q,P,K))$	$(-2(yx + z^3))$	$P^3E(Q)F(K)$
$\mathcal{J}_5 =$	$\frac{1}{8}\Theta(\mu_F(Q,P,K))$	$(-z^2 - 2z^2y^2 - yzx + 1 + y^2)$	$K^3E(P)F(Q)$
$\mathcal{J}_6 =$	$\frac{1}{8}\Theta(\mu_F(Q,P,K))$	$(-y^2 + 1 + z^2 - 2z^2y^2 - yzx)$	$K^3E(Q)F(P)$
$\mathcal{J}_7 =$	$\frac{1}{8}\Theta(\mu_F(Q,P,K))$	$(-2(zx + y^3)$	$Q^3E(P)F(K)$
$\mathcal{L}_1 =$	$-\frac{1}{6}\Gamma\Theta(\mu_F(Q,P,K))\Theta(\mu_U(K,P,Q))$	$(-zx - y^3 + yx^2 - y)$	$Q^3E(P)E(K)$
$\mathcal{L}_2 =$	$-\frac{1}{6}\Gamma\Theta(\mu_F(Q,P,K))\Theta(\mu_U(K,P,Q))$	$(y^2z - yx + 2z^2xy)$	$P^3E(Q)E(K)$
$\mathcal{L}_3 =$	$-\frac{1}{6}\Gamma\Theta(\mu_F(Q,P,K))\Theta(\mu_U(K,P,Q))$	$(-2z^2y^2 + xyz + 2y^2 + x^2)$	$K^3E(Q)E(P)$
$\mathcal{L}_4 =$	$\frac{1}{4}\Theta(\mu_F(Q,P,K))$	$(y^2z - yx + 2z^2xy)$	$P^3E(Q)F(K)$
$\mathcal{L}_5 =$	$\frac{1}{4}\Theta(\mu_F(Q,P,K))$	$(-2z^2 + 2)$	$K^3E(P)F(Q)$
$\mathcal{L}_6 =$	$\frac{1}{4}\Theta(\mu_F(Q,P,K))$	$(yzx + x^2)$	$K^3E(Q)F(P)$
$\mathcal{L}_7 =$	$\frac{1}{4}\Theta(\mu_F(Q,P,K))$	$(-zx - y^3 + yx^2 - y)$	$Q^3E(P)F(K)$

Table 3.1: Geometric coefficients appearing in the closed EDQNM equation (3.64)

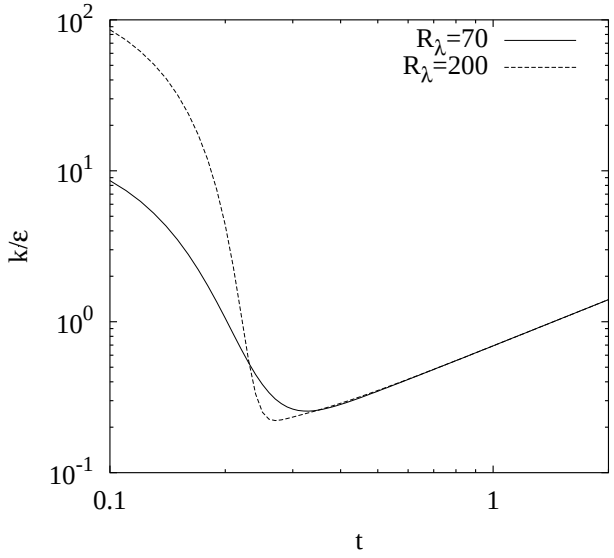

Figure 3.2: The evolution of the eddy turnover-time at two different R_λ.

3.2 Initial conditions

The energy spectrum is initialized with a *von Karmann* spectrum [61]:

$$E(K) = \frac{K^4}{(1+K^2)^{17/6}}, \tag{3.71}$$

but the precise form is of minor importance[1]. The scalar flux and scalar variance are initially zero. The calculations correspond to freely decaying turbulence. The scalar field is generated by the interaction of the isotropic velocity field with the mean scalar gradient. Results are evaluated when the decay of the velocity field becomes self-similar. As a criterion we require the eddy turnover-time k/ϵ to increase as a power law. In figure 3.2 we show the evolution of k/ϵ with time for two different Reynolds numbers. At $t = 0.5$ the evolution of $E(K)$ is considered self-similar and all results are evaluated at this time.

3.3 Calibration of the EDQNM model

3.3.1 Origin and formulation of the eddy-damping

The eddy damping is a correction of the relaxation time of the triple correlations. The need for such a correction arises when the quadruple correlations

[1] Calculations with an initial spectrum as given in equation (7.11) were also performed and no significantly different results were obtained.

are replaced by products of double correlations. Integrating and Markovianizing this 'quasi normal' expression yields the QNM approximation for the triple correlations that can be introduced in the evolution equation of the double correlations to obtain a closed set of equations. The thus obtained QNM closure of the kinetic energy spectrum underestimates the energy cascade towards the smaller scales resulting in a K^{-2} inertial range. This effect has been studied in detail by Frisch *et al.* [62]. In Nakauchi and Sega [57], a similar approach is found, which they call the modified zero-fourth-cumulant expansion (MZFC). They also apply this approach to the scalar field, but without a mean gradient. The reason for this underestimation of the spectral flux resulting in the K^{-2} slope in the inertial range is that the relaxation time of the QNM (or MZFC) approximation involves only viscous damping. The relaxation of the triple correlations is however also affected by the non-linear interaction between Fourier modes or eddies as noted by Orszag [21]. The Eddy damping is then a heuristic correction to account for this effect. The desirable relaxation or damping can be introduced by adding a spectral eddy viscosity to the viscous terms as in equation (3.36). However, the choice of this eddy viscosity is non-trivial. The original form, proposed by Orszag [21], was obtained by dimensional analysis and reads:

$$\eta(k) \sim \epsilon^{1/3} K^{2/3} \tag{3.72}$$

with λ a constant related to the kolmogorov constant. An improvement is an expression taking into account the local (in wavenumber space) behaviour of the energy spectrum:

$$\eta(K) \sim \sqrt{K^3 E(K)} \tag{3.73}$$

Another variant, non-local in wavenumber space and improving the behaviour in the dissipation range is the expression as proposed by Pouquet *et al.* [63]:

$$\eta(K) = \lambda \sqrt{\int_0^K S^2 E(S) dS} \tag{3.74}$$

All three forms are compatible with a Kolmogorov inertial range. We will retain the last form for the eddy damping term of the energy, scalar variance and scalar flux spectrum, but one should keep in mind that other forms could be envisaged. The term $\eta'(k)$ in equation (3.36) introduces the constant λ' and $\eta''(k)$ introduces λ''. In the following we will try to determine the adequate values of these constants.

The determination of the constants in the eddy damping of the kinetic energy spectrum and the scalar spectrum have been the subject of previous studies. The main results of those studies will now be resumed.

3.3.2 Choice of the model-constants for the energy spectrum and scalar spectrum

The energy spectrum $E(K)$

For the energy spectrum, the constant is related to the Kolmogorov constant. This yields the *classical* value of $\lambda_u = 0.355$. This choice is for example discussed in the book of Lesieur [56].

The scalar spectrum $E_\theta(K)$

For the eddy damping of the scalar variance spectrum the constants are chosen in order to obtain the proper Corrsin-Obukhov constant, combined with a consideration about the turbulent Prandtl number *cf.* Lesieur [56]. In Herring *et al.* [22] they choose the constants:

$$\begin{aligned} \lambda'_\theta &= 0 \\ \lambda''_\theta &= 1.3 \end{aligned} \tag{3.75}$$

Other works [64, 20, 23] use the constants $\lambda'_\theta = \lambda''_\theta = 0.36$. All values correspond to a Corrsin-Obukhov constant that is equal to 0.45 in agreement with the atmospheric measurements of Champagne *et al.* [65]. Sreenivasan [10] gives an overview of the different values found for the Corrsin-Obukhov constant in experiments. In most of the experiments a value between 0.4 and 0.5 is found. We prefer the set (3.75) because the zero value of λ'_θ is consistent with our analysis in the next section. In the following we will focus on the scalar flux spectrum. The scalar spectrum $E_\theta(K)$ will be investigated in homogeneous shear flow in chapter 5.

3.3.3 The eddy damping of the scalar flux spectrum $F_{w\theta}(K)$

The velocity-scalar correlation coefficient

For the scalar flux spectrum, up till now, no inertial range law constant has been determined. In the absence of such a law the approach followed in earlier works [20, 54, 58, 66] consisted in choosing the constants so that the one point velocity-scalar correlation coefficient $\rho_{w\theta}$ from the closure calculation corresponds to experimental results. A convenience of this parameter is that its value is relatively insensitive to Reynolds and Prandtl number. This comparison yields a set of possible correlations and an arbitrary choice is made among those combinations. Herr *et al.* [20] fit their EDQNM results to a DNS of forced turbulence that gives value of $\rho_{w\theta} = -0.55$. The DNS of Overholt and Pope [46] yields a similar value.

The relation between the sets of the two constants that where in agreement with the DNS value of $\rho_{w\theta}$ is close to linear:

$$\lambda'' = 1.03 - 1.98\lambda' \quad \text{for} \quad 0 < \lambda' < 0.52 \tag{3.76}$$

Subsequently an arbitrary choice $(\lambda', \lambda'') = (0, 1.03)$ was made [20, 54, 58, 66], but we will show in the following that this might not be the best choice.

The damping of the three-point triple-correlations

To guide the choice of the constants in the eddy-damping term, we write the derivation of the triple correlation, but this time in physical space. We do so because the influence of the pressure on the triple correlations will be the subject of our discussion and those pressure terms are not explicitly present in the Fourier representation. For convenience we introduce a short notation $u_{1i} = u_i(x_1)$.

$$\overline{u_{2i}u_{3k}\frac{\partial\theta_1}{\partial t}} = -\overline{u_{2i}u_{3k}u_{1n}}\frac{\partial\Theta}{\partial x_{1n}} - \frac{\partial}{\partial x_{1n}}\overline{\theta_1 u_{2i}u_{1n}u_{3k}} + \kappa\frac{\partial^2}{\partial x_{1n}^2}\overline{\theta_1 u_{2i}u_{3k}} \quad (3.77)$$

$$\overline{\theta_1 u_{3k}\frac{\partial u_{2i}}{\partial t}} = -\frac{\partial}{\partial x_{2n}}\overline{\theta_1 u_{2i}u_{2n}u_{3k}} - \frac{1}{\rho}\frac{\partial}{\partial x_{2i}}\overline{p_2'\theta_1 u_{3k}} + \nu\frac{\partial^2}{\partial x_{2n}^2}\overline{\theta_1 u_{2i}u_{3k}} \quad (3.78)$$

$$\overline{\theta_1 u_{2i}\frac{\partial u_{3k}}{\partial t}} = -\frac{\partial}{\partial x_{3n}}\overline{\theta_1 u_{2i}u_{3n}u_{3k}} - \frac{1}{\rho}\frac{\partial}{\partial x_{3k}}\overline{p_3'\theta_1 u_{2i}} + \nu\frac{\partial^2}{\partial x_{3n}^2}\overline{\theta_1 u_{2i}u_{3k}} \quad (3.79)$$

The sum of these three expressions yields the evolution equation of the three-point triple correlations. We could apply the quasi normal approximation to this equation and Markovianize the solution for the triple correlation. It is at this point important to note that the pressure does not appear in equation (3.77). We now recall expression (3.37) in our derivation of the EDQNM closure:

$$\left[\frac{\partial}{\partial t} + \nu(K^2+L^2) + \alpha M^2\right] \rightarrow$$
$$\left[\frac{\partial}{\partial t} + \nu(K^2+L^2) + \alpha M^2 + \eta'(K) + \eta'(L) + \eta''(M)\right]$$

The three damping terms that are added to the triple correlation equation, $\eta''(M)$, $\eta'(K)$ and $\eta'(L)$, are damping the three contributions above, 3.77, 3.78, 3.79.

Kraichnan [67] obtained as a result of his Lagrangian History Direct Interaction Approximation (LHDIA) that: *'(...) the effective relaxation time for triple correlations of simultaneous amplitudes of wave-vector triads is determined by memory and decay times associated with the viscous and pressure forces encountered along the particle paths.'*

We assume that we can identify the *triple correlations of simultaneous amplitudes of wave-vector triads* as the triple correlations $\overline{\theta_1 u_{2i} u_{3k}}$ at a certain time t. The *effective relaxation time* corresponds to the $\Theta(K,P,Q,t)$ in our closure. The viscous damping is present in this timescale, already without eddy damping. The pressure forces are however absent in this timescale. I claim that those pressure forces are the missing non-linear damping that is re-introduced by Eddy Damping.

So the eddy damping is only required for (3.78) and (3.79), containing the pressure. which leads us the choice:

$$\lambda'' = 0 \tag{3.80}$$

and λ' to be determined. Perhaps this is not a convincing proof for the choice $\lambda'' = 0$ but at least we have a choice consistent with what can be infered from LHDIA. A confirmation of this choice will be presented below.

The spectral equilibrium between production, transfer and pressure

To choose among the combinations in Herr *et al.* [20] we have to investigate the different contributions in the evolution equation of $F_{w\theta}(K)$. The non-linear transfer, as already discussed in section 1.2.2, is obtained by spherically integrating the triple correlation term:

$$T^{NL}_{w\theta}(K) = \int_{\Sigma_K} \Big[iK_j \Big(FT_{/\boldsymbol{r}} \Big(\overline{\theta(\boldsymbol{x}) u_j(\boldsymbol{x}) w(\boldsymbol{x}+\boldsymbol{r})} - \overline{\theta(\boldsymbol{x}) u_j(\boldsymbol{x}+\boldsymbol{r}) w(\boldsymbol{x}+\boldsymbol{r})} \Big) \Big) \Big] dA(\boldsymbol{K})$$

in which the first triple correlation $\theta(\boldsymbol{x}) u_j(\boldsymbol{x}) w(\boldsymbol{x}+\boldsymbol{r})$ stems from the non linear term $u_j \partial\theta/\partial x_j$ in the scalar equation. This part corresponds to the H-terms in section 3.1.6 and was denoted $\left[T^{NL}_{w\theta}(K)\right]_\theta$. The other term, $\theta(\boldsymbol{x}) u_j(\boldsymbol{x}+\boldsymbol{r}) w(\boldsymbol{x}+\boldsymbol{r})$ from the non linear term $u_j \partial u_i/\partial x_j$ in the velocity equation, corresponds to the L-terms in section 3.1.6 was denoted $\left[T^{NL}_{w\theta}(K)\right]_U$.

We can write the two contributions to the two-point velocity-scalar cross correlation separately:

$$\overline{u_{2i} \frac{\partial \theta_1}{\partial t}} + \overline{u_{2i} u_{1n}} \frac{\partial \Theta}{\partial x_{1n}} = -\frac{\partial}{\partial x_{1n}} \overline{\theta_1 u_{2i} u_{1n}} + \kappa \frac{\partial^2}{\partial x_{1n}^2} \overline{\theta_1 u_{2i}} \tag{3.81}$$

and

$$\overline{\theta_1 \frac{\partial u_{2i}}{\partial t}} + \frac{\partial}{\partial x_{2n}} \overline{\theta_1 u_{2i} u_{2n}} = -\frac{1}{\rho} \frac{\partial}{\partial x_{2i}} \overline{p'_2 \theta_1} + \nu \frac{\partial^2}{\partial x_{2n}^2} \overline{\theta_1 u_{2i}} \tag{3.82}$$

In the stationary case we know that:

$$\frac{\partial \overline{u_{2i}\theta_1}}{\partial t} = \overline{u_{2i}\frac{\partial \theta_1}{\partial t}} + \overline{\theta_1 \frac{\partial u_{2i}}{\partial t}} = 0 \tag{3.83}$$

The quantity $\partial\theta/\partial t$ is a highly intermittent function, closely related to the fine scale structure. Its correlation with the velocity field can be expected to be small for the large scales (this is an assumption that needs verification):

$$\overline{u_i(x)\frac{\partial \theta(x+r)}{\partial t}} \approx 0 \quad \text{for large} \quad r \tag{3.84}$$

in the case that in addition the Reynolds number is high eq. (3.82) simplifies to the expression:

$$0 \approx -\overline{u_{2i}u_{1n}}\frac{\partial \Theta}{\partial x_n} - \frac{\partial}{\partial x_{1n}}\overline{\theta_1 u_{2i}u_{1n}} \tag{3.85}$$

or in spectral space:

$$\frac{2}{3}E(K)\Gamma \approx \left[T_{w\theta}^{NL}(K)\right]_\theta \quad \text{for small} \quad K \tag{3.86}$$

so that in the stationary case at small wavenumbers:

$$\begin{aligned} P(K) &= -\left[T_{w\theta}^{NL}(K)\right]_\theta \\ \left[T_{w\theta}^{NL}(K)\right]_U &= -\Pi(K) \end{aligned} \tag{3.87}$$

We verified this result by Large Eddy Simulations. LES is very appropriate in this case because we want information about the large scales at large Reynolds number. The result is shown in the next chapter in figure 4.9. Very good agreement of the LES and the relations 3.87 is observed.

We will now investigate the results of our EDQNM model to see if this equilibrium is observed.

We vary the constants along the line that interpolates the possible pairs of values according to Herr *et al.* [20] $\lambda'' = 1.03 - 1.98\lambda'$ for $0 < \lambda' < 0.52$. In figure 3.3 we show the results for four different sets of values. It is observed that best agreement with (3.87) is found for the set of constants,

$$\begin{aligned} \lambda' &= 0.52 \\ \lambda'' &= 0, \end{aligned} \tag{3.88}$$

and we note that the set of constants chosen in previous works [20, 58, 66] with $\lambda' = 0$, actually yields the worst agreement. We will proceed our calculations, using the set of constants $(\lambda'; \lambda'') = (0.52; 0)$. We point out that this result confirms our assumption that the eddy damping correction to the triple correlation relaxation time is exclusively needed to model the decorrelating effect of the pressure leading to (3.80).

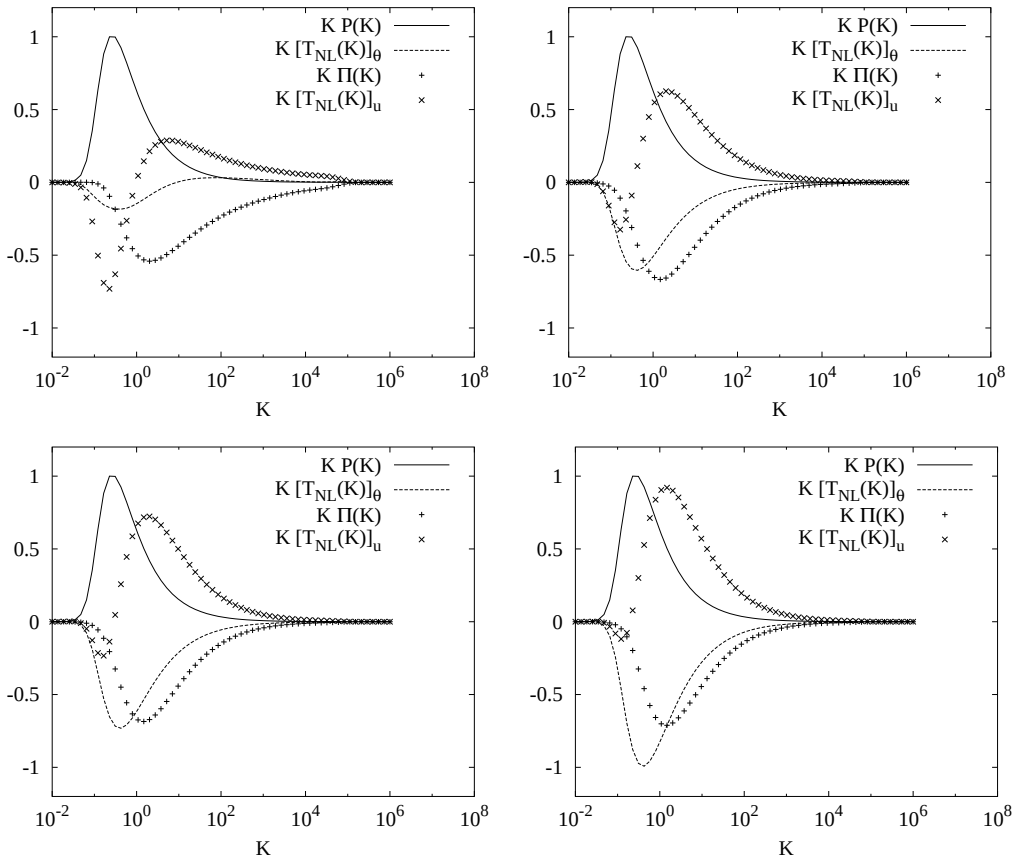

Figure 3.3: Influence of the eddy damping constants on the spectral balance at $R_\lambda = 5.\ 10^4$. Top left: $(\lambda'; \lambda'') = (0; 1.03)$, top right: $(\lambda'; \lambda'') = (0.2; 0.63)$, bottom left: $(\lambda'; \lambda'') = (0.3; 0.43)$, bottom right: $(\lambda'; \lambda'') = (0.52; 0)$

3.3.4 Influence of the scalar gradient on the non-linear transfer

The non-linear triple correlations in the equation of the scalar flux are closed by the quasi-normal approximation. In the resulting expression two different types of terms can be distinguished: the so called 'cross-terms' that contain a product of the flux spectrum and the energy spectrum, $E(A)F(B)$, and the contributions involving the mean scalar gradient, schematically $\Gamma E(A)E(B)$. The contribution of these 'gradient-terms' or 'linear terms' (because they are linearly dependent on the gradient) in the closed equation of the spectrum $F(K)$ has been obtained, as we mentioned before, by a double Eddy Damping and Markovianization procedure. We consequently introduced the designation EDM-EDQNM for those terms. Hence, we should bare in mind that the gradient-terms involve a more crude approximation than the other contributions. Therefore, before proceeding our exploitation of the EDQNM model we will investigate their behaviour.

We should mention here that for the velocity-field subjected to deformation the EDQNM approach was derived by Cambon [68], taking into account the effects of the mean gradients in the equation of the triple correlation. This was called the EDQNM2 closure. The Markovianization of this equation was in certain cases shown to be incompatible with the effect of the gradients in this equation (Bertoglio [25]). It was argued that the improvement of the model by taking into account these gradient terms could be overshadowed by the problems involving the Markovianization.

In figure 3.4 we show the influence of the gradient terms on the non linear transfer and pressure terms (we shall study those terms in more detail in the next section). The Reynolds number is equal to $R_\lambda = 100$ and 10^4 respectively. Their is no contribution to the pressure term. Apparently the gradient terms represent a pure transfer. Furthermore their influence diminishes for higher wavenumbers. In figure 3.5 we show the influence of the gradient terms on the scalar flux spectrum by comparing spectra obtained with and without these terms. We show results at Reynolds numbers of $R_\lambda = 100$ and $R_\lambda = 10^4$ as in figure 3.4. As can be seen the major difference is observed in the large scales, where the 'gradient transfer' creates an unexpected irregularity. This behaviour in the large scales encourages us to neglect the gradient terms as was done for the velocity-field by Cambon, [69], Cambon *et al.* [24] (EDQNM1) and Bertoglio [70].

3.4 Results of the Model

3.4.1 The inertial range of the kinetic energy spectrum

Before showing the results for the scalar flux spectrum we report here some results for the energy spectrum. In figure 3.6 we show $E(K)$ for Reynolds

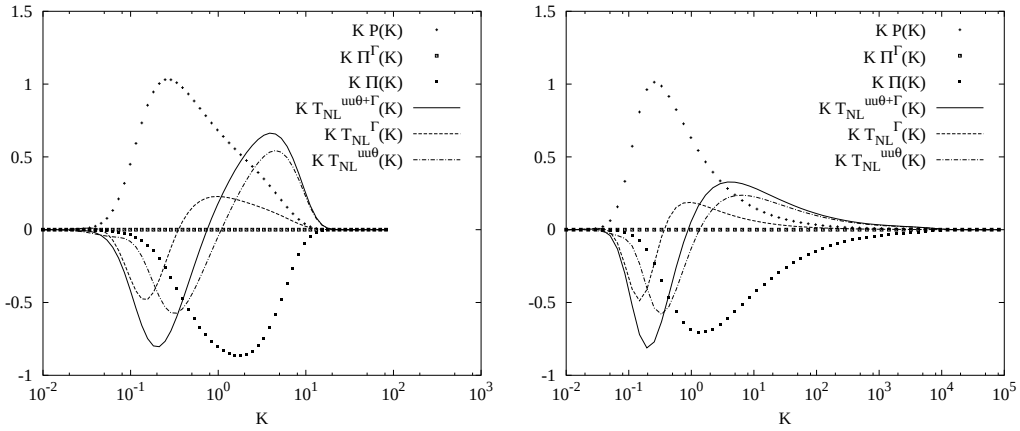

Figure 3.4: Spectra of the Gradient contributions to the non-linear transfer terms. Left: $R_\lambda = 100$, right: $R_\lambda = 10^4$

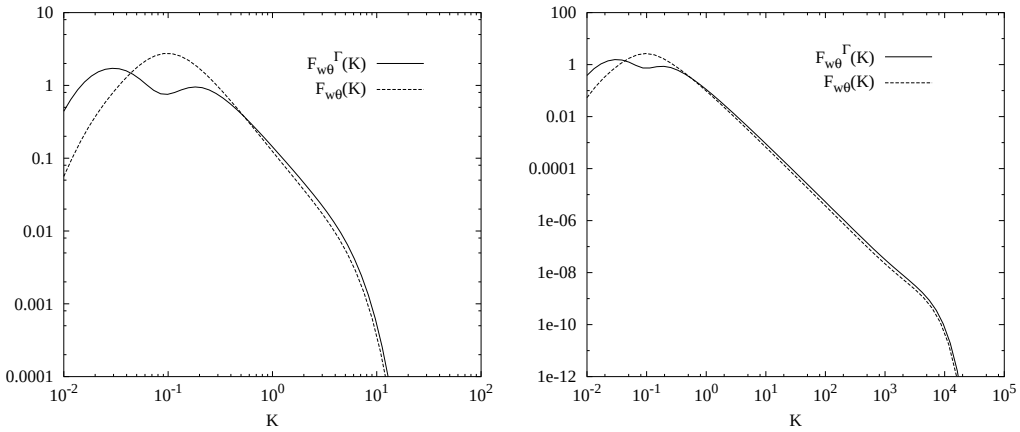

Figure 3.5: Spectra of the scalar flux calculated with and without the gradient contributions to the non-linear transfer terms. Left: $R_\lambda = 100$, right: $R_\lambda = 10^4$

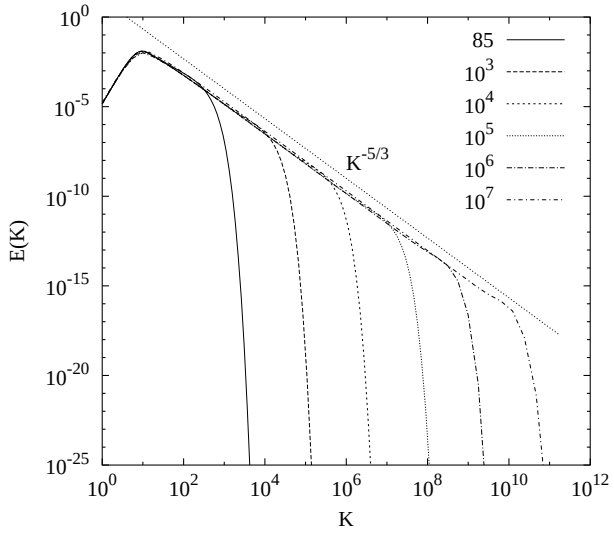

Figure 3.6: Kinetic energy spectra for Reynolds numbers from $100 < R_\lambda < 10^7$.

numbers from $85 < R_\lambda < 10^7$. We note here that an illustration of the spectral contributions (non-linear transfer and dissipation) can be found in figure 1.1, which shows results obtained with EDQNM theory. In figure 3.7 the slope of the inertial range is plotted as a function of the Reynolds number. Also drawn are the numerical fits to the experimental values of Mydlarski and Warhaft [43] in grid turbulence. The measurements were performed for $R_\lambda < 731$. The n_{uu} exponent corresponds to the measurements of the slopes of the longitudinal velocity spectrum, n_{vv} to the transversal velocity spectrum. Good agreement is observed between the EDQNM results and the experimental values[2].

3.4.2 Investigation of the different spectral contributions to the scalar flux spectrum

In this section an analysis of the contributions to the scalar flux equation is performed at different R_λ.

[2]The extrapolation of the fits of Mydlarski and Warhaft to values higher than $R_\lambda = 731$ are also shown in figure 3.7. It should be noted that the effect of intermittency is not taken into account by the EDQNM closure, and that the experimental values of the values n_{uu} and n_{vv} could be affected by the effect of intermittency, especially at higher R_λ, where the effect of intermittency is generally more noticeable. We name here the (forced) DNS of Kaneda *et al.* [71] with a remarkably steep slope around 1.76 at $R_\lambda = 1200$ and the atmospheric measurements reported by Tsuji [72] which show two distinct power law regions in the energy spectrum with slopes of 1.73 and 1.69 at a $R_\lambda = 17060$.

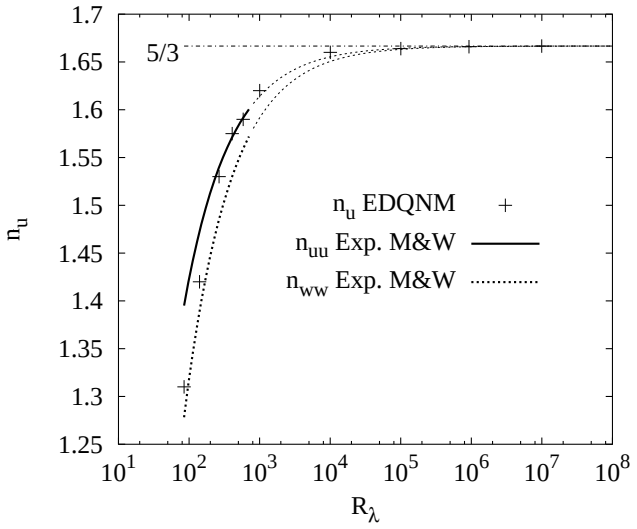

Figure 3.7: The slope of the inertial range of the kinetic energy spectra as a function of R_λ. EDQNM results compared to the experiments of Mydlarski and Warhaft [43]

The production and molecular destruction spectra given by:

$$P(K) = -\frac{2}{3}\Gamma E(K)$$
$$V(K) = (\nu + \alpha)K^2 F_{w\theta}(K)dK \tag{3.89}$$

The non-linear transfer as previously noted in chapter 2 is obtained by spherically integrating the triple correlation term:

$$T_{w\theta}^{NL}(K) = \int_{\Sigma_K} \Big[iK_j \Big(FT_{/\boldsymbol{r}} \Big(\overline{\theta(\boldsymbol{x})u_j(\boldsymbol{x})w(\boldsymbol{x}+\boldsymbol{r})} - \overline{\theta(\boldsymbol{x})u_j(\boldsymbol{x}+\boldsymbol{r})w(\boldsymbol{x}+\boldsymbol{r})} \Big) \Big) \Big] dA(\boldsymbol{K}) \tag{3.90}$$

It can easily be seen that this term vanishes in the one-point limit. The spectrum of this term integrated from wavenumber zero to infinity is thus zero and the transfer is conservative. The pressure term,

$$\Pi(K) = \int_{\Sigma_K} FT_{/\boldsymbol{r}} \left(\frac{1}{\rho} \overline{\theta(\boldsymbol{x}) \frac{\partial}{\partial z} p(\boldsymbol{x}+\boldsymbol{r})} \right) dA(\boldsymbol{K}) \tag{3.91}$$

on the contrary has an integral which is not zero: it appears to be a destruction term. $T_{w\theta}^{NL}(K)$ and $\Pi(K)$ are both functions of the triple correlation terms. The closed expressions for these two terms are obtained with the EDQNM theory. In figure 3.8 we show the balance of the terms in equation (1.48) for four different Reynolds numbers. In the figure, it can be observed

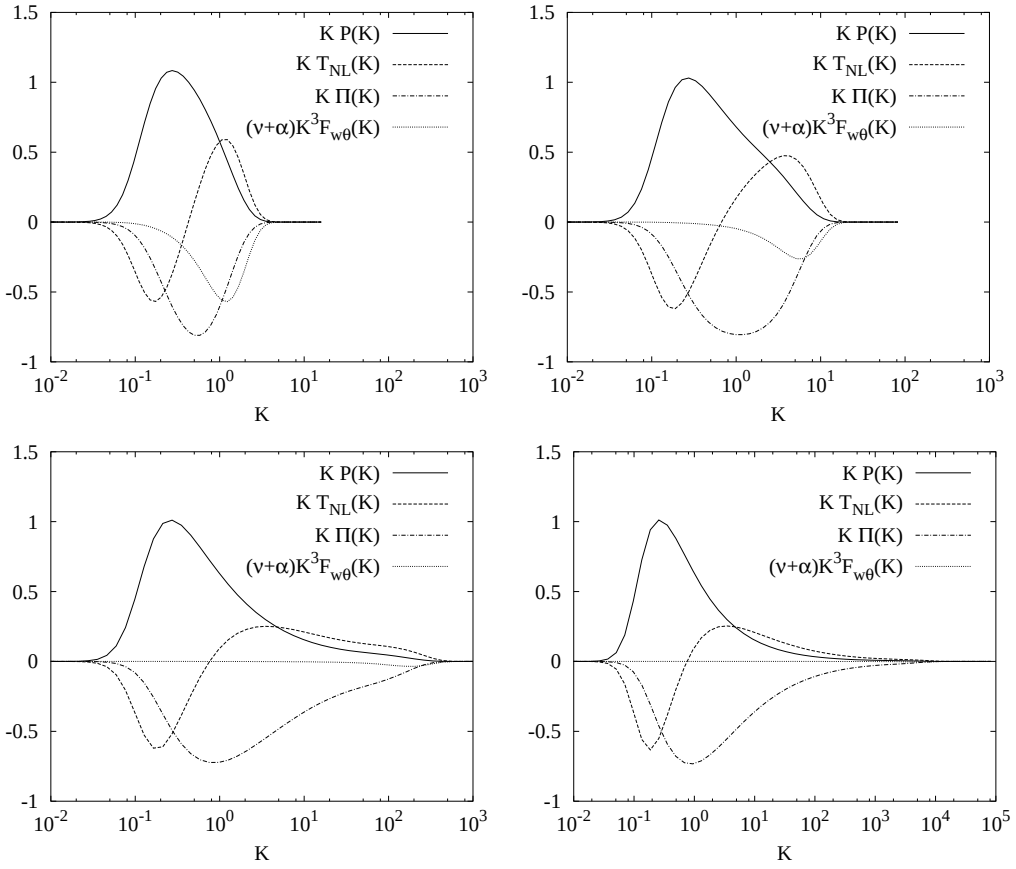

Figure 3.8: Spectral balance of the production, non-linear transfer, pressure and viscous destruction of scalar flux. Top left: $R_\lambda = 30$, top right: $R_\lambda = 100$, bottom left: $R_\lambda = 10^3$, bottom right: $R_\lambda = 10^4$

that $F_{w\theta}(K)$ is mainly produced at large scale by the mean gradient term and that it is destroyed at smaller scales by both pressure and molecular effects at small R_λ, and by pressure effects only at high R_λ. The conservative role played by the transfer term $T^{NL}_{w\theta}(K)$ also appears in the figure.

3.4.3 The spectral slope of the scalar flux in the inertial range

In chapter 2 we showed how dimensional analysis allows for an inertial range slope of the scalar flux spectrum varying from $-5/3$ to $-7/3$, depending on the behaviour of the spectral flux. The behaviour of the slope of the spectrum in the inertial range will now be investigated by EDQNM calculations.

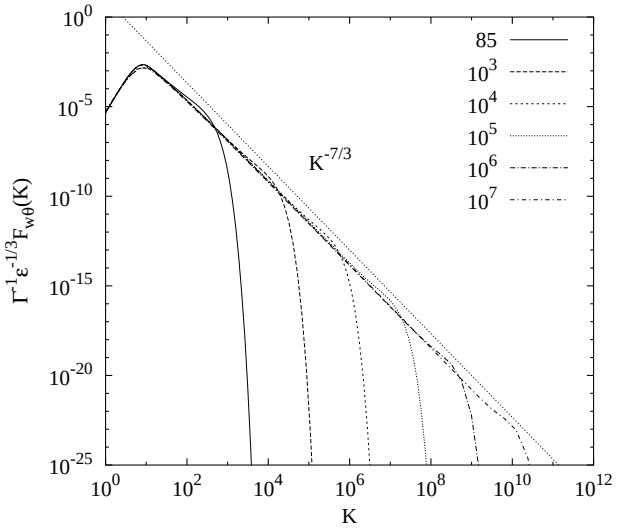

Figure 3.9: Scalar flux spectra for Reynolds numbers from $100 < R_\lambda < 10^7$.

In figure 3.9 and 3.10 we show spectra for Reynolds numbers[3] in the range $30 < R_\lambda < 10^7$.

In figure 3.11 we show the dependence of the slope on the Reynolds number. The results do not leave any doubt about the asymptotic inertial range slope. The closure shows a tendency towards a $K^{-7/3}$ slope[4]. It also shows that this value is only approached for very large values of the Reynolds number ($R_\lambda = 10^4$ yields a $K^{-2.27}$ slope). It can therefore be argued that a clear $K^{-7/3}$ will not easily be observed on earth, atmospheric experiments reaching R_λ up to 10^4. As in Mydlarski and Warhaft [43] for the velocity spectra we try to fit a power law to the results. The empirical relation $n_{w\theta} = 7/3(1 - 2.73R_\lambda^{-0.54})$ describes the data pretty well.

Furthermore, it is shown that the experimental results of Mydlarski and Warhaft [40] are in reasonable agreement with the calculations. From those results it can be concluded that a $K^{-7/3}$ slope will not be observed in DNS of decaying isotropic turbulence with a mean scalar gradient in the near

[3]The calculations for $R_\lambda = 10^6$ and 10^7 are slightly underresolved. The errors introduced hereby were estimated to be less than 1% for the inertial range slope and less than 10% for the ratio of dissipation to production as examined in section 3.4.4 and of the same order for the scaling constant $C_{w\theta}$

[4]It is worth noting that an asymptotic K^{-2} slope is obtained with this same EDQNM closure as soon as λ' is taken equal to zero, independent of the value of λ''. With this choice we omit the influence of the pressure on the triple-correlation relaxation-time stemming from equation (3.78) and (3.79). Those triple correlations are consequently only damped by viscous and diffusive effects and therefore this choice gives a significantly different wavenumber dependence. Possibly this scaling is analogous to the K^{-2} scaling of the energy spectrum in the absence of Eddy damping in which only viscous damping relaxes the triple correlations, as discussed in section 3.3.1 and the work of Frisch *et al.* [62].

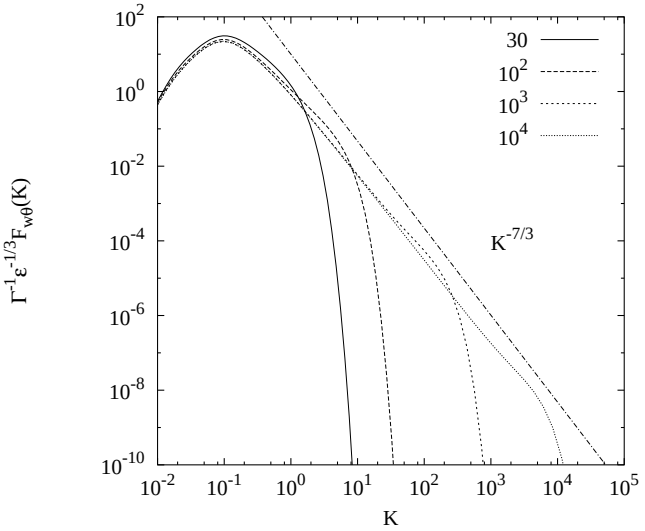

Figure 3.10: Same as 3.9 but for $30 < R_\lambda < 10^4$.

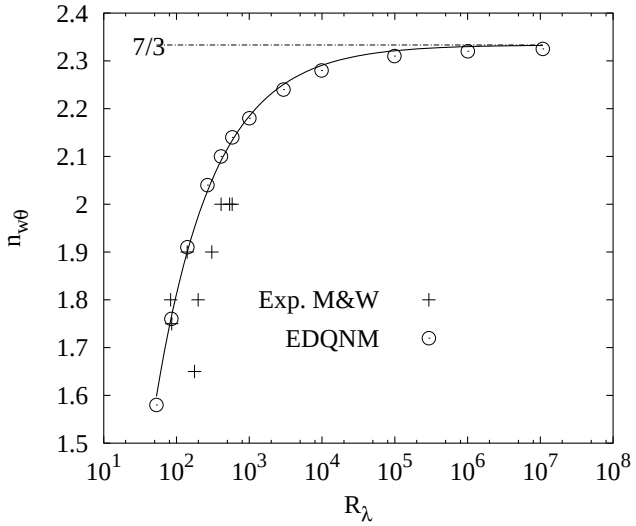

Figure 3.11: The slope of the inertial range of the velocity-scalar cross spectrum as a function of R_λ. EDQNM results compared to the experiments of Mydlarski and Warhaft [40]

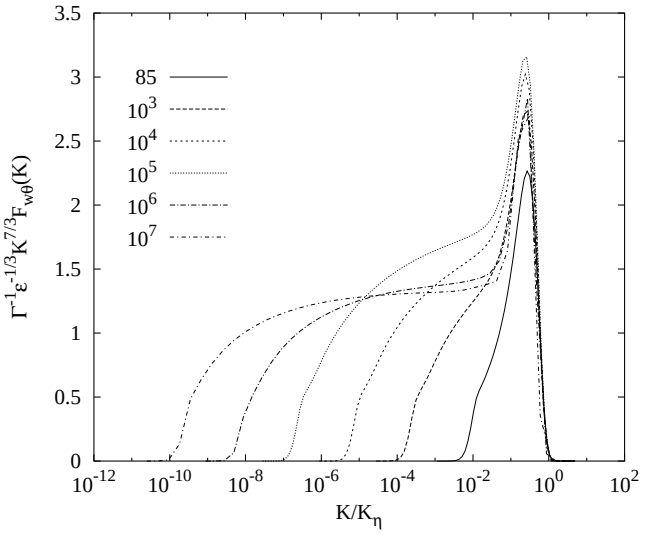

Figure 3.12: Compensated scalar flux spectra for Reynolds numbers from $100 < R_\lambda < 10^7$

future or even in wind tunnel experiments, the Reynolds number being too low in both cases.

In figure 3.12 compensated spectra are plotted for Reynolds numbers in the range $100 < R_\lambda < 10^7$. The prefactor $C_{w\theta}$ in the scaling relation:

$$F_{w\theta}(K) = C_{w\theta}\Gamma\epsilon^{1/3}K^{-7/3}, \tag{3.92}$$

appears to be of order unity. It is found $C_{w\theta} \approx 1.5$.

In figure 3.13 the present EDQNM results are compared with experimental data of Mydlarski and Warhaft [40] and DNS and SDIP results of O'Gorman and Pullin [51]. The spectra are one-dimensional spectra. An exact relation between one-dimensional and spherically averaged spectra exists in the case of isotropic turbulence and scalar fluctuations created by a uniform mean scalar gradient (see O'Gorman and Pullin [59, 51]). It reads:

$$F^{1D}(K_1) = \frac{3}{4}\int_{K_1}^{\infty} \frac{K^2 + K_1^2}{K^3} F_{w\theta}(K)dK \tag{3.93}$$

SDIP stands for sparse direct inter-interaction perturbation and corresponds to a variant of the lagrangian direct interaction approximation of Kraichnan [67]. The SDIP result is given only in the asymptotically high Reynolds number limit. It yields an overestimation of the constant $C_{w\theta}$ as explained in O'Gorman and Pullin [51]. The spectrum calculated with EDQNM theory is situated in between the DNS and the experimental results.

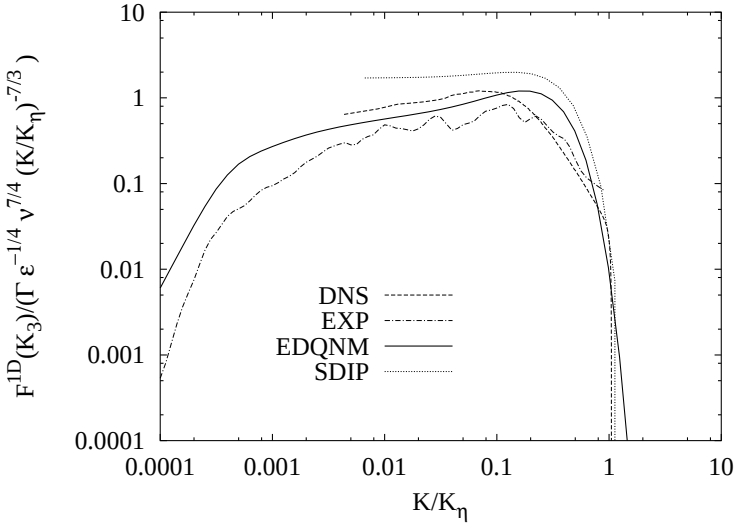

Figure 3.13: Comparison of one dimensional scalar flux spectra from DNS, SDIP (O'Gorman and Pullin [51]), and experiments (Mydlarski and Warhaft [40]) with EDQNM results.

3.4.4 The molecular dissipation of scalar flux

It was already noted in figure 3.8 that, when the Reynolds number increases, the viscous dissipation becomes small compared to the production term. We call $\Gamma\mathcal{U}^2$ the integral value of $P(K)$, $\epsilon_{w\theta}$ the integral value of $V(K)$. The dependence of the ratio, $\epsilon_{w\theta}/\Gamma\mathcal{U}^2$ has been studied in the literature. Mydlarski [41] found a decrease proportional to $R_\lambda^{-1.2}$ and in the DNS of Overholt and Pope [46] a $R_\lambda^{-0.77}$ scaling is observed. In figure 3.14 their observations are compared with the results of the EDQNM calculations. The closure is applied to a range of R_λ much wider than obtainable in DNS or wind-tunnel experiments. It can be observed that there is good agreement between the DNS of Overholt and Pope [46] and the EDQNM calculations at low R_λ, where the $R_\lambda^{-0.77}$ scaling is found. At high R_λ, the EDQNM results scale as R_λ^{-1}. This R_λ^{-1} dependence can be analytically predicted assuming Lumley's scaling (equation 3.92) for $F_{w\theta}(K)$. Substituting (3.92) in the expression for the molecular dissipation of scalar flux, one obtains:

$$\epsilon_{w\theta} = (\nu+\alpha)\int^{K_\eta} K^2\left[C_{w\theta}\Gamma\epsilon^{1/3}K^{-7/3}\right]dK \tag{3.94}$$

ignoring the lower bound of the integral by assuming a very high R_λ. With the expressions for the Kolmogorov scale and R_λ:

$$K_\eta = \left(\frac{2}{3C_K}\right)^{3/4}\frac{\epsilon^{1/4}}{\nu^{3/4}},\quad R_\lambda = \sqrt{15\frac{\mathcal{U}^4}{\nu\epsilon}}$$

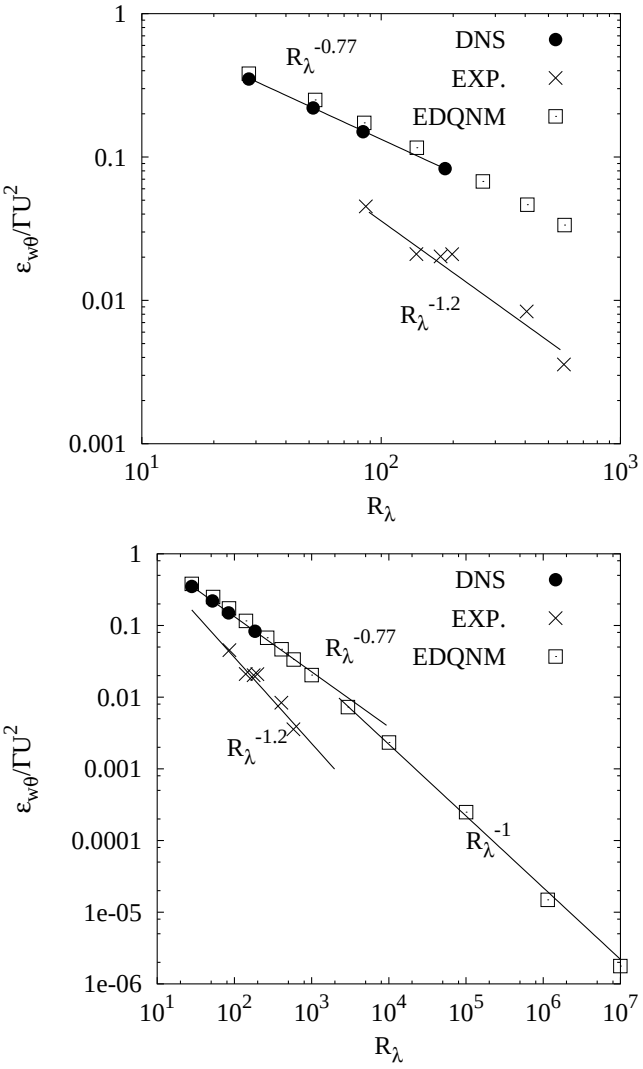

Figure 3.14: The ratio of molecular destruction to production of $\overline{w\theta}$ as a function of R_λ, compared to the results of the DNS of Overholt and Pope [46] and the values of Mydlarski [41]. Top: $28 < R_\lambda < 582$, bottom $28 < R_\lambda < 10^7$.

it is immediately found that:

$$\epsilon_{w\theta}/\Gamma\mathcal{U}^2 \sim R_\lambda^{-1}. \tag{3.95}$$

In the intermediate range of R_λ, the $R_\lambda^{-1.2}$ scaling found in the experiment of Mydlarski [41] is not found with the EDQNM closure. It has to be pointed out that Mydlarski only measures one component of the dissipation.

3.5 Conclusions

We discussed in this chapter the derivation of the equations for the EDQNM closure of the velocity scalar cross correlation, previously derived by Herr *et al.* [20]. The constants in the eddy damping term were determined and the effect of the mean scalar gradient on the non-linear transfer was studied.

At moderate Reynolds numbers the one dimensional spectra are shown to agree with experimental results and DNS. The low computational cost of the closure calculations allows to perform calculations at very high Reynolds numbers where the dimensional analysis of [31] was verified: a $K^{-7/3}$ scaling is found. This scaling is however only found for very high Reynolds numbers and at Reynolds numbers corresponding to laboratory experiments, the spectral exponent is found to be closer to -2 as observed in the experiments of Mydlarski and Warhaft [40]. The empirical relation $n_{w\theta} = 7/3(1 - 2.73R_\lambda^{-0.54})$ gives the evolution of the spectral exponent according to our calculations. The prefactor $C_{w\theta}$ in the scaling relation:

$$F_{w\theta}(K) = C_{w\theta}\Gamma\epsilon^{1/3}K^{-7/3}, \tag{3.96}$$

was found to be $C_{w\theta} \approx 1.5$. At low R_λ, the molecular destruction of scalar flux normalized by the production was shown to obey the $R_\lambda^{-0.77}$ power law proposed by [46]. For higher values this quantity tends towards an asymptotic R_λ^{-1} behaviour that can easily be predicted by dimensional analysis.

We have to note that analytical closures are, uptil now, not capable to reproduce the intermittent character of a turbulent field that is even more pronounced for the scalar field. The effect of intermittency on second order quantities such as energy spectra and cospectra is known to be rather small at low and moderate Reynolds numbers. The good agreement observed in this chapter between experimental results, DNS and the EDQNM theory is a good illustration. The influence of intermittency at high R_λ and for higher order moments is known to be greater. We will not further address the subject of intermittency in this work.

Chapter 4

Large Eddy Simulations

4.1 Introduction

In the previous chapter it was clearly shown that EDQNM theory predicts a $-7/3$ inertial range slope for the scalar flux spectrum at high Reynolds numbers. In this chapter we investigate in more detail the LES results already presented in chapter 2. In particular we analyze the fact that these LES were found to support the existence of a K^{-2} behaviour of the scalar flux spectrum.

We use the EDQNM closure derived in the previous chapter as a tool to analyze several effects that are likely to influence the LES results, namely the influence of forcing, resolution and subgrid modelling. After this analysis we perform additional LES in order to check the influence of large scale forcing and to check assumptions about the spectral balance of the different contributions to the scalar flux evolution equation.

4.2 Filtering

LES is based on the observation that the small turbulent scales are much more universal than the large scales. Most of the important properties of a turbulent flow are governed by the large scales. Those large scales are calculated exactly in LES, whereas the small scales and the interaction between large and small scales are represented by a model. In Pope [3] we find a good illustration of the computational gain obtained by not resolving the full wavenumber spectrum. It is, for example, shown that for a Reynolds number of 70, the dissipation range contains 99.98% of the wavemodes and that this percentage grows with increasing Reynolds number.

To split the turbulent field into large scales and small scales, a filtering operator is applied to the Navier-Stokes and scalar equations. For homogeneous fields a uniform filtering procedure is usually introduced and one writes (filtered quantities will be denoted by a tilde):

$$\tilde{u}_i(x,t) = \int_\Omega G(x-x')u_i(x',t)d^3x' \tag{4.1}$$

or in Fourier space:

$$\widetilde{\hat{u}_i}(\boldsymbol{K},t) = G(K)\hat{u}_i(\boldsymbol{K},t) \tag{4.2}$$

and the same procedure can be applied to the scalar field. For homogeneous fields a spectral low pass, or top hat filter, with a cut-off frequency K_c,

$$\begin{aligned} G_{LP}(K) &= 1 \quad \forall \quad K \leq K_c \\ G_{LP}(K) &= 0 \quad \forall \quad K > K_c, \end{aligned}$$

turns out to be convenient

This procedure yields the situation schematically shown for the energy spectrum in fig. 4.1. The solid line represents the resolved part and the dashed line the scales with a wavenumber larger than the cut-off wavenumber K_c, that are removed by filtering. There is a spectral flux through this cut-off wavenumber that is the difference between a forward flux ϵ_f and a reverse flux ϵ_b, usually named backscatter. It is the modeling of those fluxes from and towards removed scales that constitutes the major challenge in LES. After filtering we find the following equations for the resolved part of the turbulent fields:

$$\frac{\partial\tilde{u}_i}{\partial t} + \frac{\partial}{\partial x_j}(\widetilde{\tilde{u}_i\tilde{u}_j}) = -\frac{1}{\rho}\frac{\partial\tilde{p}}{\partial x_i} + \frac{\partial}{\partial x_j}\left(\nu\frac{\partial\tilde{u}_i}{\partial x_j}\right) - \frac{\partial\tau_{ij}^{sg}}{\partial x_j} \tag{4.3}$$

$$\frac{\partial\tilde{u}_i}{\partial x_i} = 0 \tag{4.4}$$

$$\frac{\partial\tilde{\theta}}{\partial t} + \frac{\partial}{\partial x_j}(\widetilde{\tilde{\theta}\tilde{u}_j}) = \frac{\partial}{\partial x_j}\left(\alpha\frac{\partial\tilde{\theta}}{\partial x_j}\right) - \frac{\partial g_{u_i\theta}^{sg}}{\partial x_j} \tag{4.5}$$

with

$$\tau_{ij}^{sg} = \widetilde{u_iu_j} - \widetilde{\tilde{u}_i\tilde{u}_j} \tag{4.6}$$

$$g_{u_i\theta}^{sg} = \widetilde{u_i\theta} - \widetilde{\tilde{u}_i\tilde{\theta}} \tag{4.7}$$

For the last two expressions, the subgrid stress and subgrid scalar flux, an appropriate model is needed to reconstruct properly the interaction of the large scales with the subgrid-scales. This will be the issue of the next section.

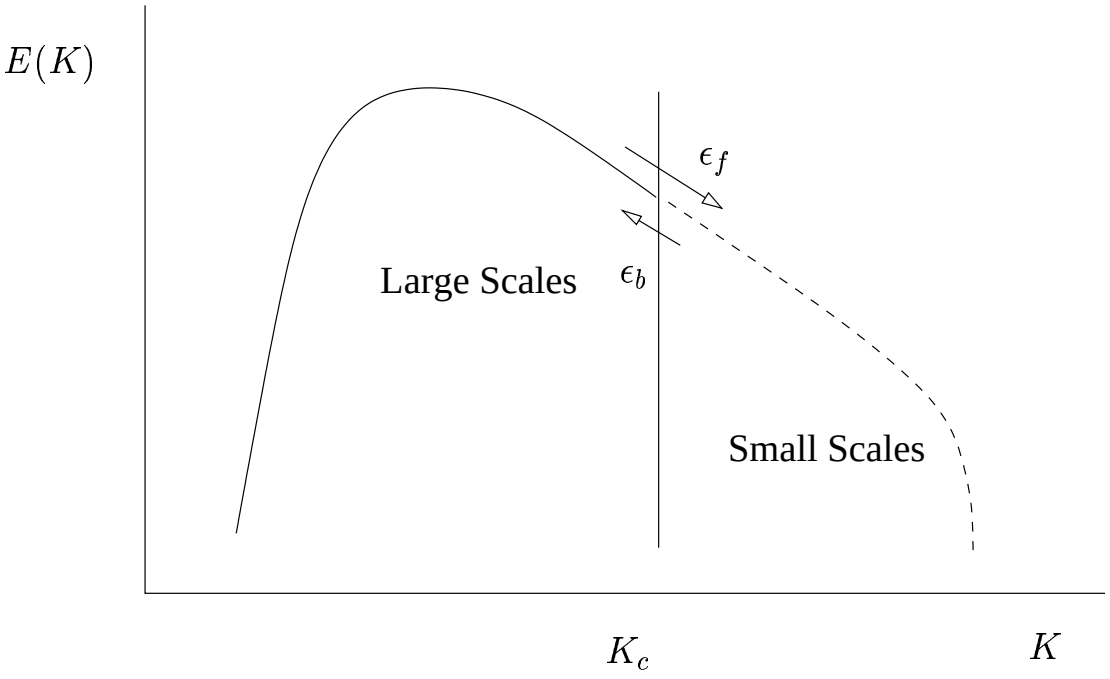

Figure 4.1: Schematic representation of the LES approach. The large scales are resolved and the small scales as well as the spectral fluxes have to be modeled.

4.3 Subgrid modelling

4.3.1 The eddy-viscosity closure assumption for LES

The most common way to represent the effect of turbulent fluctuations on the mean velocity field is the so-called Boussinesq closure assumption. The interaction between the fluctuating and mean fields is herein represented by an eddy viscosity. This concept was extended to LES, leading to the following model for the subgrid stress:

$$\tau_{ij}^{sg} - \frac{1}{3}\tau_{kk}^{sg}\delta_{ij} = -2\nu_e \tilde{S}_{ij} \tag{4.8}$$

with

$$\tilde{S}_{ij} = \frac{1}{2}\left(\frac{\partial \tilde{u}_i}{\partial x_j} + \frac{\partial \tilde{u}_j}{\partial x_i}\right) \tag{4.9}$$

The trace of τ_{ij}^{sg} is absorbed into the pressure term in equation (4.3). One can similarly introduce an eddy diffusivity for the subgrid scalar flux:

$$g_{u_i\theta}^{sg} = -2\alpha_e \frac{\partial \tilde{\theta}}{\partial x_i} \tag{4.10}$$

The eddy viscosity models most widely used are the Smagorinsky model [73] and more recently its dynamic formulation by Germano *et al.* [74].

4.3.2 The spectral eddy viscosity

In homogeneous turbulence, where (pseudo-)spectral methods are generally applied, one can more advantageously use a spectral formulation of the eddy viscosity, easily compatible with those methods. To understand the idea of a spectral eddy viscosity, we write the equation for the resolved part of the isotropic energy spectrum in Fourier space:

$$\frac{\partial E^{<}(K)}{\partial t} = T^{<}(K) + T^{>}(K) + 2\nu K^2 E^{<}(K) \tag{4.11}$$

This is the usual Lin equation, except that we splitted the non-linear transfer into $T^{<}(K)$, a part entirely resolved by the simulation and $T^{>}(K)$ a part that involves scales smaller than the filter size and, therefore, interactions between small and large scales. If we would assume the small scales to be isotropic it is reasonable to assume that we can model the effect of the latter by an eddy-viscosity (in the following we omit the superscript $<$ on the energy spectrum):

$$T^{>}(K) = 2\nu_e K^2 E(K) \tag{4.12}$$

with ν_e in the ideal case independent of the wavenumber K. The use of such a subgrid model was partially supported by the study of Chollet and Lesieur [52] who showed that in isotropic turbulence the quantity:

$$\frac{T^{>}(K)}{K^2 E(K)} \tag{4.13}$$

was constant in the inertial range and proportional to $\sqrt{E(K_c)/K_c}$, except near the cut-off where (4.13) rises sharply due to local interactions between wavemodes across the cut-off, as predicted by Kraichnan [75]. This effect can be taken into account by adding a *cusp* to the eddy viscosity as proposed by Chollet and Lesieur [52, 76]:

$$\nu_e(K) = \sqrt{\frac{E(K_c)}{K_c}} \left(\frac{1}{6\sqrt{3}\lambda} + 0.4724 \left(\frac{K}{K_c} \right)^{3.742} \right) \tag{4.14}$$

with λ the eddy damping constant in the EDQNM closure for the energy spectrum. The eddy viscosity concept has however some fundamental deficiencies (c.f. Bertoglio [25]). First the fact that the effect of backscatter (energy going from small to large scales) is modeled by a statistically averaged quantity which can not truly represent the instantaneous and local interaction effects. Instantaneous information initially beyond the cut-off can not influence the large scales.

Secondly, the analysis of Chollet and Lesieur [52] was performed for isotropic turbulence. Anisotropy of the small scales can not be correctly predicted. In anisotropic turbulence the backscatter ϵ_b term shows a different degree of anisotropy compared to the drain term ϵ_f in the energy transfer. This difference in anisotropy can not be taken into account by an eddy viscosity , that models the sum of the effects of backscatter and drain together [25]. In rotating turbulence the anisotropy of the small scales is very strong (see for example Liechtenstein *et al.* [77] and Bellet *et al.* [78]), and an eddy-viscosity is bound to give incorrect results in this case. For sheared turbulence Bertoglio [25] showed, using the EDQNM approach, that at low resolution significant errors are introduced by this effect. At higher resolutions these errors are expected to diminish. This is illustrated by the work of Cui *et al.* [79] that shows that the eddy viscosity formulation gives reasonable results in turbulent channel flow. The study of Casciola *et al.* [80] shows that shear has a negligible influence on the spectral cascade in the inertial range.

4.3.3 The spectral eddy diffusivity

To model the subgrid scalar field, the diffusivity is similarly replaced by an eddy diffusivity, assumed to be proportional to the eddy viscosity:

$$\alpha_e(K) = \frac{\nu_e(K)}{Pr_T} \tag{4.15}$$

in which Pr_T is a turbulent Prandtl number that is usually assumed to be equal to 0.6. The eddy-diffusivity assumption was shown to be less reliable than its viscous counterpart. In Rogallo and Lesieur [53] $\alpha_e(K)$ was shown not to exhibit the nice wavenumber independent plateau as did the eddy viscosity for the velocity field. The same discussion about the difficulties in predicting anisotropy as in the previous section could be repeated here. We can for example mention the work of Kang and Meneveau [81] who study experimentally the anisotropy of a scalar field and analyze its implications for subgrid-models.

Especially as we are studying the scalar-velocity cross correlation which is per definition an anisotropic quantity, we should be careful with drawing conclusions from the LES results.

4.3.4 Eddy viscosity and diffusivity based on the Kolmogorov equation

An alternative approach for modeling the subgrid scales was proposed by Shao *et al.* [82] (see also Cui *et al.* [79] and Shao *et al.* [83]). This work still uses the eddy viscosity concept, but expresses its form using the Kolmogorov equation. The model could also be extended towards a tensorial approach. An expression for the Eddy viscosity and diffusivity was derived, based on the Kolmogorov [4] and Yaglom [84] relation for the second-order structure functions $D_{ll}(r)$ and $D_{\theta\theta}(r)$. We will summarize the model here and for details we refer to Cui *et al.* [79] and Shao *et al.* [82, 83].

At high Reynolds numbers, the equation for the resolved part of the velocity structure function, assuming stationarity of the small scales, is:

$$-\frac{4}{5}\epsilon r = \tilde{D}_{lll}(r) - 6T_{l,ll}(r) \tag{4.16}$$

with ϵ the subgrid dissipation; $\tilde{D}_{lll}(r)$ is the resolved part of the third order longitudinal structure function and $T_{l,ll}(r)$,

$$T_{l,ll}(r) = \overline{\tilde{u_1}(x_1)\tau_{11}(x_1+r)} \tag{4.17}$$

is the energy transfer between resolved and unresolved scales.

Similarly, the equation for the resolved part of the scalar structure function reads:

$$-\frac{4}{3}\epsilon_\theta r = \tilde{D}_{\theta\theta l}(r) - 4T_{\theta,\theta l} \tag{4.18}$$

with ϵ_θ the subgrid dissipation of scalar variance; $\tilde{D}_{\theta\theta l}(r)$ is the resolved part of the third order mixed scalar-velocity longitudinal structure function and $T_{\theta,\theta l}$,

$$T_{\theta,\theta l}(r) = \overline{\tilde{\theta}(x_1) g^{sg}_{u\theta}(x_1 + r)\rangle} \tag{4.19}$$

represents the scalar variance transfer between resolved and unresolved scales. Using the eddy viscosity (and diffusivity) concept the subgrid terms are expressed:

$$\tau_{ij}(x) = -2\nu_e \tilde{S}_{ij}(x) \tag{4.20}$$

$$g^{sg}_{u_i\theta}(x) = -2\alpha_e \frac{\partial\tilde{\theta}(x)}{\partial x_i} \tag{4.21}$$

as well as the dissipation and diffusion at high Reynolds number:

$$\epsilon = 2\nu_e \overline{\tilde{S}_{ij}\tilde{S}_{ij}} \tag{4.22}$$

$$\epsilon_\theta = \alpha_e \overline{\frac{\partial\tilde{\theta}}{\partial x_i}\frac{\partial\tilde{\theta}}{\partial x_i}} \tag{4.23}$$

Using the relation between second order correlation and structure functions:

$$\tilde{D}_{ll} = 2\overline{\tilde{u}^2} - 2\overline{\tilde{u}_1(x)\tilde{u}_1(x+r)} \tag{4.24}$$

in equation (4.16) Shao finally expresses the eddy viscosity (details in Cui *et al.* [79]):

$$\nu_e = -\frac{5\tilde{D}_{lll}}{8\overline{\tilde{S}_{ij}\tilde{S}_{ij}}r - 30(\partial\tilde{D}_{ll}/\partial r)} \tag{4.25}$$

and the diffusivity [83]:

$$\alpha_e = -\frac{3\tilde{D}_{\theta\theta l}}{4\overline{\frac{\partial\tilde{\theta}}{\partial x_i}\frac{\partial\tilde{\theta}}{\partial x_i}}r - 6(\partial\tilde{D}_{\theta\theta}/\partial r)} \tag{4.26}$$

An advantage of this eddy diffusivity is that it is not assumed to be proportional to the eddy viscosity at all wavenumbers. Furthermore there is no adjustable parameter in the diffusivity. Shao *et al.* [83] show that the mean value of the turbulent Prandtl number obtained with this model is equal to 0.559. We stress that the turbulent Prandtl number is here a result of the model and not an adjustable parameter.

4.4 Description of the code

The code used for the LES results in the present chapter, as well as for the LES and DNS in chapter 2, is a pseudo spectral code developed by Bertoglio [25] and largely modified by Shao [85]. The time scheme is a second order Adams-Bashford scheme. The calculations were performed at a 128^3 resolution. The subgrid model used for the results in chapter 2 is the Chollet and Lesieur eddy viscosity model [52] for the velocity field with a constant subgrid Prandtl number for the scalar field, assumed to be $Pr_T = 0.6$. The results in section 4.6 and 4.7 are obtained with the model described in the previous section. In the following we will refer to this model as the Shao Structure Function (SSF) Model. All calculations are performed at infinite Reynolds number, ignoring all molecular effects.

4.5 Discussion of the results in chapter 2

4.5.1 Investigation of the effect of the resolution and the subgrid model using the EDQNM closure

In this section we use the EDQNM model to mimic the conditions of the LES performed in chapter 2 and then we use the model to analyze in detail the LES results. The advantage of EDQNM is that it is not restricted to low resolutions. To analyze the LES of the first chapter, the Chollet-Lesieur subgrid model, equation (4.14), is used in the EDQNM calculations as well as a constant turbulent Prandtl number of 0.6. The equations that we solve are:

$$\frac{\partial E(K)}{\partial t} = T^{<}(K) + 2\nu_e K^2 E(K) \tag{4.27}$$

and

$$\frac{\partial}{\partial t} F_{w\theta}(K)^{<} + (\nu_e + \nu_e Pr_t^{-1}) K^2 F_{w\theta}(K)^{<} = P^{<}(K) + T_{w\theta}^{NL<}(K) + \Pi^{<}(K) \tag{4.28}$$

For $K < K_c$, the non-linear transfer $T_{w\theta}^{NL<}(K)$ and pressure term $\Pi^{<}(K)$ are defined as in the rest of this manuscript with the difference that all interactions involving wavenumbers larger than K_c are set equal to zero. In the following we will also omit the superscript $<$ on the scalar flux spectrum.

We force the spectrum by maintaining a constant K^4 forcing range at the lowest wavenumbers of the energy spectrum $E(K)$. That is: we fix the kinetic energy at the first wavenumber $E(K_1)$. The second wavenumber is fixed at a value:

$$E(K_2) = E(K_1) \left(\frac{K_2}{K_1} \right)^4, \tag{4.29}$$

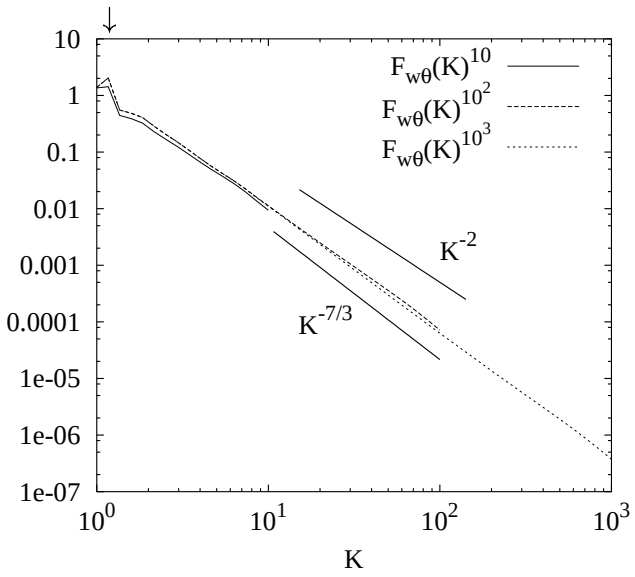

Figure 4.2: For three different resolutions we show the scalar flux spectrum as a result of EDQNM calculations for a velocity field forced at the first two wavenumbers and a Chollet-Lesieur subgrid model. The little arrow indicates the forced wavenumber K_f

and so on up to K_f, where the maximum of the forcing range is attained. In this range the values of $E(K)$ remain constant during the calculation. The rest of the spectrum can freely evolve.

We define the resolution R of our calculation,

$$R = \frac{K_c}{K_1}, \tag{4.30}$$

as the ratio of cut-off wavenumber to first wavenumber. This resolution R will be used as a superscript to the different spectra. In the following:

$$F_{w\theta}(K)^R$$

will mean the $F_{w\theta}(K)$ spectrum as a result of a calculation with resolution R.

The resolution is varied and the steady state results are shown in figure 4.2. The little arrow indicates the forced wavenumber K_f. In this representation it is not easy to draw conclusions about the spectral slope. The same data is therefore shown in compensated form in figure 4.3. The spectra are multiplied by K^2 and $K^{7/3}$ respectively. The following observations can be made:

- For all three spectra the first wavenumber decade ($K \leq 10$) shows a power law behaviour. In the case of the lowest resolution, $R = 10$,

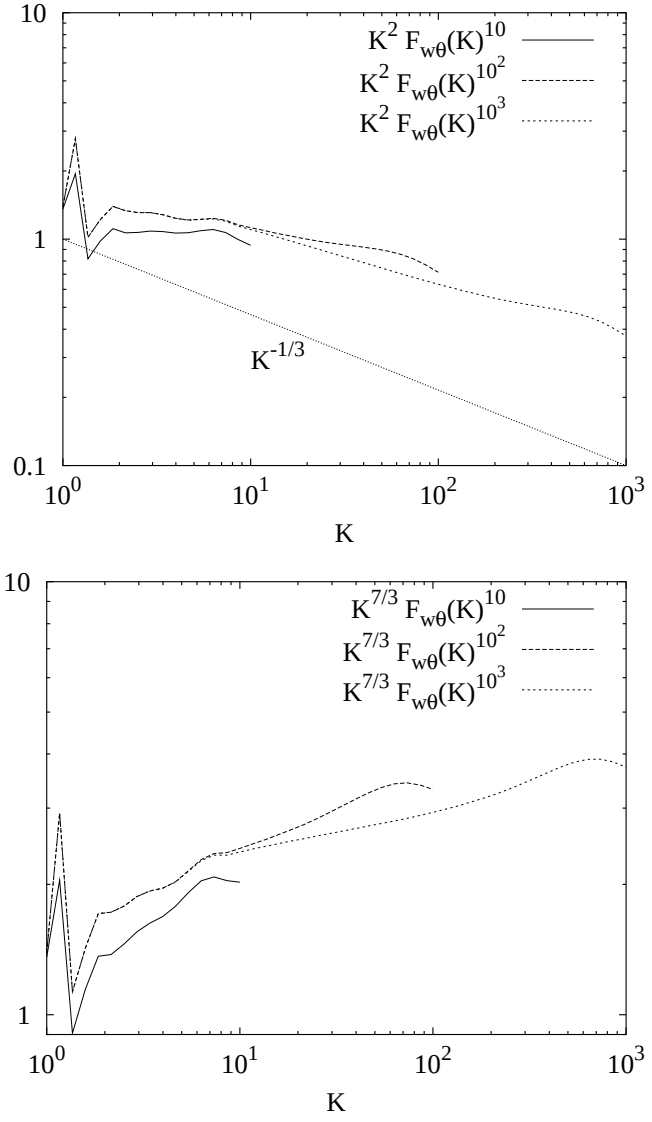

Figure 4.3: Same as in figure 4.2 but compensated by K^2 (top) and $K^{7/3}$ (bottom).

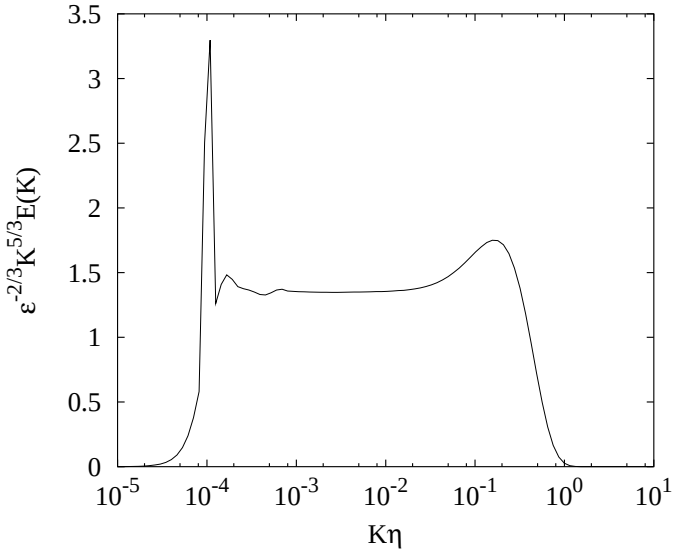

Figure 4.4: Forced turbulence, $R_\lambda = 2400$ compensated kinetic energy spectrum

the spectrum compensated by K^2 shows a neat plateau between the forcing wavenumber and the cut-off: the slope of this wavenumber zone is -2 for this resolution. For the two other spectra this zone is slightly steeper.

- The slope of the spectra at $R = 100$ and $R = 1000$ increases beyond this first decade. Even for a resolution of 1000, the slope is not equal to $K^{-7/3}$ and we observe a similar slow tendency towards $K^{-7/3}$ as for the complete EDQNM calculation between the Reynolds number and the slope as shown in the previous chapter (figure 3.11).

- Comparing the spectra at a resolution of 100 and 1000 in fig. 4.3 we note that the spectral cut-off and subgrid model affect approximately the entire last decade of the spectra.

Apparently, in this particular situation, i.e. forced LES using the Chollet-Lesieur subgrid model and a constant turbulent Prandtl number, the $-7/3$ slope will probably not appear, unless calculations at very large resolutions are performed. The K^{-2} behaviour is not observed either, except close to the forcing frequency where the slope is close to -2.

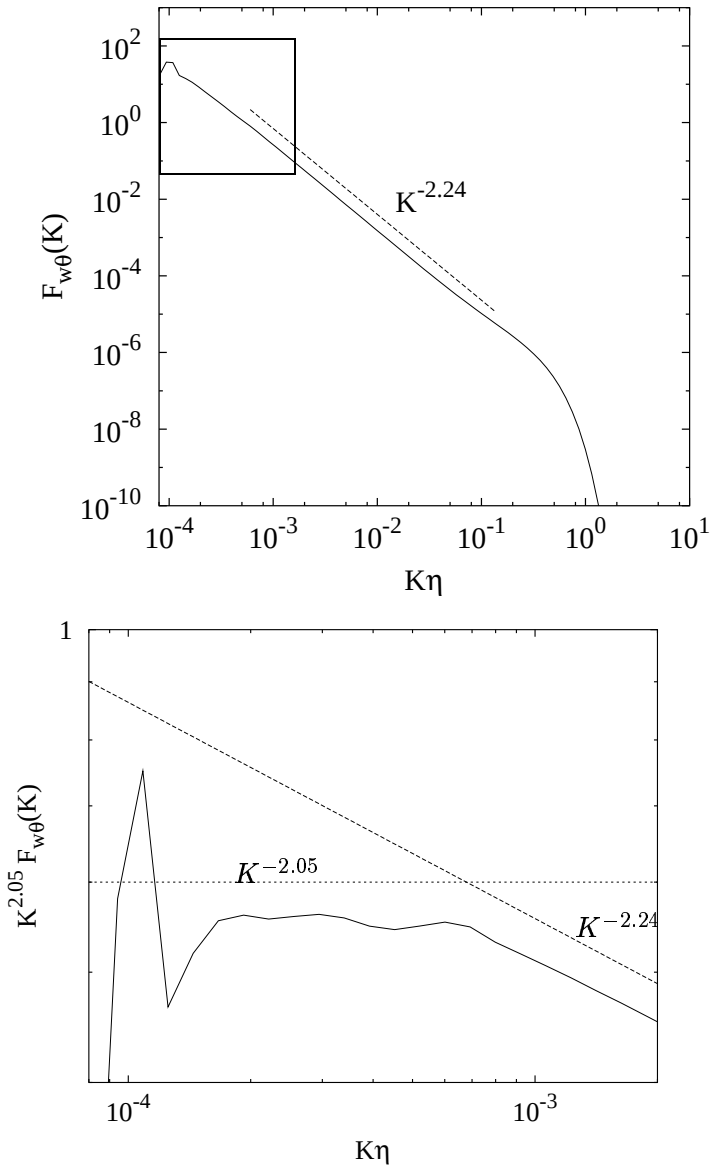

Figure 4.5: Forced turbulence $R_\lambda = 2400$. Top: uncompensated scalar flux spectrum. Bottom: zoom of the region influenced by forcing compensated by $K^{2.05}$.

4.5.2 The influence of forcing on the inertial range in a fully resolved EDQNM calculation

We just saw the effect of the resolution, together with the effect of forcing and a subgrid model, we will now investigate the effect of forcing separately. Again we force the spectrum by maintaining a constant K^4 forcing range in the low wavenumbers, up to a wavenumber K_f. Contrary to the last section, we perform a full EDQNM calculation (without subgrid model). The calculation is performed at a (arbitrarily chosen) $R_\lambda = 2400$. At this Reynolds number we find an inertial range for over two wavenumber decades of the energy spectrum and the inertial range of the scalar flux spectrum at this Reynolds should be significantly steeper than -2 (around -2.24 as can be concluded from figure 3.11).

We first show the compensated energy spectrum in 4.4. This spectrum shows a large peak at the forcing frequency, and also a clear $K^{-5/3}$ range, starting immediately after the forcing frequency.

For the scalar flux spectrum the situation is quite different as can be observed in figure 4.5. We also show a zoom of the low-wavenumber zone. The peak is present, the -2.24 slope as well, but in between we also observe a significantly large zone with a slope close to -2 (we observe a slope of -2.05). It seems that the peak in the energy spectrum, induced by the forcing, is responsible for a zone in the scalar flux spectrum with a slope equal or close to -2.

We can try to explain the observed behaviour of the wavenumber spectrum by a dimensional analysis. We first consider the energy spectrum in figure 4.4. The large peak in the energy spectrum corresponds to one or more wavemodes that are largely dominant in their spectral vicinity. We could connect this mode to spatial structures, or eddies, with size $\sim K_f^{-1}$. In the range where these eddies are dominant compared to the 'local' eddies of size $\sim K^{-1}$, we will not observe the inertial behaviour, governed by ϵ and K. The parameters in this range will rather be determined by the typical velocity scale $\mathcal{U}_f$ of the forcing frequency and the local wavenumber K so that

$$F_{w\theta}(K) = \Gamma f(\mathcal{U}_f, K) \rightarrow F_{w\theta}(K) \sim \Gamma \mathcal{U}_f K^{-2} \tag{4.32}$$

We note here that also in the paper of Alvelius and Johansson [86] we observe a K^{-2} inertial range for the pressure spectrum that is expected to obey a $K^{-7/3}$ law. Their paper also concerns forced LES results, with the forcing method, isotropically forcing the large wavenumbers, described in Alvelius [87].

4.6 The influence of the forcing on LES

In section 4.5.1, we observed that using the Chollet-Lesieur subgrid model in our EDQNM calculations, the scalar flux spectrum showed slopes shallower than $-7/3$ for low and intermediate resolutions. The slope increases with Reynolds number, but this tendency is slow, as in the full EDQNM calculations of Chapter 3.

In this section we perform LES. The subgrid model that we use is the SSF model discussed in section 4.3.4.

We remove the influence of the forced wavenumbers on the scalar field. To accomplish this we set to zero the scalar flux production by the forced wavemodes. We also remove the contributions to the non-linear transfer that contain the forced wavemodes. Physically we remove from the scalar field all the convective effects due to the forced wavenumbers *i.e.* the scalar field acts as if those modes were zero.

The results are shown in figure 4.6 for the energy, scalar flux and scalar variance spectrum. They all show their expected asymptotic behaviour:

$$\begin{aligned} E(K) &\sim \epsilon^{2/3} K^{-5/3} \\ E_\theta(K) &\sim \epsilon^{-1/3} \epsilon_\theta K^{-5/3} \\ F_{w\theta}(K) &\sim \Gamma \epsilon^{1/3} K^{-7/3} \end{aligned}$$

In figure 4.7 we show the scalar flux spectrum in compensated form. As in chapter 3, the constant $C_{w\theta}$ is of order unity.

4.7 The balance of the different terms in the scalar flux equation

To finish this chapter we analyze the spectra of the different terms that govern the scalar flux spectrum. The results correspond to the LES, performed in the previous section in which the influence of the wavenumber-peak in the energy spectrum on the scalar field is removed and the subgrid-model is the SSF model.

We recall the equation governing the scalar flux spectrum in LES:

$$\begin{aligned} &\frac{\partial}{\partial t} F_{w\theta}(K) + (\nu_e + \alpha_e) K^2 F_{w\theta}(K) = \\ &\qquad P^<(K) + T_{w\theta}^{NL<}(K) + \Pi^<(K) \end{aligned} \tag{4.33}$$

The different terms are shown in fig. 4.8 introducing the notation:

$$V^{SG} = (\nu_e + \alpha_e) K^2 F_{w\theta}(K) \tag{4.34}$$

This eddy-viscous term is small except near the cut-off. The non linear transfer is negative at small K and positive at large K. The pressure is a

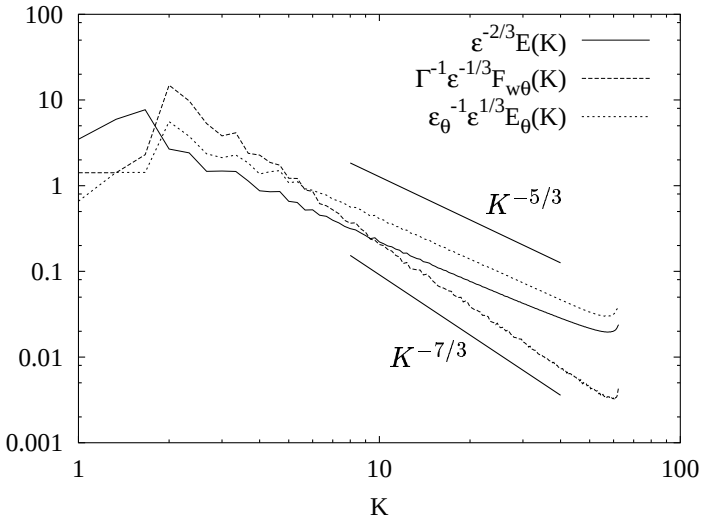

Figure 4.6: The kinetic energy, scalar flux and scalar variance spectrum calculated with the SSF model after exclusion of the effect of the first two wavenumbers of the energy spectrum on the scalar field

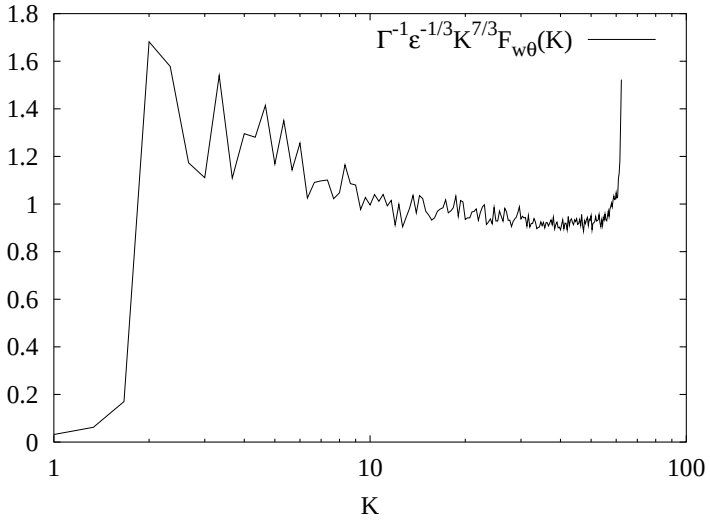

Figure 4.7: The scalar flux as in figure 4.6, but in compensated form.

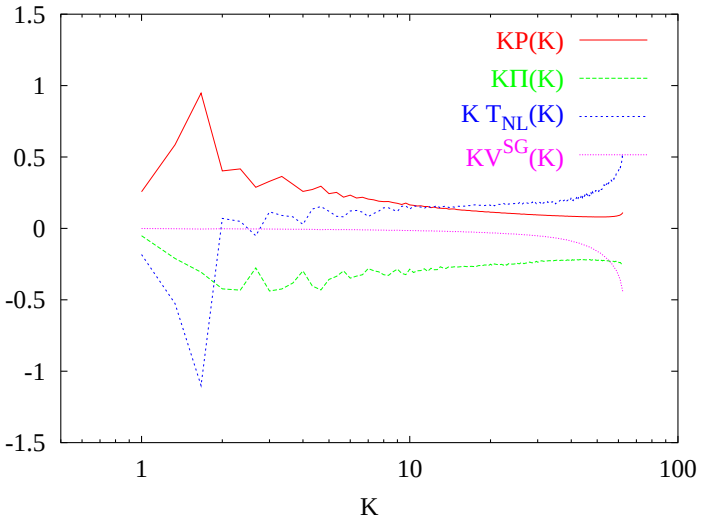

Figure 4.8: Spectral balance of the production, non-linear transfer, pressure and subgrid dissipation of scalar flux.

destructive term and the production is positive. In section 1.2.2, we decomposed the transfer term into two contributions. Subsequently, in chapter 3, we used the assumption that in the stationary case at small wavenumbers for large Reynolds:

$$\begin{aligned} P(K) &= -\left[T_{w\theta}^{NL}(K)\right]_{\theta} \\ \left[T_{w\theta}^{NL}(K)\right]_{U} &= -\Pi(K) \end{aligned} \tag{4.35}$$

In figure 4.9 we verify this result and observe excellent agreement for practically the whole spectrum: LES supports the assumption made when choosing the constants in the eddy damping term in section 3.3.

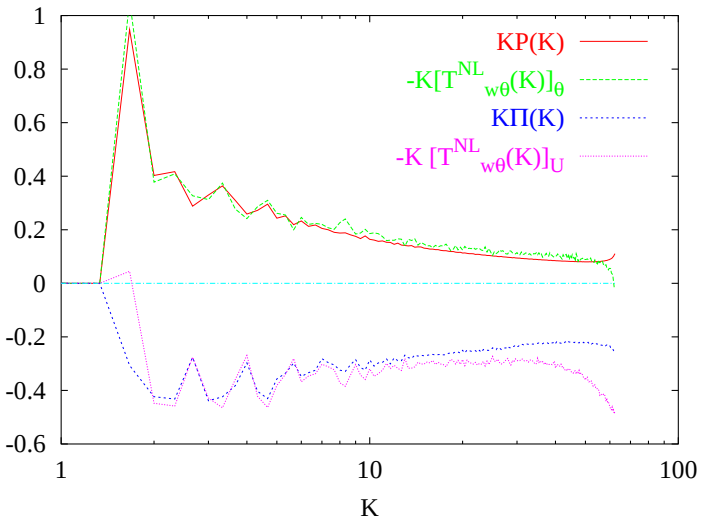

Figure 4.9: Spectral balance of the two contributions to the non-linear transfer and the production and pressure term in the scalar flux equation.

Chapter 5

Scalar mixing in uniformly sheared turbulence

In chapter 3 we found good agreement between the EDQNM theory and results from DNS and experiments in the case of isotropic turbulence with a uniform scalar gradient. In the present chapter we will apply the same theory to describe homogeneous shear flow. We choose to model the spherically averaged spectra of the scalar flux and variance spectra. The mean velocity gradient then introduces unclosed terms in the spectral evolution equations. These terms will be modelled by tensor invariant theory. A detailed comparison is performed with experimental results.

5.1 Introduction

Homogeneous turbulence subjected to uniform shear is one of the classical problems in turbulence. As shear appears in almost all practical flows in geophysical studies as well as in industrial applications, its understanding is a fundamental need in the development of turbulence models. The mixing of a scalar in a turbulent shear flow might even be of more practical importance. To date, the understanding of both shear flow and a sheared scalar field is not complete, partially because of the practical difficulties in generating a homogeneous shear flow in laboratory experiments and partially because of computational limitations in direct numerical simulations. The understanding and modelling of mixing of pollutant, temperature or concentration fluctuations in the presence of shear remains a challenging issue.

The first nearly homogeneous shear flow was generated by Rose [88]. Improvements of this flow by various authors led to the experimental setup by Karnik and Tavoularis [89]. The different aspects of this flow were studied in the work of Tavoularis and Karnik [90] and the paper of Tavoularis [91]. A mean temperature gradient was added to this flow and the behaviour

of the temperature fluctuations was studied in the works of Tavoularis and Corrsin [92, 93, 94]. The diffusion of heat from a line source in homogeneous shear flow was investigated by Karnik and Tavoularis [95]. The Taylor scale Reynolds number R_λ in these flows was estimated around 150.

Information at higher R_λ can be obtained by atmospheric measurements. These flows, although generally subject to shear can not at all be considered to be subject to a uniform shear. The Reynolds number in these flows is typically within the range $10^3 < R_\lambda < 10^4$ (see for example the paper of Bradley *et al.* [96]). A major problem with atmospheric experiments are the difficultly predictable and uncontrolable meteorological conditions. The mean shear can not be kept constant over a time interval and the initial and boundary conditions are not easily controlable by the experimentalist.

Exactly the opposite is the case with direct numerical simulations (DNS): the initial conditions as well as the boundary conditions are entirely determined by the scientist or engineer. The limits of those 'numerical experiments' are only dependent on the available computer power. Those computational limits restricted the DNS study of Rogers *et al.* [97] to a $R_\lambda \approx 40$. This Reynolds number limitation can be removed by performing Large Eddy Simulations (LES) in which only the large scales are resolved. We mention the work of Kaltenbach *et al.* [98]. The problem of filtering and subgrid modelling was discussed in the case of isotropic turbulence in chapter 4. An additional problem in homogeneous shear flow is that the integral length-scale increases monotonically[1] so that sooner or later its size will become superior to the computational domain.

In this chapter we study scalar mixing in homogeneous shear flow. By using the EDQNM approach and some additional modelling hypotheses we intend to fill up, at least partially, the gap between the low Reynolds number experiments and atmospheric measurements. We also try to provide answers or at least insights into three particular questions: why show the atmospheric measurements of Kaimal *et al.* [33] and Kader and Yaglom [34] of the horizontal heat flux spectrum an inertial slope of 2.5 instead of the K^{-3} scaling as proposed by Wyngaard and Coté [32]? Why find Antonia and Zhu [99] for this same spectrum a $K^{-5/3}$ slope? What is the influence of the mean shear on the scalar variance and its spectral distribution?

In the following we will discuss and derive, where necessary, the models needed to simulate a scalar field in the presence of mean shear. The basis ingredient of this model is the EDQNM theory to represent the non-linear transfer. The formulation of the closure as derived and validated for isotropic turbulence in chapter 3 will be used. In the case of a fluctuating scalar field produced by the interaction of an isotropic turbulence with a mean scalar field, there is an exact relation between the 3D spectrum $\mathcal{F}_{u_i\theta}(\boldsymbol{K})$ and its

[1] and much faster than in the case of isotropic turbulence

integral over a sphere with radius K (Herr *et al.* [20]):

$$\mathcal{F}_{u_i\theta}(\boldsymbol{K}) \sim (1-\mu^2)F_{u_i\theta}(K) \tag{5.1}$$

with μ the cosine of the angle between the scalar gradient axis and the wavevector. In the presence of shear (5.1) does not hold anymore; nor the spectral tensor Φ_{ij} can be expressed exactly as a function of the wavenumber only. A full EDQNM approach of the problem would then require to build and numerically integrate a wavevector dependent closed set of equations. In order to simplify the numerical task that would result of this complete approach, we integrate the equation over spherical shells with radius K to obtain the variable:

$$F_{u_i\theta}(K,t) = \iint_{\Sigma K} \mathcal{F}_{u_i\theta}(\mathbf{K},t)d\Sigma K \tag{5.2}$$

The main quanities in this chapter are then the spherically averaged spectra: $\varphi_{ij}(K,t)$, $E_\theta(K,t)$ and $F_{u_i\theta}(K,t)$. For the velocity field, the approach of considering and modelling only the spherically averaged spectra, was introduced by Cambon *et al.* [24]. The averaging procedure introduces unclosed terms in the equations of $\varphi_{ij}(K,t)$, $E_\theta(K,t)$ and $F_{u_i\theta}(K,t)$. The unclosed terms that are related to the interaction with the mean velocity field (linear transfer and rapid pressure terms) are modelled by tensor invariant theory. The non-linear terms are modeled by EDQNM theory with additional assumptions about the anisotropy of the spectra.

We will validate the resulting model by comparison with experimental results and apply it to different situations, ranging from low Reynolds numbers, attainable by DNS and laboratory experiments, upto Reynolds numbers that represent the highest Reynolds numbers observed in atmospheric measurements.

5.2 Modelling the velocity field

We recall here the equation for the spectral tensor $\Phi_{ij}(\boldsymbol{K},t)$ in homogeneously sheared turbulence that can be found in the work of Craya [100] or Cambon *et al.* [24]:

$$\begin{aligned}\left[\frac{\partial}{\partial t}+2\nu K^2\right]\Phi_{ij} + \frac{\partial \overline{U}_i}{\partial x_l}\Phi_{lj} + \frac{\partial \overline{U}_j}{\partial x_l}\Phi_{il} = \\ +\frac{\partial \overline{U}_l}{\partial x_n}\frac{\partial K_l\Phi_{ij}}{\partial K_n} + 2\frac{\partial \overline{U}_l}{\partial x_n}\left(\frac{K_lK_i}{K^2}\Phi_{nj}+\frac{K_lK_j}{K^2}\Phi_{in}\right) \\ +P_{il}(\mathbf{K})K_nT_{lnj}+P_{lj}(\mathbf{K})K_nT^*_{lni}\end{aligned} \tag{5.3}$$

in which $\Phi_{ij}=\Phi_{ij}(\mathbf{K},t)$ is a function of the wavevector. The T_{ijk} terms express the non-linear interaction involving triple velocity correlations. These terms are unclosed.

As proposed by Cambon *et al.* [24], we can reduce the computational cost of resolving this equation by integrating the spectral tensor over spherical shells with radius K, the wavenumber. The variable then becomes:

$$\varphi_{ij}(K,t) = \iint_{\Sigma k} \Phi_{ij}(\mathbf{K},t) d\Sigma K \tag{5.4}$$

involving one spatial variable K instead of the three-dimensional wavevector $\mathbf{K}$. The equation for $\varphi_{ij}(K,t)$ reads:

$$\left[\frac{\partial}{\partial t} + 2\nu K^2\right]\varphi_{ij} + \frac{\partial \overline{U}_i}{\partial x_l}\varphi_{lj} + \frac{\partial \overline{U}_j}{\partial x_l}\varphi_{il} = T_{ij}^L(K) + \Pi_{ij}^L(K) + T_{ij}^{NL}(K) \tag{5.5}$$

The T_{ijk} terms representing the non-linear interactions are non-closed terms in equation (5.3). After integration over wavenumber shells the other terms on the right hand side of equation (5.5), the linear transfer $T_{ij}^L(K)$ and rapid pressure term $\Pi_{ij}^L(K)$, have to be modeled as well. The modelling of the $\varphi_{ij}(K,t)$ equation is not the subject of the present work and we will use the model proposed by Touil [1]. The model is briefly resumed in appendix B.

5.3 Modelling the scalar flux spectrum

In homogeneously sheared turbulence with a mean scalar gradient we can derive an equation for the scalar flux spectrum.

$$\begin{aligned}\left[\frac{\partial}{\partial t} + (\nu+\alpha)K^2\right]\mathcal{F}_{u_i\theta} + \frac{\partial \overline{U}_i}{\partial x_j}\mathcal{F}_{u_j\theta} + \frac{\partial \Theta}{\partial x_j}\Phi_{ij} = \\ + \frac{\partial \overline{U}_l}{\partial x_n}\frac{\partial K_l \mathcal{F}_{u_i\theta}}{\partial K_n} + 2\frac{\partial \overline{U}_n}{\partial x_j}\frac{K_i K_n}{K^2}\mathcal{F}_{u_j\theta} \\ -iK_n\left(T_{\theta in} - T^*_{\theta in}\right) + i\frac{K_i K_n K_j}{K^2}T_{\theta jn}\end{aligned} \tag{5.6}$$

as for the velocity field, $\mathcal{F}_{u_j\theta}$ is a function of the wavevector and time. We similarly integrate the equation to obtain the variable:

$$F_{u_i\theta}(K,t) = \iint_{\Sigma k} \mathcal{F}_{u_i\theta}(\mathbf{K},t) d\Sigma K \tag{5.7}$$

Integration yields the following equation:

$$\left[\frac{\partial}{\partial t} + (\nu+\alpha)K^2\right]F_{u_i\theta}(K) + \frac{\partial \overline{U}_i}{\partial x_j}F_{u_j\theta}(K) + \frac{\partial \Theta}{\partial x_j}\varphi_{ij}(K) = T_{i\theta}^L(K) + \Pi_{i\theta}^L(K) + T_{i\theta}^{NL}(K) + \Pi_{i\theta}(K) \tag{5.8}$$

The terms on the left hand side of this equation do not require modelling: the dissipation and the production by shear and the mean scalar gradient respectively are exact. On the RHS we find similar terms as for the velocity field[2]. They are now explicited and modeled.

Rapid Pressure

The rapid pressure is:

$$\Pi_{i\theta}^L = 2\frac{\partial \overline{U}_n}{\partial x_j}\int_{\Sigma_K}\frac{K_i K_n}{K^2}\mathcal{F}_{u_j\theta}d\Sigma K = 2\frac{\partial \overline{U}_n}{\partial x_j}\int_{\Sigma_K} H_{in}^j d\Sigma K \tag{5.9}$$

We will model the term H_{in}^j assuming that it can be represented as an isotropic tensorial function of $F_{u_i\theta}$ and $\alpha_i = K_i/K$. We find the model (as shown below):

$$\Pi_{i\theta}^L = (12A^L - 4)\frac{\partial \overline{U}_i}{\partial x_j}F_{u_j\theta} - (8A^L - 3)\frac{\partial \overline{U}_j}{\partial x_i}F_{u_j\theta} \tag{5.10}$$

We use the theory of representation by tensorial isotropic functions (as in Eringen [101] or Schiestel [102]). We propose the form:

$$\begin{aligned} H_{in}^j &= A\delta_{in}F_{u_j\theta} + B^I\delta_{ij}F_{u_n\theta} + B^{II}\delta_{jn}F_{u_i\theta} \\ &+C\alpha_i\alpha_n F_{u_j\theta} + D^I\alpha_i\alpha_j F_{u_n\theta} + D^{II}\alpha_j\alpha_n F_{u_i\theta} \end{aligned} \tag{5.11}$$

This expression needs to satisfy three conditions:

- Symmetry in α: $H_{in}^j = H_{ni}^j$. This condition yields $B^I = B^{II} = B$ and $D^I = D^{II} = D$
- Continuity: $H_{ij}^j = 0$. This gives $A + 4B + D = 0$ and $C + D = 0$
- The definition of $F_{u_j\theta}$:

$$\int_{\Sigma_K} H_{ii}^j d\Sigma K = \int_{\Sigma_K}\frac{K_i K_i}{K^2}\mathcal{F}_{u_j\theta}d\Sigma K = \int_{\Sigma_K}\mathcal{F}_{u_j\theta}d\Sigma K = F_{u_j\theta} \tag{5.12}$$

This last constraint yields the equation: $3A + 2B + C + 2D = 1$. The integrals of the angular moments can be calculated as in Cambon *et al.* [68]:

[2]The slow pressure $\Pi_{i\theta}(K)$ is separated from the nonlinear transfer term, like in the rest of this manuscript. In equation (5.5) for φ_{ij} the nonlinear term is not explicitly written. It is part of $T_{ij}^{NL}(K)$.

$$\int_{\Sigma_K} \frac{K_i K_n}{K^2} d\Sigma K = \delta_{in} \tag{5.13}$$

We can now explicit equation (5.9), calling the constant $A = A^L$.

In Schiestel [102] the same approach is followed for one point modelling of the turbulent flux. In their work only A and B are non-zero in equation (5.11) giving for the rapid pressure term:

$$\Pi^L_{i\theta} = \frac{4}{5}\frac{\partial \overline{U}_i}{\partial x_j} F_{u_j\theta} - \frac{1}{5}\frac{\partial \overline{U}_j}{\partial x_i} F_{u_j\theta} \tag{5.14}$$

We find the same expression if we substitute in expression (5.10) for A^L the value $2/5$. It is reasonable to expect that the value of A^L in our model should be close to this value.

Linear Transfer

Cambon *et al.* [24, 69] derived a model for the linear transfer of kinetic energy. The constant intervening in this model was related to the constant in the model for the rapid pressure as discussed in the last section.

The linear transfer is represented by:

$$T^L_{i\theta} = \frac{\partial \overline{U}_n}{\partial x_j} \int_{\Sigma_K} \frac{\partial K_n \mathcal{F}_{u_i\theta}}{\partial K_j} d\Sigma K \tag{5.15}$$

The linear transfer term has been described in appendix **??** for the velocity field and could be modelled in a similar way:

$$T^L_{i\theta}(K) = A^{TL}\sqrt{S_{ij}S_{ij}}\frac{\partial K F_{u_i\theta}}{\partial K} \tag{5.16}$$

with A^L to be determined by comparison with experiments. We will however follow another procedure. We rewrite eq. (5.15) (see also Clark and Zemach [103]):

$$T^L_{i\theta} = \frac{\partial \overline{U}_n}{\partial x_j}\frac{\partial}{\partial K}\int_0^K \int_{\Sigma_K} \frac{\partial K_n \mathcal{F}_{u_i\theta}}{\partial K_j} d\Sigma K dK \tag{5.17}$$

noticing that the two integrals together can be rewritten as an integral over the volume of a sphere with radius K:

$$\int_0^K \int_{\Sigma_K} d\Sigma K dK = \int_{V(\Sigma_K)} dV \tag{5.18}$$

and rewriting:

$$\frac{\partial}{\partial K_j} = \frac{\partial}{\partial K_l}\delta_{lj}, \tag{5.19}$$

we write (5.17) as:

$$T^L_{i\theta} = \frac{\partial \overline{U}_n}{\partial x_j}\frac{\partial}{\partial K}\int_{V(\Sigma_K)} \frac{\partial}{\partial K_l}\delta_{lj}K_n\mathcal{F}_{u_i\theta}dV \tag{5.20}$$

With the divergence theorem of Gauss, we can rewrite this volume integral of the divergence as a surface integral involving the outer vector K_j/K:

$$\begin{aligned} T^L_{i\theta} &= \frac{\partial \overline{U}_n}{\partial x_j}\frac{\partial}{\partial K}\int_{\Sigma_K} \frac{K_j}{K}K_n\mathcal{F}_{u_i\theta}d\Sigma K \\ &= \frac{\partial \overline{U}_n}{\partial x_j}\frac{\partial}{\partial K}K\int_{\Sigma_K} \frac{K_jK_n}{K^2}\mathcal{F}_{u_i\theta}d\Sigma K \\ &= \frac{\partial \overline{U}_n}{\partial x_j}\frac{\partial}{\partial K}K\int_{\Sigma_K} H^i_{jn}d\Sigma K \end{aligned} \tag{5.21}$$

with H^i_{jn} defined and modeled as in the last section for the rapid pressure. Our model for the linear transfer reads then:

$$T^L_{i\theta} = \left(\frac{3}{2} - 4A^L\right)\left(\frac{\partial \overline{U}_i}{\partial x_j} + \frac{\partial \overline{U}_j}{\partial x_i}\right)\frac{\partial}{\partial K}KF_{u_j\theta}(K) \tag{5.22}$$

Non linear transfer and non linear pressure

In the presence of shear the non linear transfer and pressure term can not be expressed exactly as a function of the wavenumber only. A full EDQNM approach of the problem would then require to build and numerically integrate a wavevector dependent closed set of equations. This approach is complex and numerically expensive. We will therefore treat the non-linear transfer and slow pressure term with the EDQNM model as derived in chapter 3. Even though the closure was derived for isotropic turbulence with a mean scalar gradient we will use it here in the case of an anisotropic velocity field. Obviously this approach is not rigorous and has to be seen as an approximation.

5.4 Modelling the scalar variance spectrum

For the scalar (variance) spectrum one can derive:

$$\left[\frac{\partial}{\partial t} + 2\alpha K^2\right] \Phi_\theta + \frac{\partial \Theta}{\partial x_j}\mathcal{F}_{u_j\theta} =$$
$$\frac{\partial \overline{U}_l}{\partial x_n}\frac{\partial K_l \Phi_\theta}{\partial K_n} - iK_n\left(T_{\theta\theta n} - T^*_{\theta\theta n}\right) \tag{5.23}$$

with $\mathcal{F}_{u_j\theta}(\mathbf{K}, t)$ the spectrum of the velocity scalar cross-correlations. Once again we integrate over wavenumber shells:

$$E_\theta(K,t) = \iint_{\Sigma k} \Phi_\theta(\mathbf{K},t) dA(\mathbf{K}) \tag{5.24}$$

and similarly we need to model the right hand side of the resulting equation:

$$\left[\frac{\partial}{\partial t} + 2\alpha K^2\right] E_\theta(K) + \frac{\partial \Theta}{\partial x_j} F_{u_j\theta}(K) = T^L_\theta(K) + T^{NL}_\theta(K) \tag{5.25}$$

Linear Transfer

The linear transfer, integrated over spherical shells can be rewritten (see also section 5.3):

$$T^L_\theta(K) = \int_\Sigma \frac{\partial \overline{U}_l}{\partial x_n}\frac{\partial K_l \Phi_\theta}{\partial K_n} dA(\mathbf{K}) = \frac{\partial \overline{U}_l}{\partial x_n}\frac{\partial}{\partial K} K \int_{\Sigma K} \frac{K_l K_n}{K^2}\Phi_\theta dA(\mathbf{K})$$
$$= \frac{\partial \overline{U}_l}{\partial x_n}\frac{\partial}{\partial K} K \int_{\Sigma K} H_{ln} dA(\mathbf{K}) \tag{5.26}$$

In the case of homogeneous shear,

$$\frac{\partial \overline{U}_1}{\partial z} = S\delta_{l1}\delta_{n3}, \tag{5.27}$$

we can, introducing spherical coordinates

$$K_1 = K sin\theta\ cos\phi, \quad K_2 = K sin\theta\ sin\phi, \quad K_3 = K cos\theta$$
$$\int_{\Sigma K} dA(\mathbf{K}) = \int_0^\pi \int_0^{2\pi} K^2 sin\theta\ d\phi\ d\theta, \tag{5.28}$$

rewrite expression 5.26 as:

$$S\frac{\partial}{\partial K} K \int_{\Sigma K} \frac{K_1 K_3}{K^2}\Phi_\theta(\mathbf{K}) dA(\mathbf{K}) = \tag{5.29}$$
$$S\frac{\partial}{\partial K} K \int_0^\pi \int_0^{2\pi} sin\theta\ cos\theta\ K^2 sin\theta\ \Phi_\theta(\mathbf{K}) cos\phi\ d\phi\ d\theta \tag{5.30}$$

As long as $\Phi_\theta(\mathbf{K})$ is not a function of ϕ, thus in the isotropic case and even in the case that $\Phi_\theta(\mathbf{K})$ is axisymmetrical around the z-axis, the integral is zero. It is therefore justified, at least at small St, to neglect this term. The influence at long time has to be investigated.

We conclude that if we try to model H_{ln} as a function of the isotropic scalar spectrum $E_\theta(K,t)$, it is found that the whole term disappears. We will neglect this linear transfer. As long as $\Phi_\theta(\mathbf{K},t)$ is close to isotropy, this approximation might not introduce a large error.

Non-linear transfer

In the absence of scalar and velocity gradients, the EDQNM expression for the non-linear transfer reads [22]:

$$T_\theta^{NL}(K) = \iint \Theta_\theta^{KPQ} \frac{K}{PQ}(1-y^2)E(Q)\left[K^2E_\theta(P) - P^2E_\theta(K)\right] \tag{5.31}$$

The details of the closure can be found in for example Lesieur [56]. In the case of a non-zero scalar gradient, the non-linear transfer contains terms involving this gradient and an exact EDQNM expression can be found in Herr *et al.* [20]. In the case of sheared turbulence the expression gets even more difficult and the closure has at present not yet been derived for this case. We will neglect the contributions stemming from the mean scalar gradients and shear and we also neglect its spectral anisotropy: we use the isotropic formulation (5.31).

5.5 Final formulation of the model for scalar mixing in homogeneous shear flow

We recall the equations for $\varphi_{ij}(K,t)$, $E_\theta(K,t)$ and $F_{i\theta}(K,t)$ that were discussed and derived in the last three sections. For the velocity field we have the equation:

$$\left[\frac{\partial}{\partial t} + 2\nu K^2\right]\varphi_{ij}(K) + \frac{\partial \overline{U}_i}{\partial x_l}\varphi_{lj}(K) + \frac{\partial \overline{U}_j}{\partial x_l}\varphi_{il}(K) = T_{ij}^L(K) + \Pi_{ij}^L(K) + T_{ij}^{NL}(K) \tag{5.32}$$

with the linear transfer $T_{ij}^L(K)$, rapid pressure $\Pi_{ij}^L(K)$ and nonlinear transfer $T_{ij}^{NL}(K)$ discussed in Touil [1]. The evolution of the scalar flux spectrum is calculated by:

$$\left[\frac{\partial}{\partial t}+(\nu+\alpha)K^2\right]F_{u_i\theta}(K)+\frac{\partial\overline{U}_i}{\partial x_j}F_{u_j\theta}(K)+\frac{\partial\Theta}{\partial x_j}\varphi_{ij}(K)= T^L_{i\theta}(K)+\Pi^L_{i\theta}(K)+T^{NL}_{i\theta}(K)+\Pi_{i\theta}(K) \qquad (5.33)$$

with $\Pi^L_{i\theta}(K)$ given by equation (5.10), $T^L_{i\theta}(K)$ by (5.22) and the nonlinear transfer (and non-linear pressure) as described in chapter 3, equation (3.64). The scalar spectrum evolution equation reads:

$$\left[\frac{\partial}{\partial t}+2\alpha K^2\right]E_\theta(K)+\frac{\partial\Theta}{\partial x_j}F_{u_j\theta}(K)=T^{NL}_\theta(K) \qquad (5.34)$$

with

$$T^{NL}_\theta(K)=\iint\Theta^{KPQ}_\theta\frac{K}{PQ}(1-y^2)E(Q)\left[K^2E_\theta(P)-P^2E_\theta(K)\right].$$

5.6 Results

5.6.1 Model calibration

The velocity field

For a detailed study of the performance of the model-equation for the velocity field (5.32) we refer to Touil [1]. We just want to recall a few results of the model when applied to homogeneous sheared turbulence. The results of the model were compared to the experiments of Tavoularis and Karnik [90] and were found in satisfactory agreement with the asymptotic analysis of Tavoularis [91] for the different quantities. The components of b_{ij}, the dimensionless Reynolds stress-tensor,

$$b_{ij}=\frac{\overline{u_iu_j}}{\overline{q^2}} \qquad (5.35)$$

with $q^2=u^2+v^2+w^2$, tended to constant values in fairly good agreement with the experimental values. The uw-cospectrum showed a $K^{-7/3}$ inertial range and for large St, $\overline{q^2}$ increased exponentially with time. This last issue, has been the subject of the work of Rohr *et al.* [104], who identified $St=4$ as a threshold, and noted that for lower values of St the turbulent kinetic energy decays whereas for larger values it starts to grow. Tavoularis and Karnik [90] found that for $4<St<8$, $\overline{q^2}$ remains approximately constant, and tends to exponential growth for larger St. In figure 5.1 we show the result of the model of Touil for three different Reynolds numbers. The calculations are in good agreement with the experimental observations.

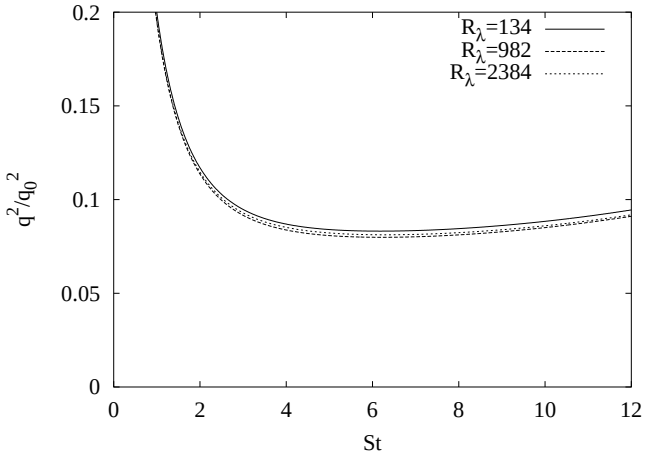

Figure 5.1: Model results for the evolution of the kinetic energy in homogeneous turbulent shear flow. We observe a decay upto $St = 4$, an approximately constant value in between $4 \lesssim St \lesssim 8$, and an increasing value for larger St. The Reynolds numbers are determined at $St = 12$.

The scalar variance

The model for the scalar variance spectrum contains no adjustable constants apart from the EDQNM closure for the non-linear transfer. The two constants are taken equal to their classical 'isotropic' values so that we recover the isotropic formulation in the case of vanishing scalar and velocity gradients.

The scalar flux

The model for the scalar flux spectrum contains three constants. The two EDQNM constants as determined in chapter 3, and the constant A^L that appears in the linear transfer and rapid pressure. This last constant is determined in section 5.6.3 by comparison with DNS and experimental results.

5.6.2 The decay of scalar fluctuations in homogeneous shear flow

In the absence of a mean scalar gradient there is no scalar flux and subsequently no production of scalar fluctuations. This case is thus independent of the choice of the model constant A^L. The case of a homogeneously sheared scalar wihout mean scalar gradient has to our knowledge not been studied experimentally. This was already noticed by Gonzalez [105]. Gonzalez performed a self preservation analysis on the large time decay of the scalar

spectrum in homogeneous shear flow in the absence of mean scalar gradients. His approach consists in looking for self-similar solutions of equation (5.34).

One of the conclusions of this analysisis is that the scalar variance should decay exponentially. In isotropic turbulence this decay obeys a power law. In the absence of experimental data to verify his results he used the data of Karnik and Tavoularis [95] who report measurements of the scalar field behind a line-source in uniform shear flow. Gonzalez conjectures that on the centerline behind the line source the budget of scalar variance reduces to a convection-dissipation equilibrium. In other words the turbulent diffusion can be neglected, and, invoking the Taylor hypothesis, a locally-homogeneous scalar field is observed. Obviously this is not exactly true. Mean scalar gradients might play a role and inhomogeneous effects might be present. However, the exponential decay that Gonzalez proposed fits satisfactorily the experimental data. We recall the expression here:

$$\overline{\theta^2} \sim exp\left(-\alpha \frac{x_\theta}{M}\right) \tag{5.36}$$

with α a constant, equal to 0.037, M the height of one of the 12 shear-generating channels (which is related to the typical initial lengthscale of the turbulent velocity field) and x_θ the downstream distance from the source. The time dependence is recoverered by invoking the Taylor-hypothesis replacing x_θ by $\overline{U}_c t$, with $\overline{U}_c$ the centerline velocity. One can write:

$$\overline{\theta^2} \sim exp\left(-\beta St\right) \tag{5.37}$$

The relation between α and β is subsequently:

$$\beta = \frac{\alpha \overline{U}_c}{MS} \tag{5.38}$$

Using the values M, x_θ and $\overline{U}_c$ from Karnik and Tavoularis [95] we find $\beta = 0.235$. In Gonzalez [105] this exponential function is shown to describe the data for $8.75 < St < 17.5$, where $St = 17.5$ is the limit imposed by the experimental facility.

To simulate this experiment we use a *von Karmann* spectrum [61] to initialize both the energy and scalar spectrum. The shear rate ($47s^{-1}$) and the Reynolds number (varying from $130 < R_\lambda < 160$ in the test section [92]) are taken the same as in the experiment. The result of the calculation is shown in figure 5.2. The decay exponent of the scalar variance is very close to the experimental value, but approaches this decay rate at a somewhat larger St than in the experiment. This difference could perhaps be explained by the difference in initial conditions. The spectral distribution at $St = 0$

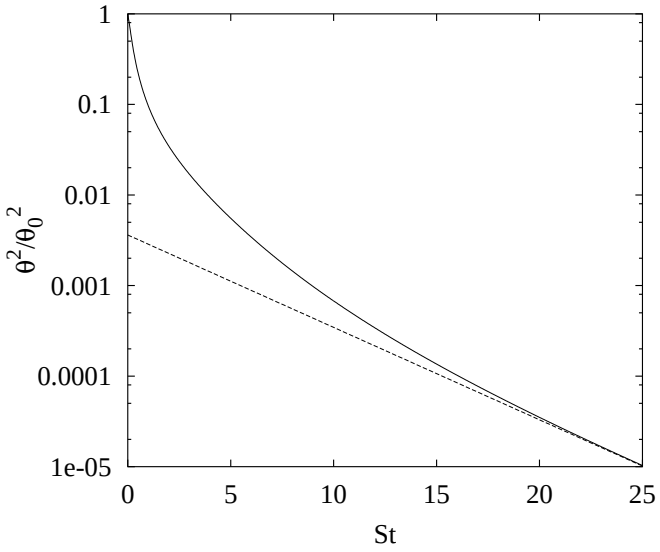

Figure 5.2: Model results for the decay of scalar variance with time in homogeneous turbulent shear flow (solid line). The decay for $St > 8.7$ in the Karnik and Tavoularis experiment [95] obeys an exponential $exp(-0.235St)$. This exponential is also drawn.

in the experiment is not known and might be very different from the *von Karmann* spectrum used in our calculation.

Taking into account that no model constant was adjusted to obtain this result, finding the same exponential decay as in the experiment is an encouraging result. It shows that the influence of the mean shear on the scalar field is at least partially present in the model through the evolution of the energy spectrum that intervenes in the nonlinear transfer of $E_\theta(K)$. A typical scalar spectrum at $St = 15$ is shown in fig. 5.3.

5.6.3 Comparison of one point statistics with experimental results of homogeneous shear flow with a cross-stream mean scalar gradient

To validate our model and to determine the constant A^L, we compare the results of our calculations with the results of previous works using various methods (Experiment, DNS, LES, Rapid Distortion Theory). In all these works we compare with the situation where the shear and scalar gradient are given by

$$S = \frac{\partial \overline{U_x}}{\partial z}, \quad \Gamma = \frac{\partial \Theta}{\partial z}$$

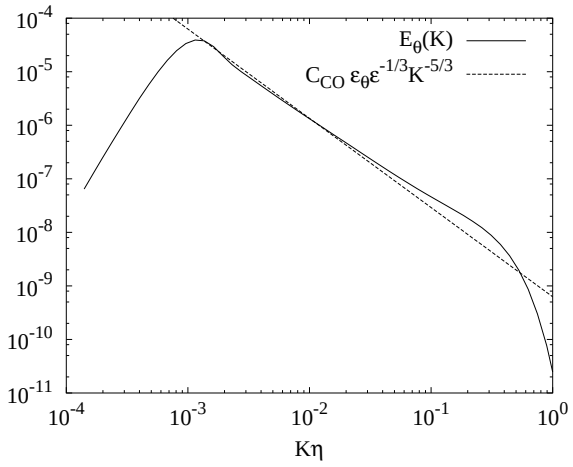

Figure 5.3: Scalar variance spectrum in homogeneous turbulent shear flow at $St = 12$.

Because the mean shear deforms the scalar field it is found in this case that the scalar flux has two components: one in the z and one in the x direction. In the following we will call those fluxes the vertical and horizontal scalar flux respectively[3].

The best overall agreement with the different results is obtained for the value $A^L = 0.385$. Those results are summarized in table 5.1. The difference between RUN1 and RUN2 is the Reynolds number of the initial energy spectrum, chosen so that at $St = 12$ the R_λ was equal to respectively 43 and 150. This allows a comparison with the DNS values ($R_\lambda = 43$ at $St = 12$) and the experiment of Tavoularis and Corrsin [92] ($R_\lambda = 150$ at $St = 12$). All quantities are determined at $St = 12$ which is chosen as a reference time because in literature most results are shown at this non-dimensional time.

Details about the DNS can be found in the report of Rogers *et al.* [97]. To take the mean shear into account in their pseudo spectral code, the numerical mesh moved along with the mean velocity field so that the numerical domain had to be remeshed several times during the calculation. They also report results about the scalar field with other orientations of the mean scalar gradients: $\partial\Theta/\partial x_1$ and $\partial\Theta/\partial x_2$, but those cases will not be treated in this manuscript.

We compare also with the Rapid Distortion Theory (RDT) analysis of Rogers [106]. The idea of RDT is to neglect all non-linear terms in the equations of the spectral tensor, scalar flux spectrum and scalar spectrum. RDT is known to yield valuable information, because the non-linear effects

[3]In this chapter we choose the value of Γ positive so that the vertical scalar flux becomes negative

Table 5.1: Comparison of the EDQNM results with experimental results and Simulations. All values are determined at $St = 12$.

Authors	RMR [97]	Present RUN1	T&C [92]	Present RUN2	R91 [106]	KGS [98]
Approach	DNS	EDQNM	Exp	EDQNM	RDT	LES
Re_λ	43	43	150	150	-	-
Pr_T	0.85	0.94	1.12	1.1	0.9	0.74
D_{13}/D_{33}	-2.57	-3.01	-2.2 (-2.9)	-2.9	-	-2.1
$\rho_{u\theta}$	0.68	0.87	0.59	0.76	0.9	0.6
$\rho_{w\theta}$	-0.5	-0.73	-0.45	-0.61	-0.65	-0.5
R	1.62	2.26	2.55	2.5	-	-
B	1.05	1.39	1.53	1.55	-	-

(absent in RDT) do often respond slower to rapid deformations than the linear terms so that the neglection of the non-linear terms does not introduce large errors at short deformation times. The rapid pressure and linear transfer are linear terms so that comparison with RDT might be useful. We can however question if $St = 12$ corresponds to a short deformation time.

The paper of Kaltenbach *et al.* [98] reports uniformly sheared stable and unstable vertically stratified flows. The case $Ri = 0$ (Ri stands for Richardson number) corresponds to a passive scalar field so that a comparison with our work can be made.

The experimental results of Tavoularis and Corrsin [92] are wind tunnel results in which the mean shear is generated by using an array of jets discharging air at different speeds. The scalar gradient was introduced by heating cylindrical rods at the exits of the different jets. A detailed comparison is performed between this experiment and the results of our model. This comparison is shown in figure 5.4. We will now define and discuss the different quantities.

Turbulent prandtl number

The turbulent Prandtl number is defined as:

$$Pr_T = \frac{\nu_T}{\alpha_T} \tag{5.40}$$

In this expression the turbulent viscosity and diffusivity are defined by:

$$\nu_T = \frac{\overline{uw}}{S}$$
$$\alpha_T = \frac{\overline{w\theta}}{\Gamma}$$

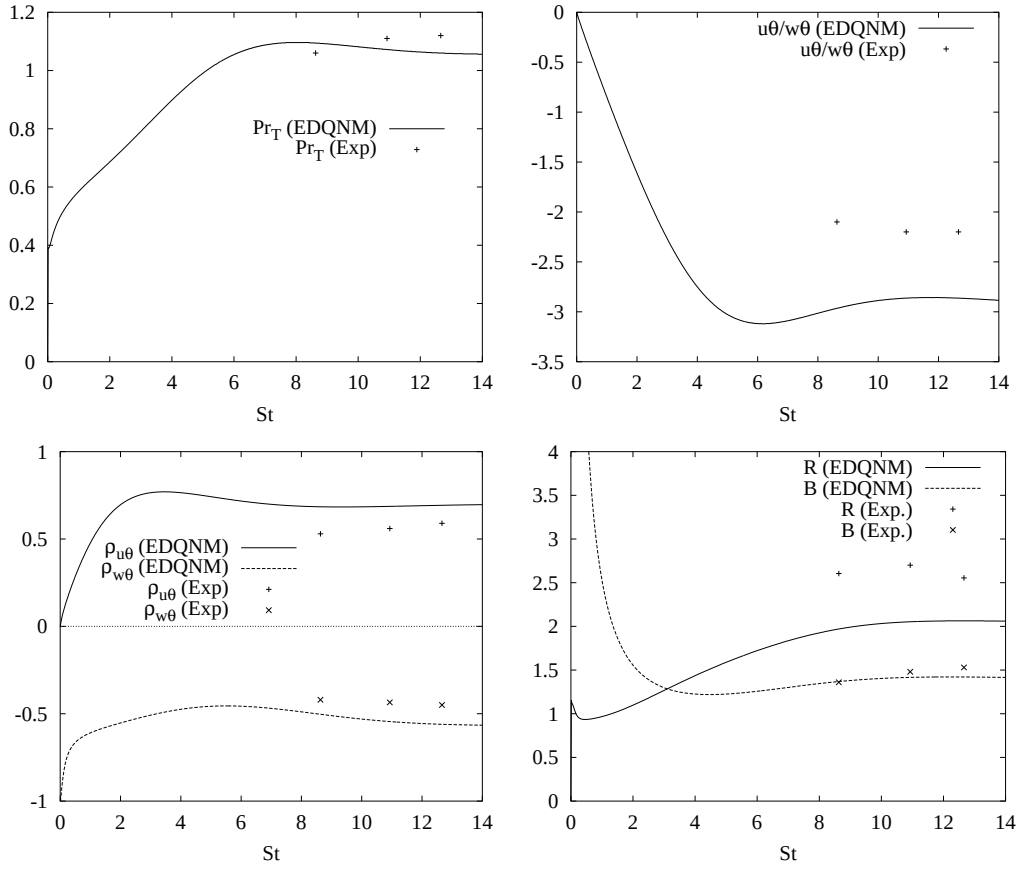

Figure 5.4: $R_\lambda \approx 150$ Top left: Turbulent Prandtl number, top right: diffusivity ratio, bottom left: correlation coefficients, bottom right: time scale ratio R and relative fluctuation intensity parameter B

The turbulent Prandtl number is thus the ratio of the Reynolds stress to the vertical turbulent heatflux, normalized by the mean gradients:

$$Pr_T = \frac{\Gamma}{S}\frac{\overline{uw}}{\overline{w\theta}}. \tag{5.41}$$

In figure 5.4 we show that the agreement with the Tavoularis and Corrsin [92] experiment is good. A spectral extension of Pr_T was proposed in Fulachier and Antonia [107]:

$$Pr_T(K) = \frac{\Gamma}{S}\frac{\varphi_{uw}(K)}{F_{w\theta}(K)}. \tag{5.42}$$

They analyzed this quantity in various shear flows and observed that it was a decreasing function in the inertial range. This observation is compatible with a tendency towards a $K^{-7/3}$ inertial range behaviour slower for the vertical scalar flux spectrum than for the Reynolds-stress spectrum. The Reynolds number dependency of the spectral slope of the scalar flux spectra in homogeneous shear flow is investigated in section 5.6.5.

The turbulent diffusivity tensor

The turbulent diffusivity tensor D_{ij} is defined as:

$$-\overline{u_i\theta} = D_{ij}\frac{\partial\Theta}{\partial x_j} \tag{5.43}$$

In this chapter the two non-zero components of this tensor are D_{13} and D_{33}, corresponding to the horizontal and vertical scalar flux. The ratio of those two components is equal to the ratio of the two scalar fluxes:

$$\frac{D_{13}}{D_{33}} = \frac{\overline{u\theta}}{\overline{w\theta}} \tag{5.44}$$

It has been studied in several works[4]. In fig. 5.4 the comparison of the model with Tavoularis and Corrsin [92] is shown. The value obtained with our model (-2.9 at $St = 12$) is lower than the value measured in the Tavoularis and Corrsin [92] experiment.

In another work by the same authors [94], the experimental results are analysed using a quasi-lagrangian analysis, invoking several assumptions

[4]Rubinstein and Barton [108] perform a renormalization group analysis of this ratio and derive the expression:

$$\overline{u\theta}/\overline{w\theta} = -0.641\frac{Sk}{\epsilon} \tag{5.45}$$

with k the kinetic energy. Substituting in this expression the values for the kinetic energy, dissipation and shear rate from our calculation at $St = 12$, we obtain the value $D_{13}/D_{33} = -2.82$.

relating eulerian and lagrangian statistics. The ratio was then estimated to be -2.9, in agreement with our calculation but no estimation could be made of the errors induced by the approximations so that the perfect agreement of their value with our calculation could be a lucky coincidence.

Heat flux correlation coefficients

The scalar flux correlation coefficients corresponding to the two components of the scalar flux are defined by:

$$\rho_{u\theta} = \frac{\overline{u\theta}}{\sqrt{\overline{u^2}\,\overline{\theta^2}}}, \quad \rho_{w\theta} = \frac{\overline{w\theta}}{\sqrt{\overline{w^2}\,\overline{\theta^2}}} \tag{5.46}$$

We observe in fig. 5.4 reasonable agreement with the experimental values. The absolute value of both coefficients are over-estimated by our model. $\rho_{u\theta}$ and $\rho_{w\theta}$ calculated by the model are ~ 0.8 and ~ -0.6 respectively compared to the experimental values ~ 0.6 and -0.5.

Time scale ratio

We define the ratio of the velocity timescale and the passive scalar time scale as:

$$R = \frac{k/\epsilon}{\overline{\theta^2}/\epsilon_\theta} \tag{5.47}$$

We find acceptable agreement with the experiment (fig. 5.4).

Relative intensity ratio

The relative strength of the fluctuating velocity field compared to the scalar field can be expressed by the parameter B:

$$B = \frac{k^{1/2}/S}{\overline{\theta^2}^{1/2}/\Gamma} \tag{5.48}$$

Figure 5.4 shows that the agreement is good.

5.6.4 The inertial range of the scalar spectrum

We show in figure 5.5 two scalar spectra at $St = 12$ for two different Reynolds numbers: $R_\lambda = 134$ corresponds approximately to the situation in the Tavoularis and Corrsin experiments [92]. The spectral slope is less steep than $-5/3$. At $R_\lambda = 2384$, a typical atmospheric value, a $-5/3$ inertial range slope is observed.

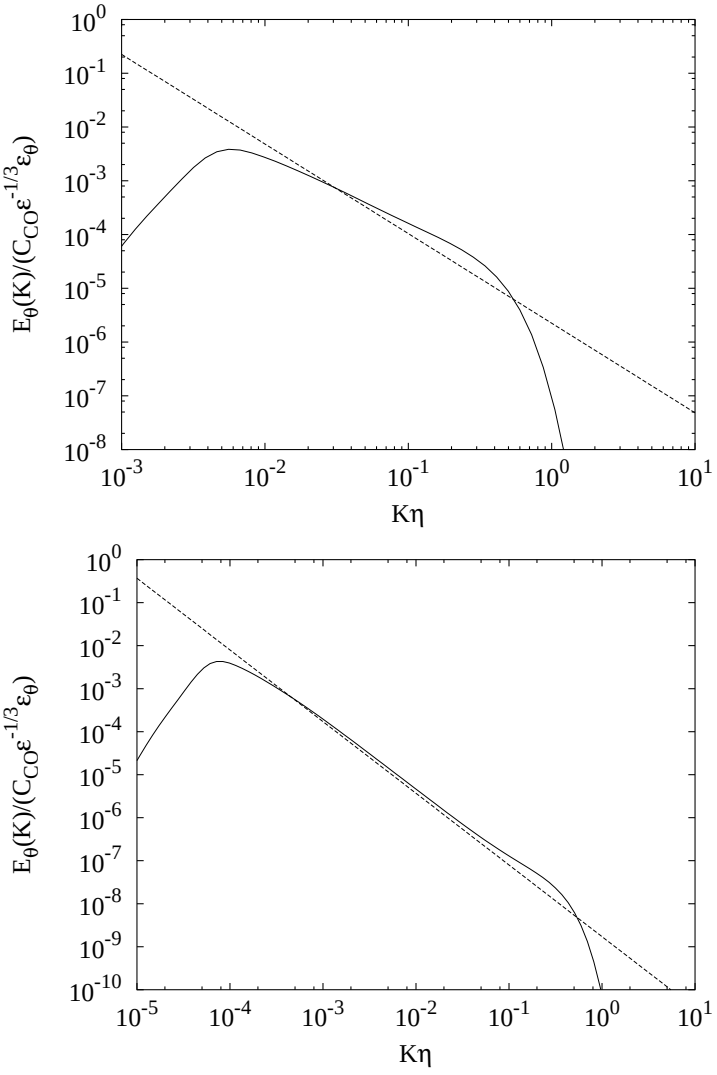

Figure 5.5: Scalar spectra at $St = 12$ for two different Reynolds numbers. Top: $R_\lambda = 134$, bottom: $R_\lambda = 2384$. Straight lines correspond to $K^{-5/3}$

In figure 5.6 we plot the slope of the scalar spectrum at $St = 12$ for varying Reynolds number. The results are compared to the compilation of experimental results by Sreenivasan [6]. The different experiments in this compilation (the Tavoularis and Corrsin experiments [92], a heated boundary layer, the wake of a heated cylinder and atmosperic measurements) are compared in one graph because the non-dimensional shear rate is comparable in all different experiments. The slopes deduced from our calculations show that the same tendencies are observed. At low R_λ (~ 150) a value close to $n_\theta = 1.3$ is found, both with our model and in the experiments. When R_λ increases the slope changes and tends towards $-5/3$, a value which is nearly reached at R_λ of a few thousands. However the results of our model tend faster towards their asymptotic value of $-5/3$ than the experimental slopes.

The slope determined by Sreenivasan corresponds to the slope of the one-dimensional scalar spectrum $E_\theta(K_x)$. Our model provides only the spectra integrated over wavenumber shells and we do not consider the anisotropy of the scalar spectrum. This might explain the difference of our results with the experimental values. Another reason, closely related, might be the neglection of the direct influence of the shear on the non-linear interactions and the linear transfer[5]. Those anisotropic terms which act especially at the lower wave-numbers might cause the inertial range to be shallower at lower R_λ.

5.6.5 The scalar flux spectrum

In figure 5.7 we show the spectra of the horizontal and vertical heatflux at $St = 12$, normalized by the RMS values of θ, u and w. $F_{u\theta}(K)$ shows a steeper inertial range slope than $F_{w\theta}(K)$. The two spectra intersect at a certain wavenumber.

The different contributions to the equation of the scalar flux

The different contributions to the evolution equation of the scalar flux spectra, equation (5.8), are shown in figures 5.8 and 5.9. The two figures correspond to the two different cases shown in figure 5.7, $R_\lambda = 134$ and $R_\lambda = 2384$.

We define in these figure the production terms:

[5] It would be interesting to consider the results in this chapter in comparison with the recent work of Celani *et al.* [109], who also study the effect of shear on the scalar spectrum and propose a model to explain the shallow scalar spectra in the presence of uniform shear.

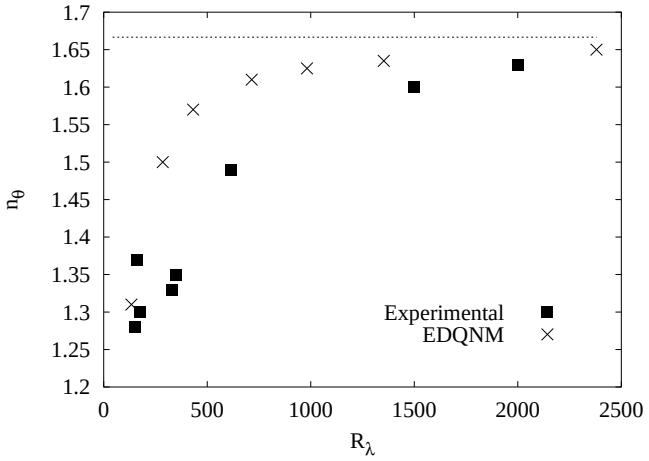

Figure 5.6: Spectral slope of the scalar variance spectrum. Results of Sreenivasan [6] compared to the present EDQNM results. The dotted line corresponds to a $-5/3$ slope.

$$P_i^\Gamma(K) = -\frac{\partial \Theta}{\partial z}\varphi_{i3}(K)$$
$$P_i^S(K) = -\frac{\partial \overline{U}_i}{\partial x_j}F_{u_j\theta}(K) \tag{5.49}$$

the dissipative term:

$$V_i(K) = -(\nu+\alpha)K^2 F_{u_i\theta}(K)$$

For simplicity the indices are dropped (all contributions to $F_{u\theta}(K)$ should have an index 1, the contributions to $F_{w\theta}(K)$ an index 3). All the contributions to $F_{w\theta}(K)$ which is a negative spectrum, are multiplied with -1 to simplify the comparison with $F_{u\theta}(K)$, which is a positive spectrum.

We observe that for the vertical heatflux spectra $F_{w\theta}(K)$, the main contributions are the same as in the isotropic case. The *new* terms (compared to isotropic turbulence with a mean scalar gradient) are small: the production by shear $P^S(K)$ is zero as can directly be seen from eq. (5.6.5). The linear transfer $T^L(K)$ and rapid pressure $\Pi^L(K)$ terms are small, especially for higher wavenumbers. The behaviour of the *old* terms (production by the scalar gradient $P^\Gamma(K)$, pressure $\Pi(K)$, non-linear transfer $T^{NL}(K)$ and dissipation $V(K)$) is roughly the same as in the isotropic case.

The horizontal heatflux spectrum $F_{u\theta}(K)$ does not exist in the isotropic case. We see three production terms: $P^S(K)$, $P^\Gamma(K)$ and the rapid pressure term $\Pi^L(K)$. We see, especially in the high Reynolds number case,

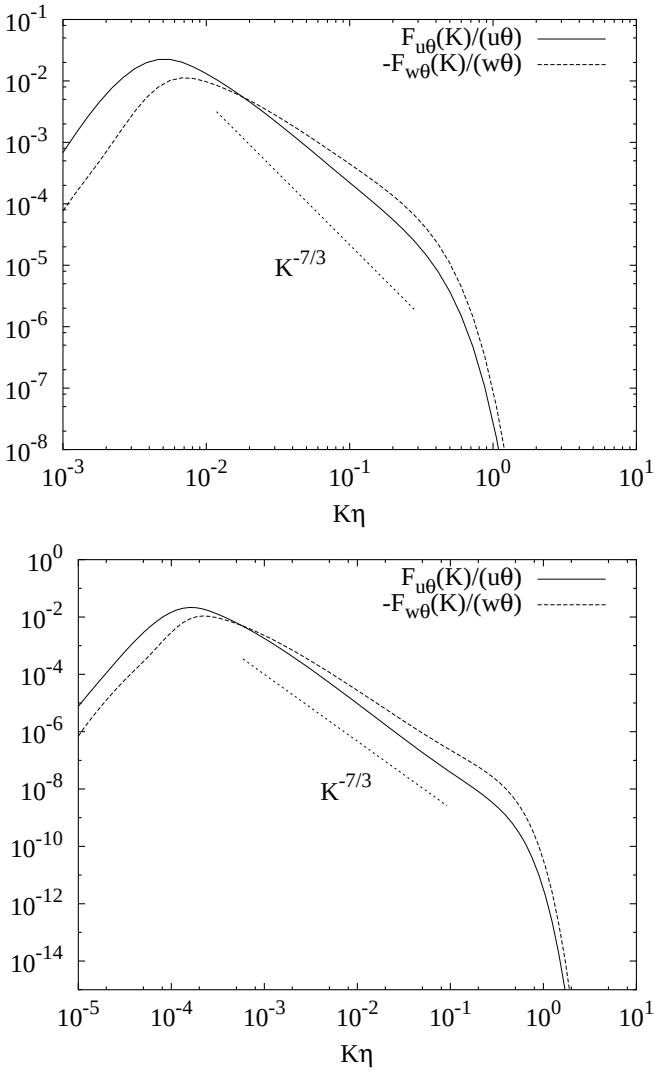

Figure 5.7: Horizontal and vertical heatflux spectra at $St = 12$ for two different Reynolds numbers. Top: $R_\lambda = 134$, bottom: $R_\lambda = 2384$

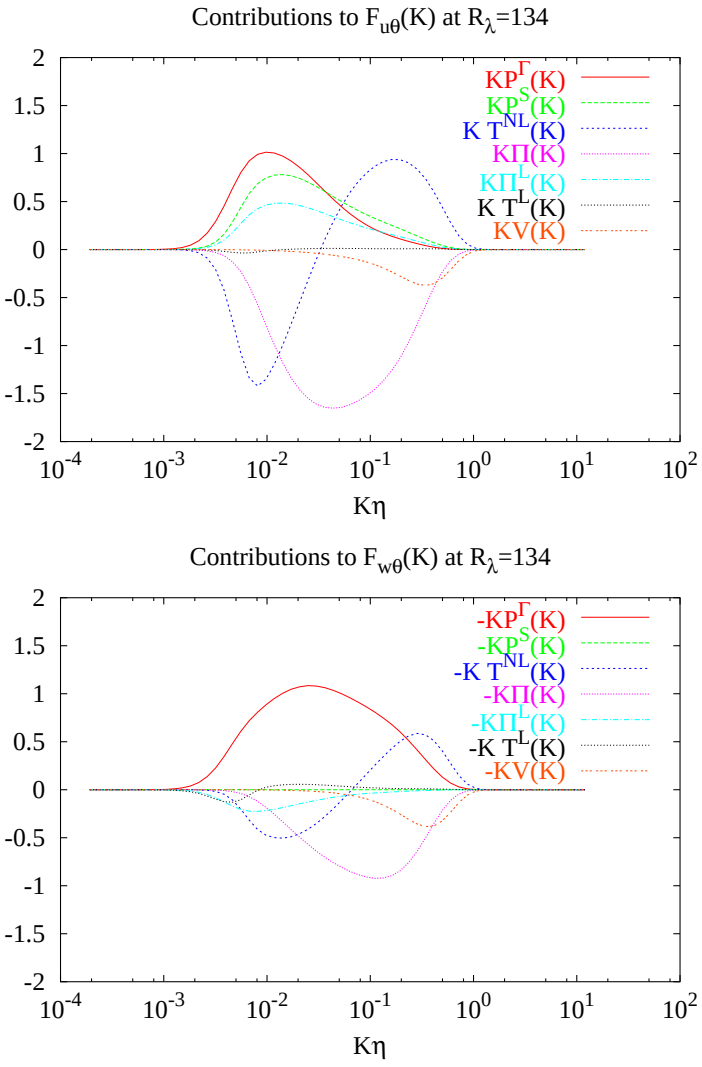

Figure 5.8: Contributions to the equations of the horizontal and vertical heatflux spectra at $St = 12$ and $R_\lambda = 134$.

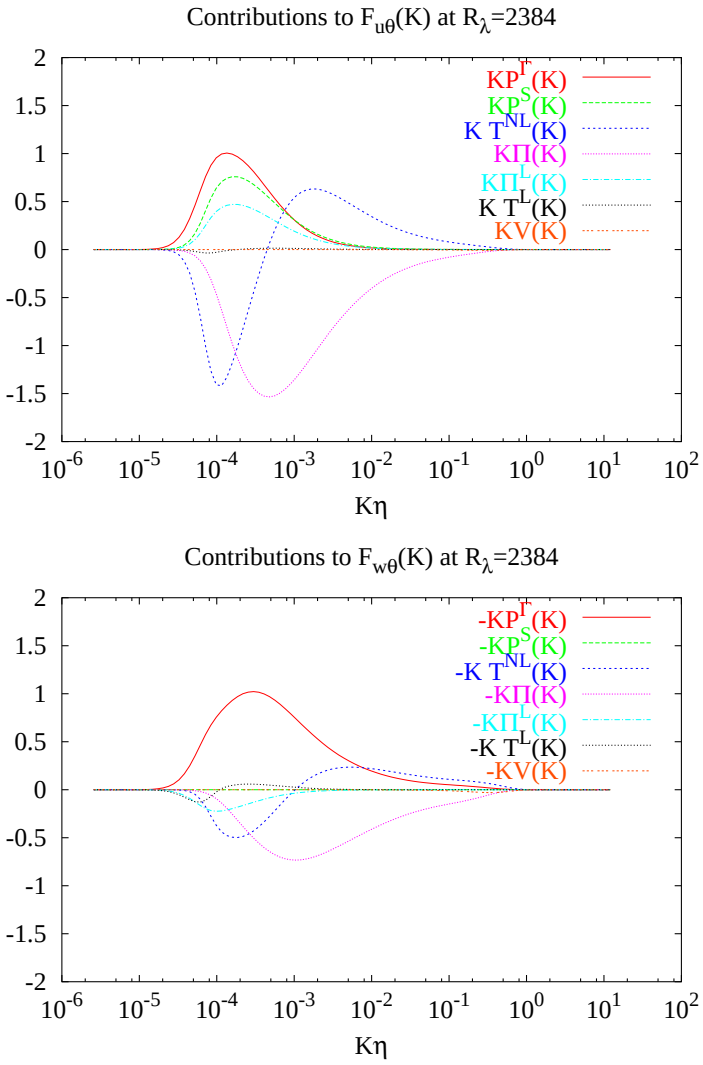

Figure 5.9: Contributions to the equations of the horizontal and vertical heatflux spectra at $St = 12$ and $R_\lambda = 2384$.

that in the inertial range, there are only two dominant terms, the pressure term $\Pi(K)$ and the non-linear transfer $T^{NL}(K)$. Already for the vertical spectrum those terms where dominant, but for $F_{u\theta}(K)$ the production terms fall off as $K^{-7/3}$, compared to $K^{-5/3}$ for the production term of the vertical heatflux, so that the non-linear interactions are even more dominant in the inertial range.

The inertial range of the scalar flux spectra

We show in figure 5.10 the slopes of the vertical and horizontal heatflux spectra as a function of the Reynolds number.

At two different times, $St = 0.5$ and $St = 12$ the slopes are determined. It is observed that the difference between the slopes at different times decreases with increasing Reynolds number.

The vertical heat-flux spectrum tends to the $n_{w\theta} = -7/3$ asymptote for large R_λ, like in an isotropic turbulence with a mean scalar gradient. Apparently the asymptotic value is not changed by the presence of shear. In fig. 5.11 we show the compensated spectra for different Reynolds numbers.

The exponent of the horizontal spectrum, $n_{u\theta}$ (fig. 5.10 bottom) is found to tend to a value larger than 7/3. However, the high Reynolds number asymptote seems to be smaller than the value $n_{u\theta} = 3$ proposed by Wyngaard and Coté [32]: $n_{u\theta} = 23/9$ appears a more plausible value. This can also be observed in figure 5.12, where the spectra compensated by $K^{23/9}$ are plotted. It is interesting to point out that measurements in the atmosphere have found values values close to 2.5 (Wyngaard and Coté [32], Caughey [110], Kader and Yaglom [34]) and that $23/9 \approx 2.555$.

Dimensional analysis based on the quantities S, ϵ and K provides the following expression for the spectrum:

$$F_{u\theta}(K) \sim \frac{\partial \Theta}{\partial z} S^{\alpha} \epsilon^{\frac{1-\alpha}{3}} K^{-\frac{7+2\alpha}{3}} \tag{5.50}$$

This expression is linear in the scalar gradient, as it has to be to reflect the linearity of the scalar equation. Linearity in S is not mandatory since the Navier-Stokes equations are not linear; if linearity in S is assumed, (5.50) reduces to the Wyngaard and Coté (1972) formulation:

$$F_{u\theta}(K) \sim \frac{\partial \Theta}{\partial z} S K^{-3}. \tag{5.51}$$

This formulation can also be found by assuming

$$F_{u\theta}(K) \sim \frac{\varphi_{uw}(K)}{E(K)} F_{w\theta}(K) \tag{5.52}$$

and using (2.5) to express $F_{w\theta}(K)$ and a classical expression for the $\varphi_{uw}(K)$ spectrum:

$$\varphi_{uw}(K) \sim S \epsilon^{1/3} K^{-7/3}. \tag{5.53}$$

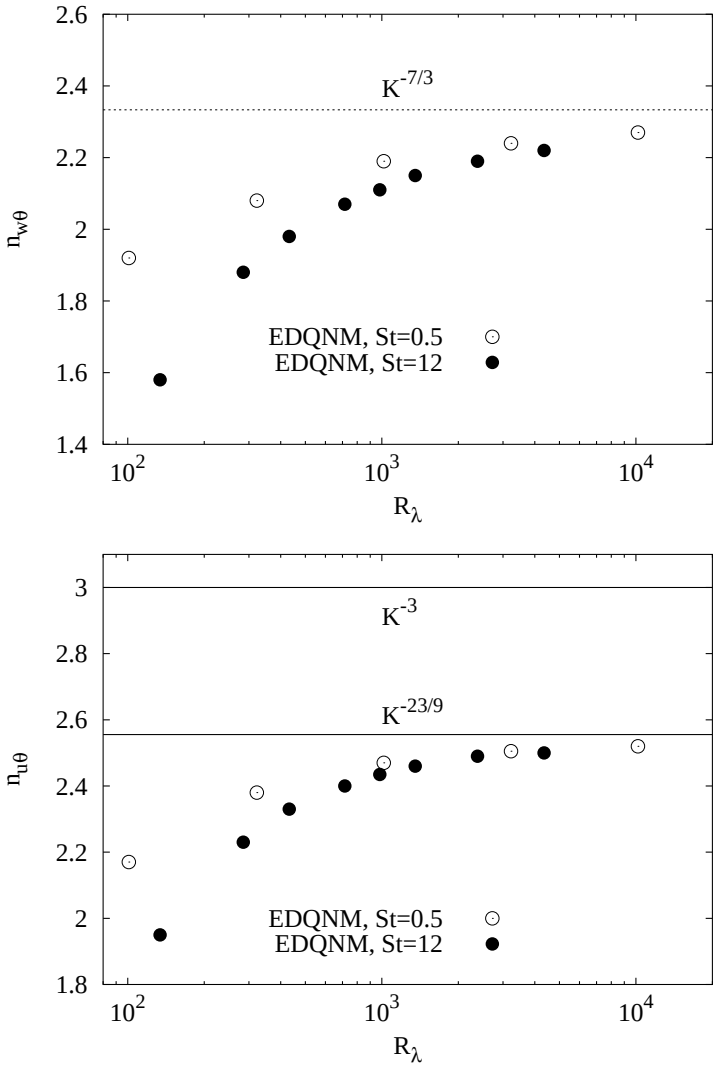

Figure 5.10: Inertial range slopes of the scalar flux spectra as a function of the Reynolds number. Top: vertical scalar flux, dotted line corresponds to $K^{-7/3}$. Bottom: horizontal scalar flux, dotted line corresponds to $K^{-23/9}$.

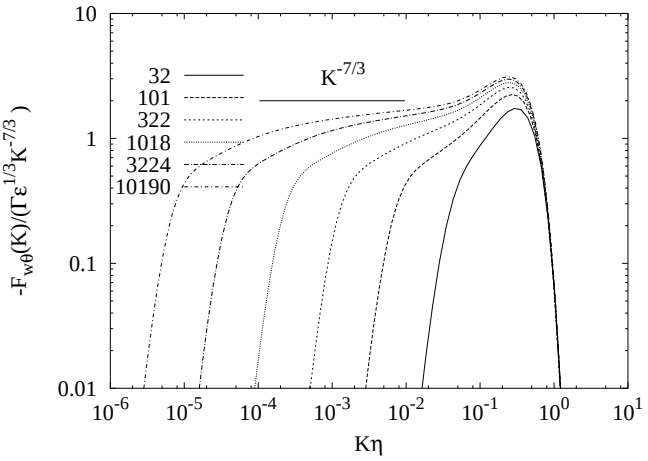

Figure 5.11: Compensated vertical heatflux spectra for $32 < R_\lambda < 10^4$ at $St = 0.5$.

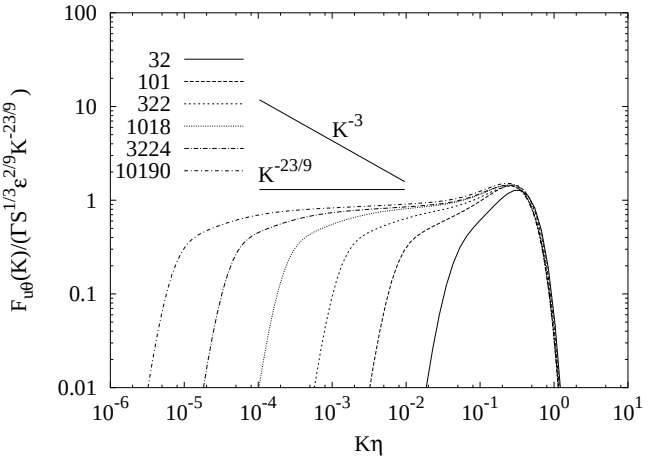

Figure 5.12: The $K^{-23/9}$ scaling (5.56) for the horizontal heatflux spectrum tested in the range $32 < R_\lambda < 10^4$ at $St = 0.5$.

If instead, one uses a tensorial extension of (2.5):

$$F_{u_i\theta}(K) \sim \frac{\partial \Theta}{\partial x_j}\epsilon_{ij}(K)^{1/3}K^{-7/3}, \tag{5.54}$$

and expresses $\epsilon_{uw}(K)$ by arguments similar to the ones leading to (5.53):

$$\epsilon_{uw}(K) \sim S\epsilon^{2/3}K^{-2/3} \tag{5.55}$$

it is found:

$$F_{u\theta}(K) \sim \frac{\partial \Theta}{\partial z}S^{1/3}\epsilon^{2/9}K^{-23/9}, \tag{5.56}$$

a scaling in good agreement with the present EDQNM results (see figure 5.12) as well as with the results of atmospherical measurements leading to $n_{u\theta} \sim 2.5$.

5.6.6 The $K^{-5/3}$ horizontal scalar flux spectrum of Antonia and Zhu

Antonia and Zhu [99] show two cases in which the horizontal heatflux spectrum shows a $K^{-5/3}$ inertial range for over two decades of the spectrum. Those observations are based on two experimental runs in the work of Bradley *et al.* [96]. The horizontal heatflux coefficient and Reynolds number in those two runs are $\rho_{u\theta} = 0.04$ at $R_\lambda = 7190$ and $\rho_{u\theta} = 0.05$ at $R_\lambda = 7673$. The small values for the correlation coefficient $\rho_{u\theta}$ compared to the typical values summed in table 5.1 for $St = 12$ let us suspect that the effective value of St is small in these atmospheric experiments. An exact quantitative comparison with our calculations is impossible because the atmospheric measurements do not correspond to pure homogeneous shear flow. We observe however, that in our EDQNM calculations at very small St we also see this $K^{-5/3}$ slope. The explanation might be that the production terms of both the Reynolds stress spectrum $\varphi_{13}(K)$ and the horizontal heatflux spectrum at small St are superior to the non-linear terms over most of the spectrum. Only near the dissipation range, the triadic interactions are strong enough to react to the sudden introduction of shear. In figure 5.13 we show the spectrum of $u\theta$ at four different times in the beginning of the calculation.

The parameters of our calculation (viscosity, shear) are chosen so that we find a $\rho_{u\theta} = 0.05$ at $R_\lambda \approx 7500$. At $St = 0.001$ we observe two decades of $K^{-5/3}$ in the inertial range. However, this behaviour vanishes fastly when the calculation procedes. At $St = 0.05$, the time at which $\rho_{u\theta} = 0.05$ and $R_\lambda \approx 7500$, it has practically disappeared. We find no direct agreement between the observations of Antonia and Zhu [99] and our model, i.e. at comparable Reynolds number and $\rho_{u\theta}$, we do not observe the $K^{-5/3}$ slope for the horizontal heatflux spectrum.

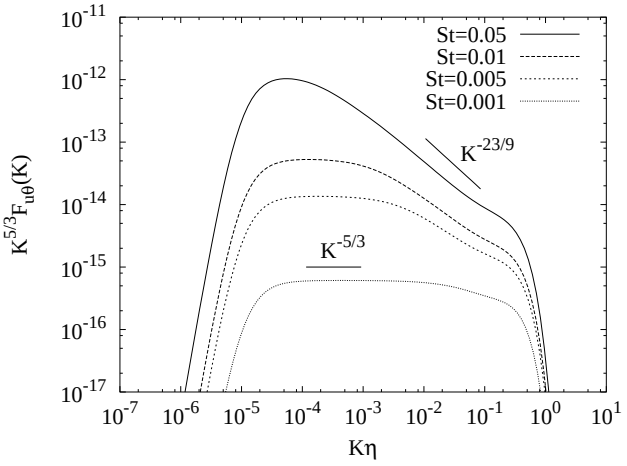

Figure 5.13: The horizontal heatflux spectrum at four different times in the beginning of the calculation. The spectra are compensated by $K^{5/3}$.

A more detailed analysis, taking into account the influence of inhomogeneity and instationarity of the mean velocity field on the horizontal scalar flux spectrum, could provide insights in this issue.

Chapter 6

Towards a spectral closure for inhomogeneous scalar fields

6.1 Introduction

In the previous chapter we succesfully applied the EDQNM theory to predict the non-linear transfer of scalar flux and variance in homogeneous shear flow. In the present chapter the equations to extend the model to scalar mixing in inhomogeneous and wall bounded flows are derived.

6.1.1 Two-point modelling of inhomogeneous turbulence

The first attempts to derive the EDQNM equations for inhomogeneous turbulence can be found in the works of Menoret [26] and Burden [27]. Numerically exploitable equations were not derived until the work of Laporta [28] who derived the extension of the EDQNM theory to weakly inhomogeneous turbulence.

A first approach to take into account the influence of boundaries on the EDQNM equations was proposed by Bertoglio and Jeandel [29], who introduced a spectral cut-off to model the scale limitation introduced by the finite size of a wall-bounded domain. Experimentally this influence was tested by Skrbek and Stalp [111] and by DNS, LES and closure calculations by Touil *et al.* [112]. The first numerical computer code based on the EDQNM equations that could be applied to complex flows including walls was created by Parpais [30]. He used the scalar energy spectrum $E(K, \boldsymbol{x}, t)$ as its main variable. The anisotropy was in this work modelled using a spectral extension of the Shih and Lumley [113] approach. This result was extended by Touil [1] refining the anisotropy of the model, the variable now being $\varphi_{ij}(K, \boldsymbol{x}, t)$. The equation in this work reads:

$$\left(\frac{\partial}{\partial t}+\overline{U}_n\frac{\partial}{\partial x_n}\right)\varphi_{ij}(\boldsymbol{x},K,t)-2\nu\left(\frac{1}{4}\frac{\partial}{\partial x^2}-K^2\right)\varphi_{ij}(\boldsymbol{x},K,t)=$$
$$\text{Production}$$
$$+\text{Linear Transfer}$$
$$+\text{Rapid Pressure}$$
$$+\text{Non-linear Transfer \& Pressure}$$
$$+\text{Inhomogeneous Transport}$$
$$+\text{Wall effects} \qquad (6.1)$$

If we compare this equation to homogeneously sheared turbulence (as considered in the previous chapter), we observe additional terms. On the LHS we find the convection by the mean velocity and the inhomogeneous dissipation. Those terms do not need any modelling. Neither does the production. The linear transfer, rapid pressure and non-linear transfer can be modeled as in the previous chapter. Inhomogeneous transport and wall effects are new terms. They are discussed in the PhD thesis of Touil [1] and will also be discussed for the scalar field in the following sections.

6.1.2 Two point modelling of an inhomogeneous scalar field

The work of Herring *et al.* [22] applied the EDQNM theory to isotropic scalar fields and also in this context the two-point approach helped the understanding of the turbulent dynamics. A first application of the EDQNM theory to isotropic turbulence with a mean scalar gradient can be found in the work of Herr *et al.* [20]. An application to inhomogeneous scalar mixing was done by Parpais and Bertoglio [114]. The principle variables in this work are the energy spectrum $E(K,\boldsymbol{x},t)$ and the scalar spectrum $E_\theta(K,\boldsymbol{x},t)$. They modelled the scalar flux spectrum in a way similar to Shih and Lumley [113]. The extension of Touil [1] for the anisotropy of the velocity field will be done in this work for the scalar field. We will propose an extension of the work of Bertoglio and Jeandel [29], Laporta [28], Parpais [30] and Touil [1] on inhomogeneous turbulence to the scalar field. The approach follows closely the work of Laporta [28] for the derivation of the equations and the work of Touil [1] for the modelling assumptions.

6.2 Derivation of the equation for the inhomogeneous scalar flux spectrum

We derive the equation for the inhomogeneous two-point correlation between a passive scalar and a turbulent velocity field.

Multiplying the transport equation of the scalar fluctuation θ in point 1 in a turbulent flow by the velocity fluctuation u in point 2, and adding this equation to the equation of the velocity fluctuation in point 2 multiplied by the scalar fluctuation in point 1 we obtain after ensemble-averaging the following equation:

$$\begin{aligned}\frac{\partial\overline{u_{2i}\theta_1}}{\partial t}+\frac{\partial}{\partial x_{2n}}\left[\overline{U}_{2n}\overline{\theta_1 u_{2i}}+\overline{U}_{2i}\overline{\theta_1 u_{2n}}+\overline{\theta_1 u_{2i}u_{2n}}\right]+\\ +\frac{\partial}{\partial x_{1n}}\left[\overline{U}_{1n}\overline{\theta_1 u_{2i}}+\Theta_1\overline{u_{2i}u_{1n}}+\overline{\theta_1 u_{2i}u_{1n}}\right]=\\ -\frac{1}{\rho}\frac{\partial}{\partial x_{2i}}\overline{p_2\theta_1}+\nu\frac{\partial^2}{\partial_{2n}^2}\overline{\theta_1 u_{2i}}+\kappa\frac{\partial^2}{\partial_{1n}^2}\overline{\theta_1 u_{2i}}\end{aligned}\qquad(6.2)$$

The indexes 1 and 2 indicating position $x_1 = x-1/2r$ and $x_2 = x+1/2r$ respectively. This choice leads to the following expressions for the partial derivatives:

$$\begin{aligned}\frac{\partial}{\partial x_{1n}}&=\frac{1}{2}\frac{\partial}{\partial x_n}-\frac{\partial}{\partial r_n}\\ \frac{\partial}{\partial x_{2n}}&=\frac{1}{2}\frac{\partial}{\partial x_n}+\frac{\partial}{\partial r_n}\end{aligned}\qquad(6.3)$$

We take the fourier transform equation (6.2) to obtain:

$$\begin{aligned}\left[\frac{\partial}{\partial t}-\nu\left(\frac{1}{4}\frac{\partial^2}{\partial x_n^2}+iK_n\frac{\partial}{\partial x_n}-K^2\right)-\kappa\left(\frac{1}{4}\frac{\partial^2}{\partial x_n^2}-iK_n\frac{\partial}{\partial x_n}-K^2\right)\right]\mathcal{F}_{u_i\theta}=\\ -\left(\frac{1}{2}\frac{\partial}{\partial x_n}+iK_n\right)\left[exp\left(\frac{i}{2}\frac{\partial\overline{U}}{\partial x}\frac{\partial}{\partial K}\right)\left(\overline{U}_n\mathcal{F}_{u_i\theta}+\overline{U}_i\mathcal{F}_{u_n\theta}\right)+T_{\theta in}\right]\\ -\left(\frac{1}{2}\frac{\partial}{\partial x_n}-iK_n\right)\left[exp\left(-\frac{i}{2}\frac{\partial\overline{U}\Theta}{\partial x}\frac{\partial}{\partial K}\right)\left(\overline{U}_n\mathcal{F}_{u_i\theta}+\Theta\Phi_{in}\right)+T^*_{\theta in}\right]\\ +\left(\frac{1}{2}\frac{\partial}{\partial x_i}+iK_i\right)\Pi\end{aligned}\qquad(6.4)$$

in this equation:

$$\begin{aligned}
\mathcal{F}_{u_i\theta} &= FT_{/\boldsymbol{r}}\left(\overline{\theta(x-\frac{1}{2}r)u_i(x+\frac{1}{2}r)}\right)\\
\Phi_{ij} &= FT_{/\boldsymbol{r}}\left(\overline{u_i(x+\frac{1}{2}r)u_j(x-\frac{1}{2}r)}\right)\\
T_{\theta in} &= FT_{/\boldsymbol{r}}\left(\overline{\theta(x-\frac{1}{2}r)u_i(x+\frac{1}{2}r)u_n(x+\frac{1}{2}r)}\right)\\
T^*_{\theta in} &= FT_{/\boldsymbol{r}}\left(\overline{\theta(x-\frac{1}{2}r)u_i(x+\frac{1}{2}r)u_n(x-\frac{1}{2}r)}\right)\\
\Pi &= FT_{/\boldsymbol{r}}\left(-\frac{1}{\rho}\,\overline{p(x+\frac{1}{2}r)\theta(x-\frac{1}{2}r)}\right)
\end{aligned} \tag{6.5}$$

We need to derive an expression for the pressure-scalar correlation Π. To do this we take the divergence of equation 6.2 in point x_2. We obtain the following Poisson equation:

$$\frac{\partial}{\partial x_{2i}}\frac{\partial}{\partial x_{2n}}\left[2\overline{U}_{2n}\overline{\theta_1 u_{2i}}+\overline{\theta_1 u_{2i}u_{2n}}\right]=-\frac{1}{\rho}\frac{\partial^2}{\partial x_{2i}^2}\overline{p_2\theta_1} \tag{6.6}$$

We will use the following coordinate transformation:

$$x=x_1 \qquad r=x_2-x_1 \qquad \frac{\partial}{\partial x_{2j}}=\frac{\partial}{\partial r_j} \tag{6.7}$$

giving us for the fourier transform of equation 6.6 (Fourier transforms in those new coordinates are denoted by a hat):

$$-K_iK_n\left(2\ exp\left(i\frac{\partial\overline{U}}{\partial x}\frac{\partial}{\partial K}\right)\overline{U}_n\hat{\mathcal{F}}_{u_i\theta}+\hat{T}_{\theta in}\right)=-K^2\hat{\Pi} \tag{6.8}$$

We can return to our original coordinates by a transformation. $\hat{\mathcal{F}}_{u_i\theta}$, $\hat{T}_{\theta in}$ and $\hat{\Pi}$ can be expressed in $\mathcal{F}_{u_i\theta}$, $T_{\theta in}$ and Π by application of the operator $exp\left(\frac{i}{2}\frac{\partial}{\partial x}\frac{\partial}{\partial K}\right)$ [28] leading to:

$$\begin{aligned}
\Pi = exp\left(-\frac{i}{2}\frac{\partial}{\partial x}\frac{\partial}{\partial K}\right)\frac{K_iK_n}{K^2}\Bigg(&exp\left(\frac{i}{2}\frac{\partial}{\partial x}\frac{\partial}{\partial K}\right)T_{\theta i,n}\\
&+2\ exp\left[i\frac{\partial}{\partial K}\left(\frac{\partial\overline{U}}{\partial x}+\frac{1}{2}\frac{\partial^{\mathcal{F}}}{\partial x}\right)\right]\overline{U}_n\mathcal{F}_{u_i\theta}\Bigg)
\end{aligned} \tag{6.9}$$

We develop the pressure correlation $\left(\frac{1}{2}\frac{\partial}{\partial x_n}-iK_n\right)\Pi$ to the first order of inhomogeneity:

$$exp\left(-\frac{i}{2}\frac{\partial\overline{U}}{\partial x}\frac{\partial}{\partial K}\right)=1-\frac{i}{2}\frac{\partial\overline{U}}{\partial x}\frac{\partial}{\partial K}+... \tag{6.10}$$

so that

$$\left(\frac{1}{2}\frac{\partial}{\partial x_i}-iK_i\right)\left(1-\frac{i}{2}\frac{\partial}{\partial x_r}\frac{\partial}{\partial K_r}\right)\frac{K_nK_j}{K^2}\left(\left(1+\frac{i}{2}\frac{\partial}{\partial x_s}\frac{\partial}{\partial K_s}\right)T_{\theta jn}+ 2\left(1+i\frac{\partial}{\partial K_s}\frac{\partial\overline{U}}{\partial x_s}+\frac{i}{2}\frac{\partial}{\partial K_s}\frac{\partial^{\mathcal{F}}}{\partial x_s}\right)\overline{U}_n\mathcal{F}_{u_j\theta}\right) \tag{6.11}$$

Neglecting terms of second order in $\frac{\partial}{\partial x}$ we find:

$$\left(\frac{1}{2}\frac{\partial}{\partial x_i}\frac{K_nK_j}{K^2}+iK_i\frac{K_nK_j}{K^2}-\frac{K_i}{2}\frac{K_nK_j}{K^2}\frac{\partial}{\partial x_s}\frac{\partial}{\partial K_s}+\frac{K_i}{2}\frac{\partial}{\partial x_r}\frac{\partial}{\partial K_r}\frac{K_nK_j}{K^2}\right)T_{\theta jn}+ 2\left(\frac{1}{2}\frac{\partial}{\partial x_i}\frac{K_nK_j}{K^2}+iK_i\frac{K_nK_j}{K^2}-K_i\frac{K_nK_j}{K^2}\frac{\partial\overline{U}}{\partial x_s}\frac{\partial}{\partial K_s}- \frac{K_i}{2}\frac{K_nK_j}{K^2}\frac{\partial^{\mathcal{F}}}{\partial x_s}\frac{\partial}{\partial K_s}+\frac{K_i}{2}\frac{\partial}{\partial x_r}\frac{\partial}{\partial K_r}\frac{K_nK_j}{K^2}\right)\overline{U}_n\mathcal{F}_{u_j\theta} \tag{6.12}$$

The continuity equation implies:

$$\left(\frac{\partial}{\partial x_{2i}}\overline{\theta_1u_{2i}}=0\right)\Rightarrow\frac{1}{2}\frac{\partial}{\partial x_i}\mathcal{F}_{u_i\theta}=-iK_i\mathcal{F}_{u_i\theta} \tag{6.13}$$

In addition we need the derivative:

$$\frac{\partial}{\partial K_r}\frac{K_nK_j}{K^2}\mathcal{F}_{u_j\theta}=\left(\frac{K_j}{K^2}\delta_{nr}+\frac{K_n}{K^2}\delta_{jr}-2\frac{K_nK_jK_r}{K^4}\right)\mathcal{F}_{u_j\theta}+\frac{K_nK_j}{K^2}\frac{\partial\mathcal{F}_{u_j\theta}}{\partial K_r} \tag{6.14}$$

Eventually this yields the expression:

$$\left(\frac{1}{2}\frac{\partial}{\partial x_i}-iK_i\right)\Pi=\left(\frac{K_nK_j}{2K^2}\frac{\partial}{\partial x_i}+\frac{K_iK_n}{2K^2}\frac{\partial}{\partial x_j}+\frac{K_iK_j}{2K^2}\frac{\partial}{\partial x_n}+ i\frac{K_iK_nK_j}{K^2}-2\frac{K_iK_nK_jK_r}{K^4}\frac{\partial}{\partial x_r}\right)T_{\theta jn}+ 2\frac{K_iK_n}{K^2}\frac{\partial\overline{U}_n}{\partial x_j}\mathcal{F}_{u_j\theta} \tag{6.15}$$

This expression for the pressure correlation can be substituted in the equation for $\mathcal{F}_{u_i\theta}$. This equation is then also developped to the first order so that we obtain the following equation for the vector $\mathcal{F}_{u_i\theta}$:

$$\left(\frac{\partial}{\partial t}+\overline{U}_n\frac{\partial}{\partial x_n}\right)\mathcal{F}_{u_i\theta}(\boldsymbol{x},\boldsymbol{K},t)-(\alpha+\nu)\left(\frac{1}{4}\frac{\partial^2}{\partial x^2}-K^2\right)\mathcal{F}_{u_i\theta}(\boldsymbol{x},\boldsymbol{K},t)=$$

$$\underbrace{-(\nu-\alpha)iK_n\frac{\partial\mathcal{F}_{u_i\theta}(\boldsymbol{x},\boldsymbol{K},t)}{\partial x_n}}_{Mixed\ Molecular\ term}\ \underbrace{-\frac{\partial\overline{U}_i}{\partial x_n}\mathcal{F}_{u_i\theta}(\boldsymbol{x},\boldsymbol{K},t)-\frac{\partial\Theta}{\partial x_n}\Phi_{in}(\boldsymbol{x},\boldsymbol{K},t)}_{Production}$$

$$+\underbrace{\frac{\partial\overline{U}_n}{\partial x_p}\frac{\partial K_n\mathcal{F}_{u_i\theta}(\boldsymbol{x},\boldsymbol{K},t)}{\partial K_p}}_{Linear\ Tranfer}\ \underbrace{+2\frac{K_iK_n}{K^2}\frac{\partial\overline{U}_n}{\partial x_j}\mathcal{F}_{u_j\theta}(\boldsymbol{x},\boldsymbol{K},t)}_{Rapid\ Pressure}$$

$$\underbrace{-iK_n\left(T_{\theta in}-T^*_{\theta in}\right)+i\frac{K_iK_nK_j}{K^2}T_{\theta jn}}_{Non\ Linear\ Tranfer\ \&\ Pressure}$$

$$\underbrace{+\left(\frac{1}{2}\frac{K_nK_j}{K^2}\frac{\partial}{\partial x_i}+\frac{1}{2}\frac{K_iK_n}{K^2}\frac{\partial}{\partial x_j}+\frac{1}{2}\frac{K_iK_j}{K^2}\frac{\partial}{\partial x_n}+-2\frac{K_iK_nK_jK_r}{K^4}\frac{\partial}{\partial x_r}\right)T_{\theta jn}+-\frac{1}{2}\frac{\partial}{\partial x_n}\left(T_{\theta in}+T^*_{\theta in}\right)}_{Inhomogeneous\ Transport}\quad(6.16)$$

We will now integrate over all directions of the wavenumbervector to reduce the computational cost of a treatment of the equations as proposed in Cambon [69]. To do this we have to introduce some modelling to be able to integrate terms containing $\mathcal{F}_{u_i\theta}(\boldsymbol{x},\boldsymbol{K},t)$ and K_i.

6.2.1 Production, advection and viscous terms

The left hand side containing the time derivative, advective term and viscous (and molecular diffusive) terms, can be integrated without introducing a model. We will neglect the first term on the RHS containing a transport by molecular effects. This term vanishes in the case of $Pr=1$. The production terms, the second group of the RHS do not need any modelling.

6.2.2 Linear transfer and rapid pressure

The linear transfer and rapid pressure are modelled as in the previous chapter.

6.2.3 Non linear transfer and non-linear pressure

The non linear transfer and pressure,

$$T_{i\theta}^{NL}(\boldsymbol{x},K,t)+\Pi_{i\theta}(\boldsymbol{x},K,t)=\int_{\Sigma_K}-ik_n(P_{ij}(K)T_{\theta jn}-\delta_{ij}T^*_{\theta jn})dA(\boldsymbol{K}) \tag{6.17}$$

are modelled by EDQNM theory. In the previous chapter the non-linear transfer derived for isotropic turbulence was shown to yield adequate results for homogeneously sheared turbulence. We will use it here without modification for the inhomogenous flowfield. Laporta [28] showed that for the kinetic energy spectrum this approach corresponds to a first order approximation with respect to inhomogeneity.

6.2.4 Inhomogeneous Turbulent Transport

The diffusion terms containing the triple correlations are modelled together, introducing an eddy-viscosity as in Parpais [30]:

$$\begin{aligned}D_{i\theta}(\boldsymbol{x},K,t)=\int_{\Sigma_K}\Bigg(&\frac{1}{2}\frac{K_nK_j}{K^2}\frac{\partial}{\partial x_i}+\frac{1}{2}\frac{K_iK_n}{K^2}\frac{\partial}{\partial x_j}+\frac{1}{2}\frac{K_iK_j}{K^2}\frac{\partial}{\partial x_n}+\\&-2\frac{K_iK_nK_jK_r}{K^4}\frac{\partial}{\partial x_r}\Bigg)T_{\theta jn}+\\&-\frac{1}{2}\frac{\partial}{\partial x_n}\left(T_{\theta in}+T^*_{\theta in}\right)dA(\boldsymbol{K})\\&=\partial x_j\left(\nu_e\partial x_jF_{\theta i}(\boldsymbol{x},K,t)\right)\end{aligned} \tag{6.18}$$

The eddy viscosity is chosen in a classical isotropic form (cf. Touil [1]):

$$\nu_e=A^Dk^2/\epsilon_H \tag{6.19}$$

with ϵ_H the homogeneous part of the viscous dissipation,

$$\epsilon_H=\int 2\nu K^2E(\boldsymbol{x},K,t)dK \tag{6.20}$$

and A^D a constant to be determined.

6.2.5 The influence of walls on scalar mixing

Spectral cut-off To mimic the effect of scale limitation by walls on the turbulent structures, Bertoglio and Jeandel [29] proposed to introduce an infrarouge spectral cut-off in the energy spectrum. This approach is here extended to the scalar flux spectrum. We impose:

$$F_{u_i\theta}(\boldsymbol{x},K,t)=\ 0 \text{ if }\quad K\leq K_w=\frac{\mu_w}{\delta_w} \tag{6.21}$$

$$F_{u_i\theta}(\boldsymbol{x},K,t)\neq\ 0 \text{ if }\quad K>K_w \tag{6.22}$$

δ_w is the distance to the nearest wall. The constant μ_w was found to yield 2 in order to get results in agreement with the log-law in wall turbulence.

Pressure reflection The influence of the pressure on the equation of the scalar flux can be subdivided in three different terms.

1. The slow or non-linear pressure term that intervenes through the two-point triple correlations. This term has been thoroughly discussed in chapter 2 and 3.

2. The rapid pressure term, that exists in the presence of a mean velocity gradient as discussed in chapter 5.

3. A wall reflection term. This term disappears in the absence of boundaries. We have to propose a model for it.

We adapt an approach from one-point turbulence models (Schiestel p.202-203 [102]) inspired by the model due to Gibson and Launder [115] and the modifications by Touil [1]. We propose the model:

$$^R\Pi_{i\theta}(\boldsymbol{x},K,t) = {}^RA\ (n_j n_i \Pi^L_{j\theta}(\boldsymbol{x},K,t))\ f(y^+) \tag{6.23}$$

The constant ^RA has to be determined by comparison with experiments or DNS in the case of channel flow or flow over a flat plate. The function $f(y^+)$ is replaced as in Touil [1] by a function of R_{δ_w}, the Reynolds number based on δ_w the distance to the nearest wall, because R_{δ_w} is easier to determine than y^+ and its behaviour is roughly the same in the range considered:

$$f(R_{\delta_p}) = \left(\frac{1}{2}(\tanh(R_{\delta_w}+1) - \tanh(R_{\delta_w}-40))\right)^{1/4} \tag{6.24}$$

with the Reynolds number defined as:

$$R_{\delta_w} = \frac{k^{1/2}\delta_w}{\nu} \tag{6.25}$$

and k the kinetic energy. The function $f(R_{\delta_p})$ goes rapidly to zero for $y^+ > 40$, so that far from walls the influence becomes negligible.

6.3 Derivation of the equation for the inhomogeneous scalar variance spectrum

6.3.1 The equation

For the scalar spectrum we follow an approach identical to the one in the last section. The equation for the three-dimensional scalar spectrum reads:

$$\left(\frac{\partial}{\partial t}+\overline{U}_j\frac{\partial}{\partial x_j}\right)\Phi_\theta(\boldsymbol{x},\boldsymbol{K},t)-2\alpha\left(\frac{1}{4}\frac{\partial^2}{\partial x^2}-K^2\right)\Phi_\theta(\boldsymbol{x},\boldsymbol{K},t)=$$

$$\underbrace{-\frac{\partial\Theta}{\partial x_j}\mathcal{F}_{u_j\theta}(\boldsymbol{x},\boldsymbol{K},t)}_{Production}+\underbrace{\frac{\partial\overline{U}_j}{\partial x_p}\frac{\partial K_j\Phi_\theta(\boldsymbol{x},\boldsymbol{K},t)}{\partial K_p}}_{Linear\ Tranfer}$$

$$\underbrace{-iK_n\left(T_{\theta\theta n}-T^*_{\theta\theta n}\right)}_{Non\ Linear\ Tranfer}-\underbrace{\frac{1}{2}\frac{\partial}{\partial x_n}\left(T_{\theta\theta n}+T^*_{\theta\theta n}\right)}_{Inhomogeneous\ Transport} \tag{6.26}$$

The modelling of $E_\theta(\boldsymbol{x},K,t)$, obtained after integration over wavenumber shells does not differ from the previous section.

6.3.2 Inhomogeneous transport and wall effects

The inhomogeneous transport is modeled as in Parpais and Bertoglio [114]:

$$D_\theta(\boldsymbol{x},K,t)=\partial x_k\left(\alpha_e\partial x_k E_\theta(\boldsymbol{x},K,t)\right) \tag{6.27}$$

with an eddy diffusivity proportional to expression (6.19).

The same spectral infrared cut-off as for the spectral tensor and scalar flux is used for the scalar variance spectrum.

6.4 Perspectives

Three constants have to be determined before the described model can be employed: one for the pressure reflection near boundaries; two for the inhomogeneous transport of scalar flux and variance, which can be determined by comparison with mixing layer experiments and simulations (for example by comparison with the experiments of Larue, Libby and Seshadri [116, 117]).

Subsequently the model can be implemented in a RANS code, for example the finite element code Natur [118] in which the SCIT model is already implemented. The CFD code solves the Reynolds Averaged Navier-Stokes equations. The unclosed terms ($\overline{u_iu_j}$, $\overline{u_i\theta}$, $\overline{\theta^2}$) are obtained by integration of the spectra $\varphi_{ij}(\boldsymbol{x},K,t)$, $F_{u_i\theta}(\boldsymbol{x},K,t)$ and $E_\theta(\boldsymbol{x},K,t)$. The so obtained model of turbulent flows can be considered as a spectral equivalent of the Reynolds-stress and scalar flux one-point models. The SCIT1 model has already been implemented in this code by Touil [1] and applied to the cases

of a backward facing step, diffuser and wing profile.

The advantage of the present approach is that no dissipation equation is needed and that spectral desequilibrium can be taken into account. The price we have to pay is that we have to solve equations for the whole wave number spectrum. The model is therefore more expensive than one-point models. The approach should therefore be seen as a tool giving information on turbulent flows and scalar mixing that can not be revealed by one-point approaches and that are numerically not tractable by direct numerical simulations. A good test case would for example be the diffusion of heat from a line source in homogeneous shear flow as discussed in section 5.6.2.

Chapter 7

Inviscid turbulence, single-particle dispersion and a self-consistent Markovian two-point closure

In the first section we apply the EDQNM theory to the limit of zero viscosity: we study the evolution of the spectrally truncated Euler equations towards their equilibrium. Subsequently, in the second part of this chapter the EDQNM model is applied to a non-diffusive scalar flux to predict lagrangian single-particle diffusion. Eventually, in section 7.3, a new two-point closure is proposed based on the displacement of particles in an isotropic turbulence.

7.1 Spectral dynamics of inviscid isotropic turbulence

The evolution of the energy spectrum of the inviscid spectrally truncated Euler equations is studied by closure calculations and the results are compared to recent DNS results. The time evolution of the wavenumber that marks the beginning of the equipartition range is determined. The spectral energy flux is shown to be constant in a zone around this wavenumber.

Recently renewed interest is shown in the evolution of inviscid turbulence. Cichowlas, Bonaïtiti, Debbasch and Brachet [119] (in the following abbreviated by CBDB), show results of Direct Numerical Simulations (DNS) of the spectrally truncated 3-D incompressible Euler equations with resolutions of 256^3, 512^3 and 1024^3 wavemodes. The spherically averaged energy spectrum $E(K)$ shows at intermediate scales a $K^{-5/3}$ Kolmogorov scaling.

At larger scales a thermalized region is observed, showing a K^2 wavenumber dependence. This K^2 energy distribution corresponds to an equipartition of energy over wavenumbers in a region in which the wavemodes are in absolute equilibrium.

The Eddy-Damped Quasi-Normal Markovian theory (EDQNM) [21] is known to be compatible with both the equipartition of kinetic energy (as shown by Carnevale *et al.* [120]) and a $K^{-5/3}$ inertial range. Also, calculations at higher resolution than DNS can be performed at a much lower computational cost. EDQNM seems therefore an adequate tool to investigate the high-resolution spectral dynamics of the incompressible Euler equations.

In purpose of the present letter is to obtain information about the mechanism of relaxation towards the energy equilibrium state. We define a wavenumber K^- so that $E(K^-) \leq E(K)\ \forall\ K$. At wavenumbers larger than K^- the energy is in absolute equilibrium. The location of K^- is therefore an important parameter to describe the evolution of $E(K)$.

In the following we will analyze a freely evolving inviscid velocity field, the term decaying would be misleading because no energy is dissipated. The non linear interactions will create a $K^{-5/3}$ inertial range. This $K^{-5/3}$ Kolmogorov scaling range was studied in superfluid turbulence in the works of Nore *et al.* [121, 122]. In this range we presume the scaling:

$$E(K,t) = C_K \epsilon(t)^{2/3} K^{-5/3} \tag{7.1}$$

with $\epsilon(t)$ the spectral energy flux. The Kolmogorov range advances with time towards higher wavenumbers. At a certain time t_0 the end of the inertial range will meet the maximum wavenumber of our truncated domain K_f and an equipartition spectrum,

$$E(K,t) = A(t) K^2, \tag{7.2}$$

will build up from larger to smaller wavenumbers. $A(t)$ is a function of time. From the last two equations we can calculate the intersection of the two zones, yielding an estimate for K^-:

$$K^-_{PL}(t) \sim \left(\frac{\epsilon}{E_{th}^{3/2}} \right)^{2/11} K_f^{9/11}, \tag{7.3}$$

in which E_{th} the part of the energy contained in the equipartition range.The subscript PL indicates that a power law inertial range is presumed reaching the equipartition range at $K = K^-$. The DNS results of CBDB show however that the $K^{-5/3}$ does not extend up to the K^2 zone but that a 'dissipative' zone separates the two zones. If it is this part of the spectrum that governs the energy flux towards the equipartition zone and not the $K^{-5/3}$ zone, K^- can be estimated in another way. CBDB showed that the

local timescale τ around K^- is proportional to:

$$\tau \sim \frac{C}{K\sqrt{E_{th}}}. \tag{7.4}$$

Using this timescale to estimate the local spectral energy flux in the vicinity of K^- yields the 'dissipative estimate' of K^-:

$$K^-_{diss}(t) \sim \left(\frac{\epsilon}{E_{th}^{3/2}}\right)^{1/4} K_f^{3/4} \tag{7.5}$$

In the work of CBDB no conclusive choice could be made which estimate is the most appropriate. The relative cheapness of EDQNM calculations allows for long time, high resolution calculations that can help us to choose between the two estimates.

The evolution equation for the energy spectrum is the Lin equation without viscosity:

$$\frac{\partial E(K,t)}{\partial t} = T_{NL}(K,t) \tag{7.6}$$

The non-linear transfer T_{NL} is modeled by the EDQNM theory:

$$T_{NL}(K,t) = \iint_\Delta \Theta\ (xy+z^3)\left[K^2PE(P)E(Q) - P^3E(Q)E(K)\right]\frac{dPdP}{PQ} \tag{7.7}$$

Δ is a band in P,Q-space so that the three wave vectors $\boldsymbol{K},\boldsymbol{P},\boldsymbol{Q}$ form a triangle. x,y,z are the cosines of the angles opposite to the sides K,P,Q of the triangle formed from $\boldsymbol{K},\boldsymbol{P},\boldsymbol{Q}$. The characteristic time $\Theta(K,P,Q,t)$ is defined as:

$$\Theta(K,P,Q,t) = \frac{1-exp(\mu_{KPQ,t}\times t)}{\mu_{KPQ,t}} \tag{7.8}$$

The eddy damping is generally written

$$\mu_{KPQ} = \eta(K,t)+\eta(P,t)+\eta(Q,t)) \tag{7.9}$$

We use the formulation proposed by Pouquet *et al.* [63]:

$$\eta(K,t) = \lambda\sqrt{\int_0^K S^2E(S,t)dS} \tag{7.10}$$

λ is chosen equal to 0.36 in order to yield an adequate value for the Kolmogorov constant.

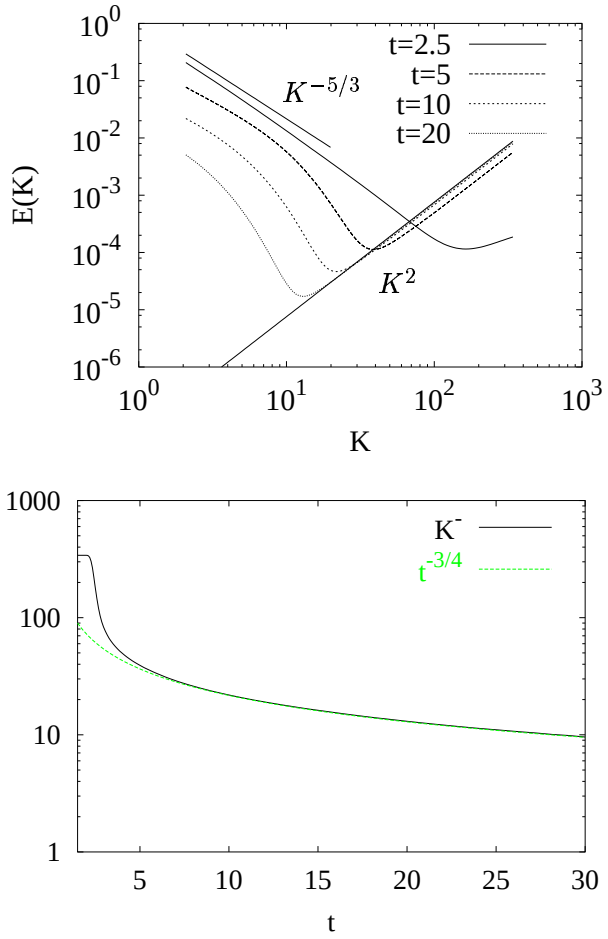

Figure 7.1: Top: evolution of the energy spectrum $E(K)$. The solid lines indicate the $K^{-5/3}$ and K^2 spectral slopes. Bottom: evolution of the parameter K^-. The dotted line corresponds to a $t^{-3/4}$ time dependence.

First we perform a calculation with a ratio of smallest to largest wavenumber $K_f/K_0 = 341$, a resolution equivalent to the 1024^3 DNS calculation of CBDB. The initial energy spectrum is given by:

$$E(K,0) = BK^S e^{-2K^2/K_L(t=0)^2}, \tag{7.11}$$

with $K_0 = 1$, $K_L(t=0) = 1$ and $K_f = 341$ and B determined so that the total kinetic energy is equal to 1. This spectrum has a maximum at $K = K_0$, the large scales are saturated from the beginning. The results are shown if figure 7.1. The evolution is shown to be comparable to the DNS results of CBDB. We observe the power law inertial range, the dissipation range and the equipartition range. The closure calculations were however performed for a longer time interval. In the top figure we see that for $t \approx 10$, A approaches its asymptotic value, which means that E_{th} approaches the total kinetic energy. The estimates K^-_{PL} and K^-_{diss} should then become proportional to ϵ^n with n equal to $2/11$ and $1/4$ respectively according to equations (7.3) and (7.5). When the size of the large scales is restricted by the size of the numerical domain the decay of spectral flux obeys:

$$\epsilon(t) \sim t^{-3} \tag{7.12}$$

as shown experimentally by Skrbek and Stalp [111] and by DNS, LES and closure calculations of Touil *et al.* [112]. At $t > 10$ one finds therefore:

$$\begin{aligned} K^-_{PL} &\sim t^{-6/11} \\ K^-_{diss} &\sim t^{-3/4} \end{aligned} \tag{7.13}$$

In figure 7.1, we plotted K^- as a function of time and it is observed that the evolution is properly described by $t^{-3/4}$.

EDQNM allows for calculations larger then the $K_f/K_0 = 341$ resolution. We performed a calculation at a $K_f/K_0 = 10^4$ resolution, with a K^4 low wavenumber zone. The results are shown in figure 7.2. This calculation is not influenced by the large scale saturation. The spectral evolution is shown in the top figure. The non-linear transfer is also shown. An interesting feature is the plateau at which no or little transfer is observed around K^-. It is thus at this zone that the spectral flux is approximately constant rather than in the inertial range. In the bottom figure it is again shown that the dissipative estimate is superior to the power-law estimate of K^-.

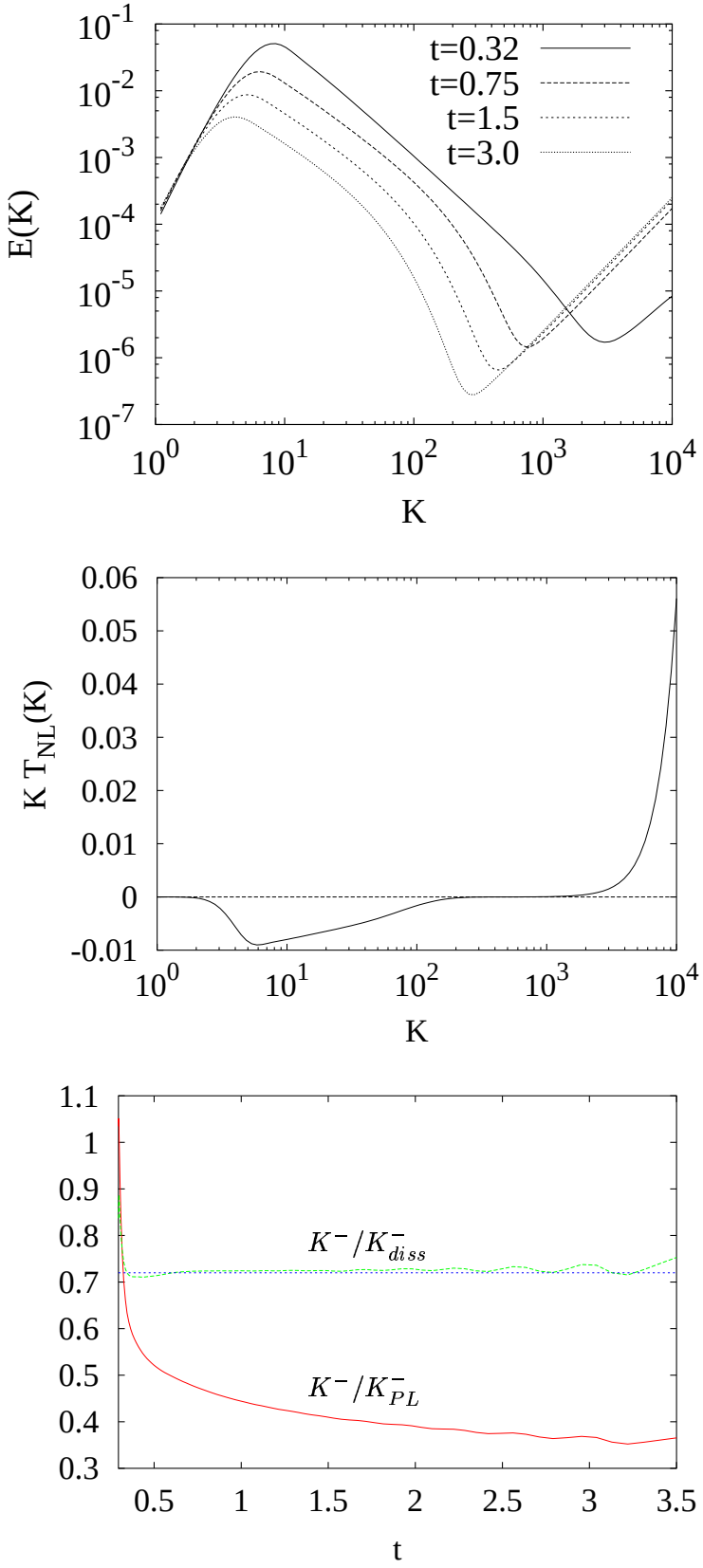

Figure 7.2: Top: spectral evolution of the high resolution energy spectrum. Middle: non-linear transfer, corresponding to the time $t = 3$. Bottom: evolution of K^-, compared to the two estimates K^-_{PL} and K^-_{diss} (equations (7.3) and (7.5)).

7.2 The non-diffusive scalar: applying the EDQNM theory to single-particle diffusion

Larcheveque and Lesieur [123] considered two-particle dispersion using the EDQNM approach. We similarly use the EDQNM equations, but our approach uses the equations derived for the scalar flux spectrum to predict single-particle dispersion, whereas they derived the equation for relative dispersion.

We consider an isotropic turbulent velocity field on which we impose a constant uniform mean temperature gradient in the z-direction. A non-diffusive scalar fluctuation obeys then the equation:

$$\frac{d\theta}{dt} + w\frac{\partial \Theta}{\partial z} = 0 \tag{7.14}$$

We define $z = 0$ as the z-position of the fluid particle at $t = 0$. The equation can subsequently be solved to yield:

$$\theta(\boldsymbol{x}, t) = -\frac{\partial \Theta}{\partial z} z'(\boldsymbol{x}, t) \tag{7.15}$$

The scalar fluctuation is directly related to the vertical separation distance z' from its initial position. The average of the squared separation distance is then:

$$\overline{z'(\boldsymbol{x}, t)^2} = \left(\frac{\partial \Theta}{\partial z}\right)^{-2} \overline{\theta(\boldsymbol{x}, t)^2} \tag{7.16}$$

The scalar variance in isotropic turbulence with a mean scalar gradient is thus directly related to one-particle dispersion.

We can write the equation for the scalar variance:

$$\frac{\partial \overline{\theta^2}}{\partial t} = -2\frac{\partial \Theta}{\partial z}\overline{w\theta} \tag{7.17}$$

To solve equation (7.17), we only need to calculate the scalar flux . We solve the EDQNM calculations for $E(K, t)$ and $F_{w\theta}(K, t)$ at a $R_\lambda = 92$. The energy spectrum is fixed. At every timestep we integrate the scalar flux spectrum to obtain $\overline{w\theta}$ and solve (7.17). The result is shown in figure 7.3. As predicted by Taylor [124], the ballistic zone with a t^2 dependence is followed by a zone of brownian motion, proportional to t. The corresponding spectra at $t = 100$ are shown in figure 7.4.

This result is an example how an Eulerian study of passive scalar mixing can be related to Lagrangian turbulence caracteristics. For an extensive review on this subject we refer to Sawford [125]. Future investigations will involve the horizontal and vertical dispersion in homogeneous shearflows, based on the model in chapter 5.

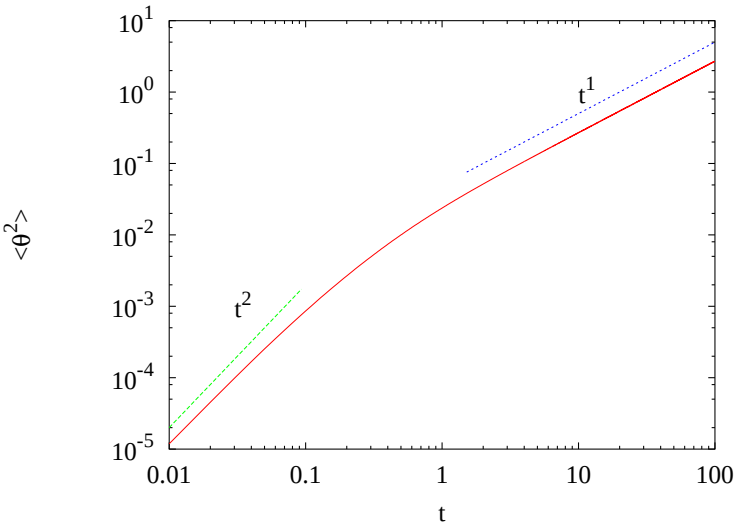

Figure 7.3: One-particle diffusion in isotropic turbulence as predicted by the EDQNM model.

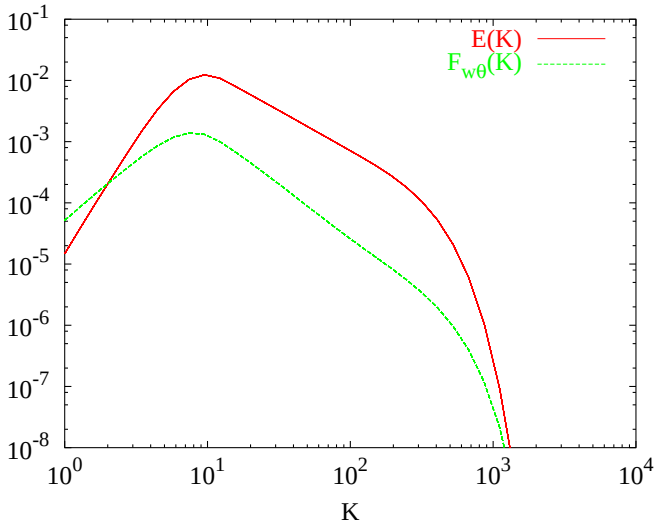

Figure 7.4: Energy and scalar flux spectrum for the case in figure 7.3 at $R_\lambda = 92$ and $t = 100$.

7.3 A Markovian two-point closure based on particle displacements in a scalar field

In the previous section, we illustrated the link between Lagrangian and Eulerian quantities, using the velocity-scalar cross correlation. In the present section it will be shown that this link allows us to use the equations derived in chapter 3 to formulate a closure for the kinetic energy, the scalar flux and the scalar variance spectra, without having to specify empirically a damping term or to adjust a numerical constant (as is the case for EDQNM). The idea is that the damping term in two-point one-time closures is the inverse of the Lagrangian correlation time of the velocity field and that this time can be deduced from the scalar-velocity correlation spectrum in the case of turbulence with a uniform mean scalar gradient. The Kolmogorov constant will be estimated with this closure. Subsequently the theory is applied to scalar mixing and an estimation of the Corrsin-Obukhov constant will be obtained.

The assumptions, leading to the EDQNM equations are the Markovianization, the Quasi-Normal assumption, and the introduction of a correction of the QNM equations, the eddy damping. The need for this correction was discussed in chapter 3. The choice of the damping is based either on pure dimensional analysis or on some crude physical assumptions. The final expression involves always an adjustable parameter that is chosen so that the model results correspond to numerical or laboratory experiments.

It is possible to give an interpretation of the damping frequency $\eta(K)$, that intervenes in the EDQNM closure if one considers the self consistent theories of turbulence i.e. theories derived from the Navier-Stokes equations, that are free from adjustable parameters. We name the two-point two-time closures such as the Direct Interaction Approximation (DIA) by Kraichnan [126] or its Lagrangian extension [67] and other variants can be found in the book of Leslie [127]. All these theories involve a similar timescale $\eta(K,t)^{-1}$ as we encounter in the eddy damping term. The following is a brief overview and details can be found in Leslie [127] or Bertoglio [25].

DIA is based, like EDQNM, on an assumption of Gaussianity. The influence of the non-linear terms is in this model treated as a perturbation of a Gaussian field. We define the two-time energy spectrum $E(K,t,t')$ as:

$$\overline{\hat{u}_i(\boldsymbol{K},t)\hat{u}_j(\boldsymbol{M},t')} = \delta(\boldsymbol{K}+\boldsymbol{M})P_{ij}(\boldsymbol{K})\frac{E(K,t,t')}{4\pi K^2} \tag{7.18}$$

The main role in DIA is played by the Green function $G(\boldsymbol{K},t,t')$, which associates the response of a mode $\boldsymbol{K}$ of the velocity field at a time t to a perturbation of this same mode at a time t'. In an isotropic turbulence we can express $G(\boldsymbol{K},t,t')$ as a function of the wavenumber. We will call the resulting expression $G(K,t,t')$. To proceed it is generally assumed that

$G(K,t,t')$ is an exponentially decaying function of $t-t'$:

$$G(K,t,t') = exp[-\eta(K)(t-t')] \tag{7.19}$$

An additional hypothesis is that one can apply the *fluctuation-dissipation* theorem that allows to write:

$$E(K,t,t') = G(K,t,t')E(K,t') \tag{7.20}$$

so that:

$$\frac{E(K,t,t')}{E(K,t')} = exp[-\eta(K)(t-t')] \tag{7.21}$$

The two-point correlation at a wavenumber K decays thus with a characteristic timescale $\eta(K)^{-1}$, that we can interpret as the correlation time at a wavenumber K:

$$\eta(K,t)^{-1} = \mathcal{T}(K,t) \tag{7.22}$$

It was subsequently shown that the Eulerian formulation of DIA was not invariant under Galilean transformation and that it is therefore incompatible with a $K^{-5/3}$ Kolmogorov inertial range. Kraichnan [67] reformulated the theory in a Lagrangian framework thus resolving the problem but yielding a very complicated set of equations. It appears that the Lagrangian history is an essential ingredient that somehow should be modeled if one tries to obtain a single-time closure. Kraichnan proposed a way to do this by considering the evolution of an auxiliary velocity field, transported by the turbulence itself, leading to his almost-Markovian closure (Test Field Model) [128]. We will proceed in a different way.

7.3.1 Presentation of the model

The starting point in deriving the model introduced in this section is the observation that in isotropic turbulence with a mean scalar gradient the value of the scalar fluctuation can be found by:

$$\theta(\boldsymbol{x},t) = -\frac{\partial\Theta}{\partial z}\int_{\mathcal{T}'}\mathcal{U}_3(\boldsymbol{x},t \mid \tau)d\tau \tag{7.23}$$

with $\mathcal{T}'$ the Lagrangian (single particle) correlation time. In the case of zero diffusivity this time will tend to infinity when t goes to infinity because the scalar value will not decorrelate from the fluid particle. In the following the scalar gradient will be taken equal to -1 to simplify the equations.

The correlation of θ with the velocity at point $\boldsymbol{x}+\boldsymbol{r}$, $w(\boldsymbol{x}+\boldsymbol{r},t)$, is then:

$$\overline{\theta(\boldsymbol{x},t)w(\boldsymbol{x}+\boldsymbol{r},t)} = \overline{\left(\int_{\mathcal{T}'}\mathcal{U}_3(\boldsymbol{x},t \mid \tau)d\tau\right)w(\boldsymbol{x}+\boldsymbol{r},t)} \tag{7.24}$$

we replace the Eulerian velocity by:

$$w(\boldsymbol{x},t) = \mathcal{U}_3(\boldsymbol{x},t \mid t) \tag{7.25}$$

and we normalize by $\overline{w(\boldsymbol{x},t)w(\boldsymbol{x}+r,t)}$, to obtain, in the case of zero diffusivity, the definition of the Lagrangian two point correlation time:

$$\frac{\overline{\theta(\boldsymbol{x},t)w(\boldsymbol{x}+\boldsymbol{r},t)}}{\overline{w(\boldsymbol{x},t)w(\boldsymbol{x}+\boldsymbol{r},t)}} = \frac{\overline{\int_{\mathcal{T}'}\mathcal{U}_3(\boldsymbol{x},t \mid \tau)\mathcal{U}_3(\boldsymbol{x}+\boldsymbol{r},t \mid t)d\tau}}{\overline{\mathcal{U}_3(\boldsymbol{x},t \mid t)\mathcal{U}_3(\boldsymbol{x}+\boldsymbol{r},t \mid t)}} = \mathcal{T}(\boldsymbol{r},t) \tag{7.26}$$

or

$$\frac{R_{w\theta}(\boldsymbol{r})}{R_{ww}(\boldsymbol{r})} = \mathcal{T}(\boldsymbol{r}). \tag{7.27}$$

in which we omitted the time dependence. A local (in wavenumber space) estimate of the Lagrangian correlation time from the velocity, and velocity-scalar correlation can then be obtained by:

$$\mathcal{T}(K) = \frac{3}{2}\frac{F_{w\theta}(K)}{E(K)}, \tag{7.28}$$

which can be identified as the eddy damping time scale (equation (7.22)) . The QNM equations for $E(K)$ and $F_{w\theta}(K)$, together with the relaxation frequency:

$$\eta(K) = \frac{2}{3}\frac{E(K)}{F_{w\theta}(K)} \tag{7.29}$$

yield a closed system, without any model constants. Using the Lumley scaling for the scalar flux and the Kolmogorov scaling for the energy spectrum, it can already be anticipated that $\eta(K)$ will show the expected inertial range behaviour, proportional to $\epsilon^{1/3}K^{2/3}$.

7.3.2 Results for the Kolmogorov and Corrsin-Obukhov constants

We use the equations in chapter 3, section 3.1.7 in which the damping $\eta(K)$ is replaced by equation (7.29). The velocity field is initialized by the form in equation (7.11). It is straight forward to apply the model to an isotropic scalar. The initial scalar spectrum is identical to the initial velocity spectrum. $R_\lambda = 1400$, the Prandtl number is 0.71.

We show the results in figure 7.5. A $K^{-5/3}$ inertial range is obtained. The value of the Kolmogorov constant is estimated to be 1.75. We remind that in the EDQNM closure this value is dependent on the constant λ. The Corrsin-Obukhov constant is estimated to be 0.32.

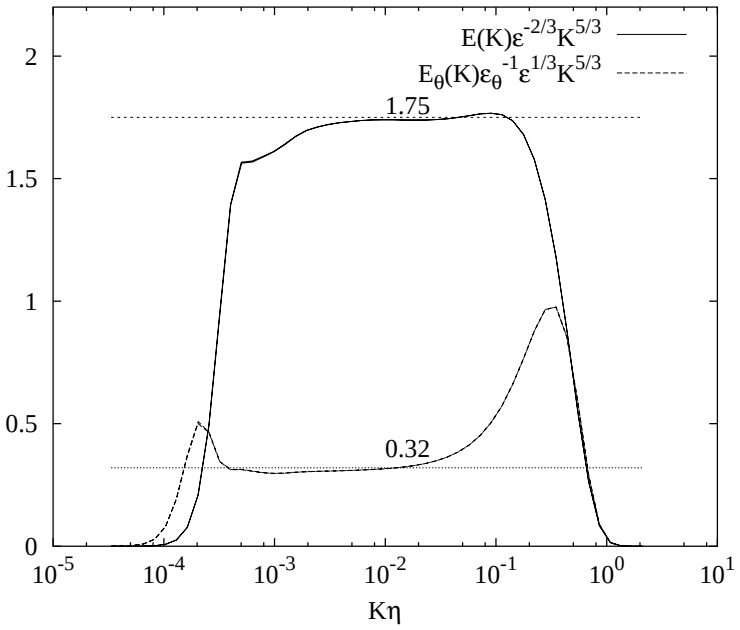

Figure 7.5: Compensated energy and scalar spectra calculated with the single-time two-point closure at $R_\lambda = 1400$, Pr=0.71.

Conclusion

The mixing of a passive scalar in a turbulent flow and in particular the scalar flux were studied in this thesis. In chapter 2 a compilation of experimental data about the spectrum of the scalar flux showed in numerous cases an inertial range behaviour different from the generally believed dimensional analysis, that predicts a $K^{-7/3}$ inertial range: a K^{-2} behaviour was observed in a number of experiments at moderate and even high R_λ. DNS showed the existence of a spectral range in which $F_{w\theta}(K)$ is not produced by the production by the mean gradient, but by the non linear interaction. This observation provides support to a cascade type of analysis. When a spectral flux of scalar flux, $\epsilon^F_{w\theta}(K)$, is introduced, dimensional analysis yields an inertial range slope for $F_{w\theta}(K)$ dependent on a parameter γ that reflects the evolution of the spectral flux in the cascade of $F_{w\theta}(K)$. In the high Reynolds number limit, the asymptotic spectrum obtained allows for a slope between $K^{-5/3}$ and $K^{-7/3}$. The LES results presented in this chapter supported a K^{-2} expression.

In chapter 3 the EDQNM theory was introduced and used to study the scalar flux. The choice of the two constants that appear in the closure is extensively discussed. The influence of the variation of these constants on the spectral balance between the terms in the evolution equation for $F_{w\theta}(K)$ was examined. The final choice of the constants is supported by LES calculations.

At moderate Reynolds numbers the one dimensional spectra obtained with the EDQNM theory are shown to agree with experimental results and DNS. The low computational cost of the closure calculations allows to perform calculations at very high Reynolds numbers. For these very high R_λ, the result of the EDQNM model is clearly that $F_{w\theta}(K)$ scales as $K^{-7/3}$, in agreement with Lumley's [31] dimensional analysis. However at R_λ corresponding to the experiment of Mydlarski and Warhaft [40], values of the exponent closer to -2 were found. An empirical relation $n_{w\theta} = 7/3\ (1 - 2.73\ R_\lambda^{-0.54})$ was shown to describe the evolution of the spectral exponent. The molecular destruction of scalar flux normalized by the production was shown to obey the $R_\lambda^{-0.77}$ power law at low R_λ in agreement with DNS. For higher values this quantity tends towards an asymptotic

R_λ^{-1} behaviour that can easily be predicted by dimensional analysis.

These results, in agreement with classical dimensional analysis, raised the question why a K^{-2} inertial range behaviour was found in the LES presented in chapter 2. The EDQNM theory was used to analyze this issue. The influence of the subgrid-model was first investigated by implementing the Chollet-Lesieur subgrid-model in the EDQNM equations. Subsequently LES were performed using an alternative subgrid-model derived by Shao. The subgrid-model was shown not to be responsible for the -2 slope. The influence of forcing was studied by EDQNM calculations forcing the smallest two wavenumbers. A K^{-2} zone of about one decade was observed as a result of the forcing. It was pointed out that this zone is not subject to inertial behaviour, but that the turbulent lengthscales corresponding to the forced wavenumbers induce this scaling. LES were performed to check this assumption: the velocity field was still forced by injecting energy at small wavenumbers, but in the calculation of the scalar field the influence of the forced wavemodes was removed. The resulting scalar flux spectrum showed a $K^{-7/3}$ inertial range.

The EDQNM closure was then applied to homogeneous shear flow with a uniform scalar gradient perpendicular to the flow direction. To reduce the numerical difficulty of solving the equation of the wavevector dependent scalar flux spectrum, $\mathcal{F}_i(\mathbf{K}, t)$, we integrated the equation over spherical shells with radius K to obtain the variable $F_{u_i\theta}(K, t)$. This approach yields unclosed terms that were modelled by tensor invariant theory. One-point statistics were compared to experimental results and good agreement was observed. The spectra associated to the streamwise and cross-stream scalar fluxes were analyzed. The spectral slope of the cross-stream spectrum tends towards a $-7/3$ value. The streamwise scalar flux spectrum is shown to behave differently from classical predictions. An asymptotic $K^{-23/9}$ behaviour is observed in agreement with experimental observations.

In chapter 6 the equations of the inhomogeneous scalar flux and variance spectra equations were derived, to extend the applicability of the two-point closure used in this work to inhomogeneous scalar mixing.

Eventually, in chapter 7 the limit of respectively zero viscosity and zero diffusivity are investigated by EDQNM theory. Zero viscosity yields the Euler equations. The evolution of the spectrally truncated Euler equations towards their equilibrium state was investigated. A good qualitative agreement with DNS results of Cichowlas *et al.* [119] was observed. Subsequently calculations were performed at higher resolutions to be able to choose between two estimates of the local minimum of the energy spectrum, proposed by Cichowlas *et al.*

Zero diffusivity yield the equation for the advection of particles by a turbulent flow: the EDQNM theory was shown to yield the correct result for lagrangian single-particle diffusion. The link between particle displacement and scalar mixing allows to formulate a single-time two-point closure that does not involve any model constants.

This thesis illustrates the role that two-point closures can still play in turbulence research next to direct simulations and experiments. At low Reynolds number their results agree with DNS. Their low computational cost allows to perform calculations at very high Reynolds numbers where dimensional analysis at asymptotic R_λ can be tested. At intermediate values, good agreement is observed with laboratory experiments and the gap between wind-tunnel measurements and atmospheric measurements can be filled. In addition, two-point closures can play an important role in the analysis of forcing and subgrid-effects present in numerical simulations. Eventually, theoretical studies can be performed in the limit of zero viscosity and diffusivity.

Interesting directions for future research would be the implementation of the inhomogeneous model (chapter 6) and its application to combustion. From a theoretical point of view it would be interesting to exploit the link between scalar mixing and particle diffusion in more detail. Finally, the model formulated in section 7.3 deserves more attention.

Chapter 8

Résumé du travail effectué

Les sections 8.1 à 8.7 sont respectivement des résumés des chapitres 1 à 7.

8.1 Mélange d'un scalaire en turbulence isotrope

On appelle scalaire passif une quantité scalaire transportée par un écoulement et qui n'exerce pas d'influence sur cet écoulement. Un exemple est la concentration d'un polluant dans l'atmosphère. Le champ de température peut également être considéré comme un champ scalaire passif si les inhomogénéités de température restent petites. Nous examinons dans ce manuscrit le mélange d'un scalaire passif dans un écoulement turbulent.

La multiplicité d'échelles d'un écoulement turbulent est fonction du nombre de Reynolds. Ce nombre s'interprète comme le rapport entre les effets convectifs (le transport de quantité de mouvement par les particules de fluide) et les effets dissipatifs (le mélange de quantité de mouvement par la viscosité moléculaire). Un écoulement à grand nombre de Reynolds contient une large gamme d'échelles de longueur différentes. Le champ de scalaire reflète ce caractère multi-échelle[1]. Ainsi l'étude du scalaire passif nous permet de visualiser et d'examiner des proprietés intrinsèques de l'écoulement sous-jacent. Sur la figure 8.1 on visualise, à titre d'exemple, un champ des fluctuations de scalaire, mélangé par un écoulement turbulent, issu d'une simulation numérique directe.

La déscription spectrale de la turbulence est une manière mathématiquement commode d'étudier son caractère multi-échelle. Simultanément, son caractère aléatoire nous amène à introduire des moyennes statistiques des quan-

[1] Le rapport entre la taille des plus petites structures scalaires et des plus petits tourbillons est une fonction croissante du nombre de Prandtl, Pr. On considerera dans ce travail le cas de $Pr \approx 1$ dans quel cas la taille des plus petits tourbillons est comparable à celle des plus petites structures du scalaire.

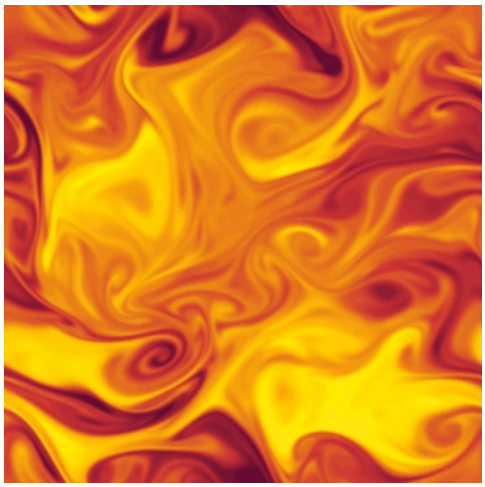

Figure 8.1: Champ des fluctuations de scalaire, mélangé par un écoulement turbulent isotrope en présence d'un gradient moyen de scalaire; DNS à $Pr = 25$, $R_\lambda = 46$. Résultat de Brethouwer [129].

tités étudiées. Ainsi nous considérons les moyennes statistiques de la distribution spectrale de l'énergie cinétique, de la variance de scalaire et du flux de scalaire comme nos variables principales. L'analyse dimensionelle prédit des comportements asymptotiques pour ces variables, pour des nombres de Reynolds qui tendent vers l'infini. A des nombres de Reynolds limités, la simulation numérique directe (DNS) permet d'examiner les mécanismes turbulents sans introduire aucune notion de moyenne statistique.

Une façon classique d'examiner ces mêmes quantités sont les théories analytiques, ou modèles en deux points. La fermeture en deux points nécessite beaucoup moins de ressources informatiques que la simulation numérique directe et peut aborder des nombres de Reynolds beaucoup plus élévés. Il y a alors complémentarité entre les méthodes de simulation directe et les techniques de fermeture en deux points. En les associant on peut examiner le comportement des écoulement turbulents dans toute la gamme de nombres de Reynolds.

8.2 Analyse dimensionelle et simulations numériques

Le spectre $F_{w\theta}(K)$ du flux d'un scalaire passif dans une turbulence isotrope en présence d'un gradient moyen de scalaire possède une zone en loi de puissance lorsque le nombre de Reynolds est assez grand. Le comportement

dans cette zone a été prédit par Lumley [17]:

$$F_{w\theta}(K) \sim \Gamma \epsilon^{1/3} K^{-7/3} \tag{8.1}$$

où Γ représente le gradient moyen, ϵ la dissipation et K le nombre d'onde. Cependant, dans les expériences de turbulence de grille, Mydlarski et Warhaft [40] trouvent un spectre qui est plus proche d'une loi d'échelle en K^{-2}. Dans les mesures atmosphériques récentes de Su *et al.* [38] le spectre vérifie également approximativement une loi en K^{-2}. Dans cette section, nous examinons la possibilité d'une loi d'échelle asymptotique décroissante en K^{-2}.

L'évolution du spectre du flux d'un scalaire passif dans une turbulence isotrope en présence d'un gradient moyen de scalaire est décrit par l'équation:

$$\frac{\partial}{\partial t} F_{w\theta}(K) + (\nu + \alpha) K^2 F_{w\theta}(K) = P(K) + T_{w\theta}^{NL}(K) + \Pi(K) \tag{8.2}$$

Le deuxième terme du membre de gauche représente la dissipation moléculaire de flux de scalaire, $P(K)$ est la production de flux de scalaire, $T_{w\theta}^{NL}(K)$ représente l'effet des corrélations triples et $\Pi(K)$ l'influence de la pression. La figure 2.3 montre ces différentes contributions. Les résultats sont issus d'une simulation numérique directe (DNS) avec une résolution spectrale de 256^3.

On observe que la dissipation est faible devant la production. C'est alors principalement le terme de pression qui équilibre la production. On note également que cet équilibre entre pression et production n'est pas local dans le spectre: la production domine la pression à petit nombre d'onde alors que c'est le contraire pour les nombres d'onde plus grands. Ce déséquilibre peut être expliqué par la présence d'un terme non-linéaire, observé également sur la figure 2.3: le terme de transfert $T_{w\theta}^{NL}(K)$. L'existence de ce terme encourage à introduire un flux spectral $\epsilon_{w\theta}^{F}(K)$ dans l'analyse visant à proposer la loi d'échelle pour spectre de flux de scalaire. L'analyse dimensionelle donne alors:

$$F_{w\theta}(K) \sim \epsilon_{w\theta}^{F}(K) \epsilon^{-1/3} K^{-5/3} \tag{8.3}$$

On remarque que (8.3) est équivalent à la loi d'échelle de Corrsin-Obukhov [9] pour le spectre de la variance de scalaire $E_\theta(K)$, dans laquelle $\epsilon_{w\theta}^{F}(K)$ remplace ϵ_θ, la dissipation de fluctuations de scalaire. Le flux $\epsilon_{w\theta}^{F}(K)$ est une quantité associée au terme de transfert non-linéaire $T_{w\theta}^{NL}(K)$. Ce flux n'est pas conservé dans la cascade, $F_{w\theta}(K)$ étant détruit par l'effet de la pression. On suppose alors que le flux diminue suivant une loi de puissance en fonction de K:

$$\epsilon_{w\theta}^{F}(K) \sim K^{-\gamma} \tag{8.4}$$

où γ est un exposant inconnu qui reste à fixer.

On utilise le fait que le coefficient de corrélation entre la vitesse et le scalaire approche une valeur constante pour les temps longs et on admet la

proportionnalité entre production et dissipation de fluctuations de scalaire ce qui mène à l'expression:

$$F_{w\theta}(K) \sim \Gamma \overline{u^2}^{(1-3\gamma/2)} \epsilon^{\gamma-1/3} K^{-(5/3+\gamma)} \tag{8.5}$$

En introduisant une hypothèse de type *Rotta* [130], on suppose que le terme de pression $\Pi(K)$ est inversement proportionnel à une échelle de temps locale $\tau(K)$, construite à partir du flux spectral d'énergie ϵ et le nombre d'onde, et à $F_{w\theta}(K)$ [50]:

$$\Pi(K) \sim \epsilon^{1/3} K^{2/3} F_{w\theta}(K) \tag{8.6}$$

de sorte que le terme de pression est proportionel à $K^{-(\gamma+1)}$. La valeur $\gamma = 0$ correspond au cas limite où le flux $\epsilon^F_{w\theta}(K)$ est constant dans la cascade, ce qui est exclu par la présence de la pression. Une valeur négative pour γ traduirait un flux croissant ce qui est également exclu. Le cas $\gamma = 2/3$ correspond à l'autre cas limite: la loi d'échelle de Lumley traduite par l'équation (8.1). Dans ce cas la production et la pression déclinent dans la zone inertielle de la même façon, en $K^{-5/3}$. Les valeurs de γ plus grandes sont exclues parce que la production ne serait alors plus équilibrée ni par la pression, ni par le transfert. Il ressort que $0 < \gamma \leq 2/3$. Dans le cas particulier $\gamma = 1/3$ on trouve:

$$\gamma = 1/3 \quad \rightarrow \quad F_{w\theta}(K) \sim \Gamma \mathcal{U} K^{-2} \tag{8.7}$$

Pour déterminer la valeur de γ dans l'équation (8.5), on a recours à la simulation des grandes échelles avec une résolution de 128^3. Le modèle de sous-maille utilisé est le modèle de viscosité turbulent de Chollet et Lesieur pour le champ de vitesse. Pour le champ de sous-maille de scalaire on choisit un nombre de Prandtl turbulent $Pr_T = 0.6$. Sur la figure 2.6 on montre le spectre de flux de scalaire sous forme compensée, d'après les relations (8.1) et (8.7). Le comportement en K^{-2} est clairement présent.

L'equation (8.6) prédit pour $\gamma = 1/3$ une pente de $-4/3$ pour le terme de pression. Sur la figure 2.7 on montre la forme compensée du terme de pression. La simulation permet effectivement de constater ce comportement en $K^{-4/3}$.

8.3 La théorie Quasi-Normale Markovianisée avec Amortissement Tourbillonnaire

Les simulations numériques directes (DNS) fournissent une information sur toutes les échelles d'un écoulement turbulent, mais la limitation des ressources informatiques fait que ces simulations ne peuvent atteindre de grands nombres de Reynolds. La simulation des grandes échelles est applicable aux

nombres de Reynolds élevés, mais elle peut difficilement renseigner sur les comportements inertiels en raison de l'utilisation de modèles pour prendre en compte les effets de sous-maille. Une troisième méthode, applicable à grand R_λ et donnant une information sur tout le spectre, est l'utilisation de fermetures en deux points. Dans le chapitre 3, on emploie la fermeture Quasi-Normale Markovianisée avec Amortissement Tourbillonnaire (EDQNM) pour étudier le comportement spectral du flux de scalaire. Une illustration de son avantage comparé aux LES et aux DNS est donnée sur la figure 1.4, où l'on voit que en EDQNM une plage spectrale très large peut être resolu à très grand nombre de Reynolds.

La fermeture EDQNM a été dérivée par Orszag [21] pour le spectre d'énergie cinétique en turbulence isotrope. Cette théorie conduit à exprimer le transfert non-linéaire T^{NL} qui intervient dans l'équation de Lin (éq. 1.17). La théorie a été étendue au cas du spectre de la variance d'un scalaire par Vignon et Cambon [23] et par Herring *et al.* [22]. Le spectre du flux de scalaire dans une turbulence isotrope en présence d'un gradient moyen de scalaire est traité dans Herr *et al.* [20]. On utilise l'approche de ces auteurs dans le présent travail. La dérivation des équations EDQNM se trouve en détail dans le chapitre 3. Le découplage des différentes contributions non-linéaires dans le bilan spectral de $F_{w\theta}(K)$ nous permet de déterminer les deux constantes dans le modèle.

Le spectre d'énergie cinétique est initialisé en utilisant l'expression de *Von Kármán* [61]. Le champ scalaire est initialement nul. Les fluctuations sont ensuite créées par l'interaction du gradient de scalaire avec les fluctuations de vitesse.

Les spectres à des Reynolds variant entre 100 et 10^7 sont représentés sur la figure 3.12. La pente de la zone inertielle du spectre à $R_\lambda = 100$ est bien inférieure à $-7/3$. Le spectre à $R_\lambda = 10^7$ possède en revanche une large zone avec une pente proche de $-7/3$. La variation de la pente a été examinée pour des R_λ variant entre 100 et 10^7 et les résultats sont donnés sur la figure 3.11. Il apparaît que la valeur asymptotique à grand R_λ est trouvée $-7/3$, en accord avec l'analyse de Lumley [31]. Cependant, cette pente n'est observée qu'à des nombres de Reynolds très élevés. Aux nombres de de Reynolds correspondant aux expériences de laboratoire, une pente proche de -2 est trouvée. A titre d'illustration on rappelle que dans l'atmosphère les valeurs typiques de R_λ sont de l'ordre de 10^4.

La dissipation moléculaire du flux de scalaire,

$$\epsilon_{w\theta} = \int_0^\infty (\nu + \alpha) K^2 F_{w\theta}(K) dK \tag{8.8}$$

a été mesurée par Mydlarski [41] et évaluée par Overholt et Pope [46] par

simulation numérique directe. La figure 3.14 montre que nos résultats sont en bon accord avec ces travaux à faible R_λ. Une dépendance en $R_\lambda^{-0.77}$ est trouvée, comme en DNS. A grand Reynolds en revanche, un comportement en R_λ^{-1} est trouvée pour le rapport $\epsilon_{w\theta}/\Gamma\mathcal{U}^2$, où $\Gamma\mathcal{U}^2$ désigne la production intégrale de flux de scalaire.

Cette étude illustre le rôle que peuvent jouer, aujourd'hui encore, les fermetures en deux points dans l'analyse des écoulements turbulents. A faible nombre de Reynolds elles reproduisent de manière satisfaisante les comportements trouvés en DNS tandis que leur faible coût de calcul permet de les appliquer à des Reynolds très élevé, et par là, d'aborder des comportements réellement asymptotiques. De plus, les comportements expérimentaux sont bien vérifiés dans la plage intermédiaire de valeurs de R_λ.

8.4 Simulation des Grandes Echelles

Les résultats de la Simulation des Grandes Echelles décrits dans le chapitre 2 font apparaitre une pente asymptotique en -2 pour la zone inertielle du spectre de flux de scalaire, tandis que les résultats de la fermeture EDQNM supportent la pente en $-7/3$ à grand Reynolds. Dans le chapitre 4, les résultats de chapitre 2 sont remis en question. L'utilisation de fermetures spectrales pour analyser l'approche LES est une pratique courante en turbulence isotrope [25, 52]. Nous employons la théorie EDQNM, dérivée dans la chapitre 3, pour analyser l'effet des différents paramètres sur les résultats issus de la LES.

Nous appliquons un filtre, avec une coupure spectrale au nombre d'onde K_c, aux équations de $E(K)$ et $F_{w\theta}(K)$ du modèle EDQNM comme pour l'approche LES (section 4.2). Les intéractions de sous-maille sont ensuite traitées par les mêmes modèles de sous-maille que dans le cadre de la LES: nous utilisons le modèle de Chollet-Lesieur, équation (4.14) et pour la diffusivité de sous-maille nous employons un nombre de Prandtl turbulent de 0.6. Les équations de notre problème sont maintenant:

$$\frac{\partial E(K)}{\partial t} = T(K) + 2\nu_e K^2 E(K) \quad \forall \quad 0 \leq K < K_c \tag{8.9}$$

et

$$\frac{\partial}{\partial t} F_{w\theta}(K) + (\nu_e + \nu_e Pr_t^{-1}) K^2 F_{w\theta}(K) = P(K) + T_{w\theta}^{NL}(K) + \Pi(K) \quad \forall \quad 0 \leq K < K_c \tag{8.10}$$

Le spectre de $E(K)$ est forcé en gardant constant les deux premiers nombres d'onde.

Nous nous intéressons d'abord à l'influence de la résolution spectrale sur le comportement inertiel de $F_{w\theta}(K)$. Sur la figure 4.2 on montre les résultats

pour 3 résolutions différentes. On observe une influence du nombre d'onde de coupure sur les spectres qui se ressent sur environ une décade. La pente varie lentement vers sa valeur asymptotique selon la résolution, d'une façon comparable aux simulations EDQNM complètes (figure 3.11).

Le forçage du spectre $E(K)$ induit une zone dans le spectre de $F_{w\theta}(K)$ qui est proche de K^{-2} (figure 4.5).

Nous reprenons les simulation des grandes échelles mais en changeant le calcul du champs scalaire: les nombres d'onde correspondant au forçage sont enlevés dans le calcul du champ scalaire. Le modèle de sous-maille de Chollet-Lesieur est également remplacé par le modèle des fonctions de structure de Shao [79, 83]. Le résultat est donné sur les figures 4.6 et 4.7. La zone inertielle de $F_{w\theta}(K)$ est maintenant effectivement proportionelle à $K^{-7/3}$.

8.5 Cisaillement homogène

Jusqu'à ce point on n'a considéré que la turbulence isotrope et son influence sur le flux d'un scalaire passif. Dans le chapitre 5 le champ turbulent est soumis à un cisaillement homogène, c'est-à-dire un gradient uniforme de vitesse. Le champ de vitesse est dans ce cas anisotrope mais est supposé homogène comme dans le cas précédent. On pose:

$$S = \frac{\partial U_x}{\partial z}$$

Nous nous concentrons sur le champ d'un scalaire passif advecté par le champ de vitesse dans le cas avec ou sans gradient moyen de scalaire. Ce gradient, quand il est non nul, est choisi parallèle au gradient de vitesse:

$$\Gamma = \frac{\partial \Theta}{\partial z}$$

Les principales quantités sont le spectre de la variance de scalaire $E_\theta(K)$ et, dans le cas où $\Gamma \neq 0$, le flux de scalaire $F_{u_i\theta}(K)$. Ce dernier possède deux composantes non-nulles: $F_{u\theta}(K), F_{w\theta}(K)$, respectivement parallèle à la direction de l'écoulement et parallèle au gradient de scalaire.

Les équations pour $E_\theta(K)$ et $F_{u_i\theta}(K)$ contiennent des termes non-fermés dans notre approche: tout d'abord le transfert non-linéaire et le terme de pression comme nous l'avons vu dans le cas d'une turbulence isotrope. Ensuite, la présence du cisaillement introduit d'autres effets: un terme de pression rapide et un terme de transfert linéaire. Ces termes sont modélisés selon la théorie des invariants. Une constante est ainsi introduite dans le modèle. Cette constante est ensuite déterminée par comparaison avec les résultats

expérimentaux de Tavoularis et Corrsin [92, 93].

Les équations fermées sont alors résolues numériquement. Dans le cas $\Gamma = 0$, la variance de scalaire décline selon une loi exponentielle (comme prédit par Gonzalez [105]) plutôt que selon une loi de puissance. Le cas $\Gamma \neq 0$ est ensuite examiné pour des nombres de Reynolds de 10^2 à 10^4. Sur la figure 5.10 on observe les pentes des spectres de $F_{u\theta}(K)$ et $F_{w\theta}(K)$. On retrouve la pente asymptotique de $F_{w\theta}(K)$ en $-7/3$ comme dans le cas isotrope. L'autre composante, absente en turbulence isotrope, est trouvée presenter une pente d'environ -2.55. Ce résultat n'est pas en accord avec l'analyse dimensionelle de Wyngaard et Coté [32], qui prédit une pente de -3. La valeur -2.55 est en revanche plus proche des valeurs observées expérimentalement [32, 34]. On propose alors une analyse dimensionelle compatible avec les résultats de nos simulations et les expériences en introduisant un flux spectral qui dépend du cisaillement. L'analyse dimensionelle donne dans ce cas:

$$F_{u\theta}(K) \sim \Gamma S^{1/3} \epsilon^{2/9} K^{-23/9} \tag{8.13}$$

8.6 Turbulence inhomogène

La thèse de Laporta [28] a montré que la théorie EDQNM s'adapte bien au calcul des écoulements turbulents faiblement inhomogènes. L'effet des parois sur les échelles turbulentes à été modélisé par Bertoglio et Jeandel [29] par l'introduction d'une coupure infrarouge sur le spectre d'énergie cinétique. On propose une extension de ce modèle au mélange d'un scalaire en turbulence inhomogène en présence de parois avec comme principaux ingrédients la fermeture EDQNM isotrope et la coupure spectrale.

8.7 Turbulence non visqueuse, dispersion d'une particule et proposition d'une nouvelle fermeture Markovienne

8.7.1 Dynamique non visqueuse du spectre d'énergie cinétique dans un domaine spectral tronqué

Le comportement d'une turbulence isotrope pour un fluide incompressible non visqueux (équation d'Euler) est examiné. On s'intéresse au cas d'un domaine spectral tronqué. Dans ce cas, une DNS effectuée par Cichowlas, Bonaiti, Debbasch et Brachet [119] a mis en évidence des phénomènes intéressants : le spectre d'énergie cinétique, initialisé aux grandes échelles, développe une zone de cascade avec une pente proche de $-5/3$. Quand cette zone est étendue jusqu'à la troncature spectrale, une zone d'équipartition d'énergie,

correspondant à un spectre en K^2, se développe. Entre la zone de cascade et la zone d'équipartition un minimum local du spectre existe.

Nous montrons que la fermeture EDQNM peut reproduire le comportement observé dans la DNS. Ensuite, un calcul sur une large plage spectrale est effectué (ce calcul correspondrait à une résolution de 30.000^3 en DNS). Ce calcul nous permet de trancher entre deux estimateurs, proposés par Cichowlas *et al.* pour le minimum du spectre. Le premier estimateur est obtenu en calculant l'intersection de la zone de cascade avec la zone d'équipartition. Le second prend en compte l'existence d'une zone de type 'dissipative' à la fin de la zone inertielle. Les résultats de la fermeture montrent que l'estimateur dissipatif est le plus approprié.

8.7.2 Dispersion d'une particule et proposition d'une nouvelle fermeture Markovienne

Si on prend la limite de diffusivité zero, l'équation de la fluctuation d'un scalaire passif en présence d'un gradient uniform de scalaire de valeur $\partial\Theta/\partial z = -1$ devient équivalent à l'équation du déplacement vertical d'un traceur passif:

$$\frac{d\theta}{dt} = w \tag{8.14}$$

Ce lien étroit entre un scalaire et un traceur nous permet d'utiliser la fermeture EDQNM pour prédire la dispersion absolute moyenne d'une particule de fluide par rapport à son origine.

Ensuite on démontre que le temps Lagrangien de décorrélation peut être estimé à partir du flux de scalaire dans le cas diffusivité zero,

$$\overline{\theta(t)w(t)} = \mathcal{T}(t)\overline{u(t)^2}, \tag{8.15}$$

ce qui nous permet de remplacer la fréquence d'amortissement dans la fermeture EDQNM par une quantité déterminée dans le modèle. Nous obtenons ainsi une fermeture sans aucune constante ajustable pour les spectres de $E(K)$, $E_\theta(K)$ et $F_{w\theta}(K)$. Les constantes de Kolmogorov et Corrsin-Obukhov sont alors estimées être 1.75 et 0.32 respectivement, ce qui est un résultat tout à fait acceptable pour un modèle sans paramètre ajusté.

Bibliography

[1] H. Touil. *Modélisation spectrale de la turbulence inhomogène anisotrope.* PhD thesis, Ecole Centrale de Lyon, 2002.

[2] F.T.M. Nieuwstadt. *Turbulentie.* epsilon, 1998.

[3] Stephen B. Pope. *Turbulent Flows.* Cambridge University Press, 2000.

[4] A.N. Kolmogorov. The local structure of turbulence in incompressible viscous fluid for very large Reynolds numbers. *Dokl. Akad. Nauk. SSSR*, 30:301–305, 1941.

[5] S.G. Saddoughi and S.V. Veeravalli. Local isotropy in turbulent boundary layers at high Reynolds number. *J. Fluid Mech.*, 268:333–372, 1994.

[6] K.R. Sreenivasan. On local isotropy of passive scalars in turbulent shear flows. *Proc. R. Soc. Lond. A*, 434:165–182, 1991.

[7] K. R. Sreenivasan and R. A. Antonia. The phenomenology of small-scale turbulence. *Annu. Rev. Fluid Mech.*, 29:435–472, 1997.

[8] A.M. Obukhov. Structure of the temperature field in turbulent flows. *Isv. Geogr. Geophys. Ser.*, 13:58–69, 1949.

[9] S. Corrsin. On the spectrum of isotropic temperature fluctuations in an isotropic turbulence. *J. Appl. Phys.*, 22:469–473, 1951.

[10] K.R. Sreenivasan. The passive scalar spectrum and the Obukhov-Corrsin constant. *Phys. Fluids*, 8:189–196, 1996.

[11] Z. Warhaft and J.L. Lumley. An experimental study of the decay of temperature fluctuations in grid-generated turbulence. *J. Fluid Mech.*, 88:659–684, 1978.

[12] Jayesh, C. Tong, and Z. Warhaft. On temperature spectra in grid turbulence. *Phys. Fluids*, 6:306–312, 1994.

[13] P.K. Yeung, S. Xu, and K.R. Sreenivasan. Schmidt number effects on turbulent transport with uniform mean scalar gradient. *Phys. Fluids*, 14(12):4178–4191, 2002.

[14] G. Brethouwer, J.C.R. Hunt, and F.T.M. Nieuwstadt. Micro-structure and Lagrangian statistics of the scalar field with a mean gradient in isotropic turbulence. *J. Fluid Mech.*, 474, 2003.

[15] S. Corrsin. Heat transfer in isotropic turbulence. *J. Appl. Phys.*, 23(1):113–118, 1952.

[16] H.K. Corrsin. A uniform gradient turbulent transport experiment. *J. Geophys. Res.*, 67(8):3033–3048, 1962.

[17] J.L. Lumley. The spectrum of nearly inertial turbulence in a stably stratified fluid. *J. Atmos. Sci.*, 21:99–102, 1964.

[18] G.K. Batchelor. The theory axisymmetric turbulence. *Proc. R. Soc. Lond. A.*, 186:480–502, 1946.

[19] S. Chandrasekhar. The theory axisymmetric turbulence. *Phil. Trans. R. Soc. Lond. A.*, 242:557–577, 1950.

[20] S. Herr, L.P. Wang, and L.R. Collins. EDQNM model of a passive scalar with a uniform mean gradient. *Phys. Fluids*, 8:1588–1608, 1996.

[21] S.A. Orszag. Analytical theories of turbulence. *J. Fluid Mech.*, 41:363–386, 1970.

[22] J.R. Herring, D. Schertzer, M. Lesieur, G.R. Newman, J.P. Chollet, and M. Larcheveque. A comparative assessment of spectral closures as applied to passive scalar diffusion. *J. Fluid Mech.*, 124:411–437, 1982.

[23] J.-M. Vignon and C. Cambon. Thermal spectral calculation using eddy-damped quasi-normal markovian theory. *Phys. Fluids*, 23:1935–1937, 1980.

[24] C. Cambon, D. Jeandel, and J. Mathieu. Spectral modelling of homogeneous non-isotropic turbulence. *J. Fluid Mech.*, 104:247–262, 1981.

[25] J.-P. Bertoglio. Etude d'une turbulence anisotrope: modélisation de sous-maille et approche statistique. *Thèse d'état, Université Claude Bernard de Lyon*, 1986.

[26] L. Ménoret. *Contribution à l'étude des écoulements faiblement inhomogènes et anisotropes.* PhD thesis, Ecole Centrale de Lyon, 1982.

[27] A.D. Burden. Towards an EDQNM closure for inhomogeneous turbulence. In *Advances in Turbulence III*, Springer Verlag, 1991.

[28] A. Laporta. *Etude spectrale et modélisation de la turbulence inhomogène.* PhD thesis, Ecole Centrale de Lyon, 1995.

[29] J.P. Bertoglio and D. Jeandel. A simplified spectral closure for inhomogeneous turbulence. *5th TSF, Springer Verlag*, 1986.

[30] S. Parpais. *Développement d'un modèle spectral pour la turbulence inhomogène. Résolution par une méthode d'éléments finis.* PhD thesis, Ecole Centrale de Lyon, 1997.

[31] J.L. Lumley. Similarity and the turbulent energy spectrum. *Phys. Fluids*, 10:855–858, 1967.

[32] J.C. Wyngaard and O.R. Coté. Cospectral similarity in the atmospheric surface layer. *Quart. J. R. Met. Soc.*, 98:590–603, 1972.

[33] J.C. Kaimal, J.C. Wyngaard, Y. Izumi, and O.R. Coté. Spectral characteristics of surface-layer turbulence. *Quart. J. R. Met. Soc.*, 98:563–589, 1972.

[34] B.A. Kader and A.M Yaglom. Spectra and correlation functions of surface layer atmospheric turbulence in unstable thermal stratification. In *Organized structures and turbulence in fluid mechanics, Grenoble*, pages 387–412, Kluwer, 1989.

[35] W.J. Massman and X. Lee. Eddy covariance flux corrections and uncertainties in long-term studies of carbon and energy exchanges. *Agr. Forest Meteorol.*, 113:121–144, 2002.

[36] C. Feigenwinter, R. Vogt, and E. Parlow. Vertical structure of selected turbulence characteristics above an urban canopy. *Theor. Appl. Climatol.*, 62:51–63, 1999.

[37] R. Kormann, H. Müller, and P. Werle. Eddy flux measurements of methane over the fen "Murnauer Moos", using a fast tunable diode laser spectrometer. *Atmos. Env.*, 35:2533–2544, 2001.

[38] H.B. Su, H.P. Schmid, C.S.B Grimmond, C.S. Vogel, and A.J. Oliphant. Spectral characteristics and correction of long-term eddy-covariance measurements over two mixed hardwood forests in non flat terrain. *Bound. Lay. Meteorol.*, 110:213–253, 2004.

[39] T.W. Horst. A simple formula for attenuation of eddy fluxes measured with first-order-response scalar sensors. *Bound. Lay. Meteorol.*, 82:219–233, 1997.

[40] L. Mydlarski and Z. Warhaft. Passive scalar statistics in high Peclet number grid turbulence. *J. Fluid Mech.*, 358:135–175, 1998.

[41] L. Mydlarski. Mixed velocity-passive scalar statistics in high-Reynolds-number turbulence. *J. Fluid Mech.*, 475:173–203, 2003.

[42] R.A. Antonia and R.J. Smalley. Velocity and temperature scaling in a rough wall boundary layer. *Phys. Rev. E*, 62:640–646, 2000.

[43] L. Mydlarski and Z. Warhaft. On the onset of high-Reynolds-number grid-generated wind tunnel turbulence. *J. Fluid Mech.*, 320:331–368, 1996.

[44] H. Zhou, G. Cui, Z. Zhang, and L. Shao. Dependence of turbulent scalar flux on molecular Prandtl number. *Phys. Fluids*, 17:2388–2394, 2002.

[45] E. Deutsch. *Dispersion de particules dans une turbulence homogène isotrope stationnaire calculeé par simulation numérique directe des grandes échelles.* PhD thesis, Electricité De France, 1992.

[46] M.R. Overholt and S.B. Pope. Direct numerical simulation of a passive scalar with imposed mean gradient in isotropic turbulence. *Phys. Fluids*, 8:3128–3148, 1996.

[47] A. Sirivat and Z. Warhaft. The effect of a passive cross-stream temperature gradient on the evolution of temperature variance and heat flux in grid turbulence. *J. Fluid Mech.*, 128:323–346, 1983.

[48] J.R. Chasnov. Similarity states of passive scalar transport in isotropic turbulence. *Phys. Fluids*, 6:1036–1051, 1994.

[49] R. Budwig, S. Tavoularis, and S. Corrsin. Temperature fluctuations and heat flux in grid-generated isotropic turbulence with streamwise and transverse mean-temperature gradients. *J. Fluid Mech.*, 153:441–460, 1985.

[50] H. Tennekes and J.L. Lumley. *A first course in turbulence.* The MIT Press, 1972.

[51] P. A. O'Gorman and D. I. Pullin. Effect of Schmidt number on the velocity-scalar cospectrum in isotropic turbulence with a mean scalar gradient. *J. Fluid Mech.*, 532:111–140, 2005.

[52] J.P. Chollet and M. Lesieur. Parameterization for small scales of three-dimensional isotropic turbulence using spectral closures. *J. Atmos. Sci.*, 38:2747–2757, 1981.

[53] M. Lesieur and R. Rogallo. Large-eddy simulation of passive scalar diffusion in isotropic turbulence. *Phys. Fluids*, 1:718–722, 1989.

[54] M. Ulitsky and L.R. Collins. On constructing realizable, conservative mixed scalar equations using the eddy-damped quasi-normal markovian theory. *J. Fluid Mech.*, 412:303–329, 2000.

[55] J.M. Vignon. *Turbulence et réaction chimique.* PhD thesis, Université Claude Bernard de Lyon, 1979.

[56] M. Lesieur. *Turbulence in fluids.* Kluwer Dordrecht, 1990.

[57] N. Nakauchi and S. Sega. The homogeneous axisymmetric passive scalar in isotropic turbulence. *Phys. Fluids*, 30(2):337–344, 1987.

[58] M. Ulitsky, T. Vaithianathan, and L.R. Collins. A spectral study of differential diffusion of passive scalars in isotropic turbulence. *J. Fluid Mech.*, 460:1–38, 2002.

[59] P.A. O'Gorman and D.I. Pullin. The velocity-scalar cross correlation of stretched spiral vortices. *Phys. Fluids*, 15, 2003.

[60] C.E. Leith. Atmospheric predictability and two-dimensional turbulence. *J. Atmos. Sci.*, 28:145–161, 1971.

[61] J.O. Hinze. *Turbulence.* McGraw-Hill, 1975.

[62] U. Frisch, M. Lesieur, and D. Schertzer. Comments on the quasi-normal markovian approximation for fully developed turbulence. *J. Fluid Mech.*, 97:181–192, 1980.

[63] A. Pouquet, M. Lesieur, J.C. André, and C. Basdevant. Evolution of high Reynolds number two-dimensional turbulence. *J. Fluid Mech.*, 72:305–319, 1975.

[64] P. Orlandi and R. A. Antonia. Dependence of a passive scalar in decaying isotropic turbulence on the Reynolds and Schmidt numbers using the EDQNM model. *J. Turbul.*, 5(009):1–13, 2004.

[65] F.H. Champagne, C.A. Friehe, J.C. LaRue, and J.C. Wyngaard. Flux measurements, flux estimation techniques and fine-scale turbulence measurements in the unstable surface layer over land. *J. Atmos. Sci.*, 34:515–530, 1977.

[66] M. Ulitsky and L.R. Collins. Application of the eddy-damped quasi-normal markovian spectral transport theory to premixed turbulent flame propagation. *Phys. Fluids*, 9:3410–3430, 1996.

[67] R.H. Kraichnan. Lagrangian-history closure approximation for turbulence. *Phys. Fluids*, 8:575–598, 1965.

[68] C. Cambon. Etude spectrale d'un champ turbulent incompressible soumis à des effets couplés de déformation et de rotation imposés extérieurement. *Thèse d'état, Université Claude Bernard de Lyon*, 1982.

[69] C. Cambon. *Modélisation spectrale en turbulence homogène isotrope.* PhD thesis, Université Claude Bernard de Lyon, 1979.

[70] J.P. Bertoglio. A model of three-dimensional transfer in non-isotropic homogeneous turbulence. In *Turbulent Shear Flows III, Davis*, pages 253–261, Springer-Verlag, 1981.

[71] Y. Kaneda, T. Ishihara, M. Yokokawa, K. Itakura, and A. Uno. Energy dissipation rate and energy spectrum in high resolution direct numerical simulations of turbulence in a periodic box. *Phys. Fluids*, 15(L21), 2003.

[72] Y. Tsuji. Intermittency effect on energy spectrum in high-Reynolds number turbulence. *Phys. Fluids*, 16(5):L43, 2004.

[73] J. Smagorinsky. General recirculation experiments with the primitive equations. *Mon. Weather Rev.*, 91:99–164, 1963.

[74] M. Germano, U. Piomelli, P. Moin, and W. Cabot. A dynamic subgrid-scale eddy viscosity model. *Phys. Fluids*, 3:1760–1765, 1991.

[75] R.H. Kraichnan. Eddy viscosity in two and three dimensions. *J. Atmos. Sci.*, 33:1521–1536, 1976.

[76] J.P. Chollet. Two-point closures as a subgrid-scale modelling for large eddy simulations. In *Turbulent Shear Flows IV, Karlsruhe*, pages 9.13–9.17, Springer-Verlag, 1984.

[77] L. Liechtenstein, F.S. Godeferd, and C. Cambon. Non-linear formation of structures in rotating stratified turbulence. In *Advances in Turbulence X, Tenth European Turbulence Conference, Trondheim*, pages 341–344, Cimne, 2004.

[78] F. Bellet, F.S. Godeferd, J.F. Scott, and C. Cambon. Wave turbulence modelling in rapidly rotating flows. In *Advances in Turbulence X, Tenth European Turbulence Conference, Trondheim*, pages 337–340, Cimne, 2004.

[79] G. Cui, H. Zhou, Z. Zhang, and L. Shao. A new dynamic subgrid eddy viscosity model with application to turbulent channel flow. *Phys. Fluids*, 16:2835–2842, 2004.

[80] C.M. Casciola, P. Gualtieri, R. Benzi, and R. Piva. Scale-by-scale budget and similarity laws for shear turbulence. *J. Fluid Mech.*, 476:105–114, 2003.

[81] H.S. Kang and C. Meneveau. Passive scalar anisotropy in a heated turbulent wake: new observations and implications for large-eddy simulations. *J. Fluid. Mech.*, 442:161–170, 2001.

[82] L. Shao, J.-P. Bertoglio, G.X. Cui, H.B. Zhou, and Z.S. Zhang. Kolmogorov equation for large eddy simulation and its use for subgrid modeling. In *ERCOFTAC Workshop, Direct and Large Eddy Simulation*, Munich, 2003.

[83] L. Shao, G. Cui, and Z. Zhang. Subgrid-diffusivity derived from the monin-yaglom equation for large eddy simulation. In *Advances in Turbulence X, Trondheim 2004*, page 862, Barcelona, 2004.

[84] A.M. Yaglom. On the local structure of a temperature field in a turbulent flow. *Dokl. Akad. Nauk. SSSR*, 69:743–746, 1949.

[85] L. Shao. *Etude d'une couche de mélange turbulente non-cisaillée par simulation des grandes échelles.* PhD thesis, Ecole Centrale de Lyon, 1992.

[86] K. Alvelius and A.V. Johansson. Les computations and comparison with kolmogorov theory for two-point pressure-velocity correlations and structure functions for globally anisotropic turbulence. *J. Fluid Mech.*, 403:22–36, 2000.

[87] K. Alvelius. Random forcing of three-dimensional homogeneous turbulence. *Phys. Fluids*, 11:1880–1889, 1999.

[88] W.G. Rose. Results of an attempt to generate a homogeneous turbulent shear flow. *J. Fluid Mech.*, 25:97–120, 1966.

[89] U. Karnik and S. Tavoularis. Generation and manipulation of uniform mean shear with the use of screens. *Exp. Fluids*, 5:247–269, 1987.

[90] S. Tavoularis and U. Karnik. Further experiments on the evolution of turbulent stresses and scales in uniformly sheared turbulence. *J. Fluid Mech.*, 204:457–478, 1989.

[91] S. Tavoularis. Asymptotic laws for transversely homogeneous turbulent shear flows. *Phys. Fluids*, 28:999–1001, 1985.

[92] S. Tavoularis and S. Corrsin. Experiments in nearly homogeneous turbulent shear flow with a uniform mean temperature gradient. part 1. *J. Fluid Mech.*, 104:457–478, 1981.

[93] S. Tavoularis and S. Corrsin. Experiments in nearly homogeneous turbulent shear flow with a uniform mean temperature gradient. part 2. the fine structure. *J. Fluid Mech.*, 104:349–367, 1981.

[94] S. Tavoularis and S. Corrsin. Effects of shear on the turbulent diffusivity tensor. *Int. J. Heat Mass Tran.*, 28:265–276, 1985.

[95] U. Karnik and S. Tavoularis. Measurements of heat diffusion from a continuous line source in a uniformly sheared turbulent flow. *J. Fluid Mech.*, 202:233–261, 1989.

[96] E.F. Bradley, R.A. Antonia, and A.J. Chambers. Turbulence Reynolds number and the turbulent kinetic energy balance in the atmospheric surface layer. *Bound. Lay. Meteorol.*, 21:183–197, 1981.

[97] M. M. Rogers, P. Moin, and W. C. Reynolds. The structure and modeling of the hydrodynamic and passive scalar fields in homogeneous turbulent shear flow. Technical report, Dept. Mech. Engng. Rep. TF-25, Stanford University, Stanford, 1986.

[98] H.-J. Kaltenbach, T. Gerz, and U. Schumann. Large-eddy simulation of homogeneous turbulence and diffusion in stably stratified shear flow. *J. Fluid Mech.*, 280:1–40, 1994.

[99] R.A. Antonia and Y. Zhu. Inertial range behaviour of the longitudinal heat flux cospectrum. *Bound. Lay. Meteorol.*, 70:429–434, 1994.

[100] A. Craya. Contribution a l'ana lyse de la turbulence associee a des vitesses moyennes. *Technical Report, Publ. Sci. Tech. Ministere de l'air*, 345, 1958.

[101] A.C. Eringen. *Continuum Physics.* Academic Press, 1971.

[102] R. Schiestel. *Modélisation et simulation des écoulements turbulents.* Hermes, 1993.

[103] T. Clark and C. Zemach. A spectral model applied to homogeneous turbulence. *Phys. Fluids*, 7:1674–1694, 1995.

[104] J.J. Rohr, E.C. Itsweire, K.N. Helland, and C.W. Van Atta. An investigation of the growth of turbulence in a uniform-mean-shear flow. *J. Fluid Mech.*, 187:1–33, 1988.

[105] M. Gonzalez. Asymptotic evolution of a passive scalar field advected by homogeneous turbulent shear flow. *Int. J. Heat Mass Tran.*, 43:387–397, 2000.

[106] M. M. Rogers. The structure of a passive scalar field with a uniform mean gradient in rapidly sheared homogeneous turbulent flow. *Phys. Fluids*, 3:144–154, 1991.

[107] L. Fulachier and R.A. Antonia. Spectral relationships between velocity and temperature fluctuations in turbulent shear flows. *Phys. Fluids*, 26:2105–2108, 1983.

[108] R. Rubinstein and J. M. Barton. Renormalization group analysis of anisotropic diffusion in turbulent shear flows. *Phys. Fluids*, 3:415–421, 1991.

[109] A. Celani, M. Cencini, M. Vergassola, E. Villermaux, and D. Vincenzi. Shear effects on passive scalar spectra. *J. Fluid. Mech.*, 523:99–108, 2005.

[110] S.J. Caughey. Boundary-layer turbulence spectra in stable conditions. *Bound. Lay. Meteorol.*, 11:3–14, 1977.

[111] L. Skrbek and S.R. Stalp. On the decay of homogeneous isotropic turbulence. *Phys. Fluids*, 12:1997–2019, 2000.

[112] H. Touil, L. Shao, and J.P. Bertoglio. The decay of turbulence in a bounded domain. *J. Turbul.*, 3(049):1–12, 2002.

[113] T.-H. Shih and J.L. Lumley. Remarks on turbulent constitutive relations. *Math. Comput. Mod.*, 18, 1993.

[114] S. Parpais and J.P. Bertoglio. Computations of heat flux and temperature fluctuation using a spectral model for inhomogeneous turbulence. In *2nd Int. Symposium on Turbulence, Heat and Mass Transfer, Delft*, pages 1–10, 1997.

[115] M.M. Gibson and B.E. Launder. Ground effects on pressure fluctuations in the atmospheric boundary layer. *J. Fluid Mech.*, 86:491–511, 1978.

[116] J.C. LaRue and P.A. Libby. Thermal mixing layer downstream of half heated turbulence grid. *Phys. Fluids*, 24:597–603, 1981.

[117] J.C. LaRue, P.A. Libby, and D.V.R. Seshadri. Further results on the thermal mixing layer downstream of a turbulence grid. *Phys. Fluids*, 24:1927–1933, 1981.

[118] G. Brun. *Développement et application d'une méthode déléments finis pour le calcul des écoulements turbulents fortement chauffés.* PhD thesis, Ecole Centrale de Lyon, 1988.

[119] C. Cichowlas, P. Bonaïti, F. Debbasch, and M. Brachet. Kolmogorov scaling in truncated 3-d euler flows. *oai:arXiv.org:nlin/0410064 (20050310)*, 2004.

[120] G.F. Carnevale, U. Frisch, and R. Salmon. H theorems in statistical fluid dynamics. *J. Phys. A: Math. Gen.*, 14:1701–1718, 1981.

[121] C. Nore, M. Abid, and M. Brachet. Kolmogorov turbulence in low-temperature superflows. *Phys. Rev. lett.*, 78:3896–3899, 1997.

[122] C. Nore, M. Abid, and M. Brachet. Decaying Kolmogorov turbulence in a model of superflow. *Phys. Fluids*, 9:2644–2669, 1997.

[123] M. Larcheveque and M. Lesieur. The application of eddy-damped markovian closures to the problem of dispersion of particle pairs. *J. Mécanique*, 20:113–134, 1981.

[124] G.I Taylor. Diffusion by continuous movements. *Proc. London Math. Soc.*, 2(20):196–212, 1921.

[125] B. Sawford. Turbulent relative dispersion. *Annu. Rev. Fluid Mech.*, 33:289–317, 2001.

[126] R.H. Kraichnan. The structure of isotropic turbulence at very high Reynolds numbers. *J. Fluid Mech.*, 5:497–543, 1959.

[127] D.C. Leslie. *Developments in the theory of turbulence.* Oxford University Press, 1973.

[128] R.H. Kraichnan. An almost-markovian galilean-invariant turbulence model. *J. Fluid Mech.*, 47:513–524, 1971.

[129] G. Brethouwer. *Mixing of passive and reactive scalars in turbulent flows.* PhD thesis, TU Delft, 2001.

[130] J.C. Rotta. Statistische Theorie nichthomogener Turbulenz. *Z. Phys*, 129:547–572, 1951.

[131] N. Nakauchi and H. Oshima. The return of strongly anisotropic turbulence to isotropy. *Phys. Fluids*, 30:6353–6360, 1987.

[132] N. Nakauchi. An application of the modified zero-fourth-cumulant approximation to homogeneous axisymmetric turbulence. *J. Phys. Soc. Jpn.*, 53:1682–1691, 1984.

Appendix A

Trigonometric relations

The definition of $x, y, z, \mu, \mu', \mu''$ is taken from Nakauchi *et al.*[131] and Lesieur [56] and not like Ulitsky and Collins [54], who define x, y, z opposite to our definitions. We define:

$$\begin{aligned} x &= -\frac{\mathbf{P}\cdot\mathbf{Q}}{PQ} \\ y &= -\frac{\mathbf{K}\cdot\mathbf{Q}}{KQ} \\ z &= -\frac{\mathbf{P}\cdot\mathbf{K}}{PK} \end{aligned} \tag{A.1}$$

The angle between the mean gradient and the wave vectors $\mathbf{K}$ is defined by:

$$\mu = \frac{K_3}{K} \tag{A.2}$$

Introducing an alternative coordinate system, Nakauchi [132] manages to express the angle between the mean gradient and the wave vectors $\mathbf{P}$ and $\mathbf{Q}$ as a function of y, z, μ, K and φ the angle of the projection on a certain plane in the new coordinate system. This φ dependence will disappear so will not go into details and refer to Nakauchi [132] or Herr *et al.* [20] for details. The expressions are:

$$\begin{aligned} \mu' &= -\frac{K_3\cdot\mathbf{P}}{PK} = -\mu z - \sqrt{(1-\mu^2)(1-z^2)}sin(\varphi) \\ \mu'' &= -\frac{K_3\cdot\mathbf{Q}}{QK} = -\mu y + \sqrt{(1-\mu^2)(1-y^2)}sin(\varphi) \end{aligned} \tag{A.3}$$

The integral in (3.48) can then be rewritten as [20]:

$$\int f(\mathbf{K},\mathbf{P}..x..\mu)\delta(\mathbf{K}+\mathbf{P}+\mathbf{Q})d\mathbf{P}d\mathbf{Q} = \iint_{\Delta} f(K,P..x..\mu)dPdQ\frac{PQ}{K}d\varphi \tag{A.4}$$

The integration domain is hereby reduced to a strip in the P, Q plane. All combinations of K, P, Q that can form triads in this plane are contributing to the non-linear interaction. To simplify the geometric functions involving the cosines x, y, z the following relations might be of use:

$$\begin{aligned}
\sqrt{1-x^2}\sqrt{1-y^2} &= xy + z \\
\sqrt{1-y^2}\sqrt{1-z^2} &= yz + x \\
\sqrt{1-x^2}\sqrt{1-z^2} &= xz + y \\
x^2 + y^2 + z^2 &= 1 - 2xyz \\
\frac{x}{K} = \frac{y}{P} &= \frac{z}{Q} \\
K^2 &= P^2 + Q^2 - 2PQx \\
P^2 &= K^2 + Q^2 - 2KQy \\
Q^2 &= P^2 + K^2 - 2PKz
\end{aligned} \tag{A.5}$$

Appendix B

Modelling the evolution equation for $\varphi_{ij}(K)$

We recall briefly the models used by Touil [1] to describe the evolution of the spherically averaged spectral tensor.

The linear transfer,

$$T_{ij}^{L}(K) = \iint_{\Sigma K} \frac{\partial \overline{U}_l}{\partial x_n} \frac{\partial K_l \Phi_{ij}}{\partial K_n} d\Sigma K \tag{B.1}$$

represents the influence of the mean velocity gradient, stretching the turbulent structures. This term is distributive in wavenumber-space, which means that it does not dissipate energy but redistributes energy over the different scales. We use the model proposed by Touil [1], inspired by Clark and Zemach [103].

$$T_{ij}^{L}(K) = A^{L} \sqrt{S_{ij} S_{ij}} \frac{\partial K \varphi_{ij}}{\partial K} \tag{B.2}$$

with

$$S_{ij} = \frac{1}{2} \left(\frac{\partial \overline{U}_i}{\partial x_j} + \frac{\partial \overline{U}_j}{\partial x_i} \right) \tag{B.3}$$

the constant A^L was determined in the work of Touil [1]. A value of -0.03 was found.

The second term on the RHS of equation (5.5) is the *rapid pressure* term. This term represents the linear part of the interaction between deformation and the pressure field.

$$\Pi_{ij}^{L}(K) = \iint_{\Sigma K} 2 \frac{\partial \overline{U}_l}{\partial x_n} \left(\frac{K_l K_i}{K^2} \Phi_{nj} + \frac{K_l K_j}{K^2} \Phi_{in} \right) d\Sigma K \tag{B.4}$$

The modeled form is taken from Cambon *et al.* [24] and can also be found in [1] with one contant $C_b = 0.77$. We note here that in the work of Cambon *et*

al. a model was derived for the linear transfer different from (B.2) and that the constant in this model was related to the constant C_b. Touil preferred the modelled form (B.2) because of its numerical robustness.

The *non-linear transfer* has been modeled by an extension of the isotropic EDQNM expression. We refer to Touil [1] for details.

Mélange d'un scalaire passif dans les écoulements turbulents

Le mélange d'un scalaire passif par un écoulement turbulent est étudié. D'abord, la simulation numérique directe (DNS), la simulation des grandes échelles (LES) et des arguments dimensionnels sont employés pour étudier le spectre du flux de scalaire dans une turbulence isotrope avec un gradient moyen uniforme de scalaire. Une loi d'échelle est dérivée. Cette loi conduit à des pentes du spectre variant entre $-5/3$ et $-7/3$ en zone inertielle. De premiers résultats de LES plaident en faveur d'un comportement en K^{-2}.

Ensuite, en utilisant une fermeture en deux points (EDQNM), nous montrons qu'aux nombres de Reynolds très élevés, le spectre de flux de scalaire dans la zone inertielle se comporte en $K^{-7/3}$. Ce résultat est en accord avec l'analyse dimensionnelle classique de Lumley (1967). Aux nombres de Reynolds correspondants aux expériences de laboratoire, la fermeture conduit à des spectres plus près de K^{-2}. Nous montrons ensuite que le comportement en K^{-2} trouvé en LES est induit par le forçage à grande échelle.

La fermeture est alors appliquée au cas des écoulements homogènes cisaillés et les spectres du flux de scalaire longitudinal et transverse sont étudiés. Le spectre du flux longitudinal est trouvé proportionelle à $K^{-23/9}$. Ce résultat est en accord avec l'expérience mais est en désaccord avec l'analyse dimensionnelle classique.

Finalement, nous montrons que le lien entre la dispersion de particules et le mélange d'un scalaire permet de formuler une fermeture en deux points et un temps qui ne nécessite l'introduction d'aucune constante dans le modèle.

Passive scalar mixing in turbulent flow

The mixing of a passive scalar in turbulent flow is studied. First, Direct Numerical Simulation (DNS), Large Eddy Simulation (LES) and dimensional arguments are used to investigate the scalar flux spectrum in isotropic turbulence with a mean scalar gradient. A scaling law allowing for inertial range slopes varying from $-5/3$ to $-7/3$ is derived. The LES results support a K^{-2} expression.

Subsequently, using a two-point closure (EDQNM), we show that at very high Reynolds numbers, the scalar flux spectrum in the inertial range behaves as predicted by the classical dimensional analysis of Lumley (1967) and scales as $K^{-7/3}$. At Reynolds numbers corresponding to laboratory experiments the closure leads to a spectrum closer to K^{-2}. It is shown that the K^{-2} scaling in the LES is induced by large scale forcing.

The closure is then applied to homogeneous shear flow and the spectra of cross-stream and streamwise scalar fluxes are investigated. The streamwise scalar flux spectrum is found to scale as $K^{-23/9}$. This result is in agreement with experiments but disagrees with classical dimensional analysis.

Eventually, we show that the link between particle dispersion and scalar mixing allows to formulate a Markovian two-point closure for the velocity and scalar that does not involve any model constant.